UNIVERSITY OF
KWAZULU-NATAL

INYUVESI
YAKWAZULU-NATALI

CYCLEN TETRAHYDROCHLORIDE INDUCES NECROPTOSIS VIA OXIDATIVE AND NITROSATIVE STRESS IN MCF-7 AND MDA-MB BREAST CANCER CELLS RESPECTIVELY

Mikayla Libby Munsamy (218016363)

Dr Rene Khan

Dr Hezekiel Kumalo

BMedSc (Physiology), BMedSci (Hons in Medical Biochemistry) (UKZN)

Submitted in fulfilment of the requirements for the degree of Master of Medical Science in the Discipline of Medical Biochemistry, School of Laboratory Medicine and Medical Sciences, College of Health Sciences, University of KwaZulu-Natal, Durban, South Africa

2023

DECLARATION

I **Mikayla Munsamy** declare that.

1. This dissertation is a rendition of original work produced by me as primary author under supervisorship. No contents of this dissertation have been previously published neither submitted to UKZN or other tertiary institutions.

2. The necessary referencing practices have been utilized to acknowledge the use of other authored sources such as journal articles, theses, ideas, and supplementary internet-based information. In the case of other quoted written sources, the following was implemented; their words have been re-written, but the general information attributed to them has been referenced.

3. The results within this dissertation are compilation of my own investigations conducted at UKZN Medical Biochemistry laboratory and were not presented towards any other awarded degree or institution.

Signed: [redacted] Date: 07/02/2024

SUPERVISOR: [redacted]

CO-SUPERVISOR: [redacted]

DEDICATION

With God, prayer, and faith nothing is impossible.

Proverbs 3 verse 5-6:

Trust in the Lord with all your heart, do not depend on your own understanding. Seek his will in all you do, and he will show you which path to take.

I dedicate this work to my loving and supportive family, not forgetting my cat who stayed up with me on countless nights.

To my mother who believes I have the potential to achieve all of my dreams as well as her own. Her sacrifices made it possible for me to obtain such a substantial academic career thus far and I strive to always make her proud.

The support of my family allowed me to focus on my education without the societal pressure a woman is often conflicted with, and I am forever grateful.

ACKNOWLEDGEMENTS

To my supervisor and co-supervisor:

A heartfelt thank you to **Dr RB Khan**. Her nurturing guidance has made the biggest difference on the standard of work I am able to produce and has greatly moulded me into a more giving young adult. To be supervised by such a kind, patient and robust woman is something I wish all upcoming scientists get to experience at least once in their academic career. I will forever cherish the fundamental values she has instilled in me in terms of work ethic, self-confidence, good research practise and overall strong morals.

A big thank you to **Dr HK Kumalo**, for the motivational support and effective lessons in grasping the very basics of science first in order to understand the more complex pathways of biochemistry.

To my laboratory mates:

A special thank you to **Miss Mayanka Naicker** and **Mr Ranesh Somaru**. The past two years would not have been so enjoyable without my dear friends. Thank you for the great memories filled with hard work, laughter, and good food.

An honourable thank you to the PhD colleagues, **Mr Mthokozisi Nxumalo, Miss Nosipho Ntanzi and Mrs Lebogang Maruma.** Your laboratory support and assistance has been greatly appreciated.

Funding:

I thank the **Council for Scientific and Industrial Research (CSIR)** for the financial and motivational support they provided me along my academic journey.

ABBREVIATIONS

ΔΨm	Mitochondrial membrane potential
ADP	Adenosine diphosphate
AKT	Serine/threonine kinase
A549	Human alveolar adenocarcinoma
APS	Ammonium persulfate
Apaf-1	Apoptotic protease activating factor-1
ATP	Adenosine triphosphate
BAK	Bcl-2 homologous antagonist killer
BAX	Bcl-2-associated X protein
BCA	Bicinchoninic acid
Bcl-2	B-cell lymphoma-2
BHT	Butylated hydroxytoluene
BID	BH3 interacting-domain death agonist
BRCA1	Breast cancer gene 1
BRCA2	Breast cancer gene 2
BSA	Bovine serum albumin
BC	Breast cancer
CAD	Caspase-activated DNase
$CaNa_2EDTA$	Calcium disodium ethylenediamine tetraacetic acid
CARDs	Caspase activation and recruitment domains
CCM	Complete culture medium
cDNA	Complementary deoxyribonucleic acid
cIAP1/2	Cellular inhibitor of apoptosis ½
Co	Cobalt
CST	Cell signalling technology.
Cu	Copper
Cyclen tetrahydrochloride	1,4,7,10-tetraazacyclododecane tetrahydrochloride
CYLD	Cylindromatosis

CYP3A4	Cytochrome p450 3A4
DAMPs	Danger-associated molecular patterns
DD	Death domain
DED	Death effector domain
DISC	Death-inducing signalling complex
DMEM	Dulbecco's Modified Eagle Medium
DMC	1,7-dimethyl-1,4,7,10-tetraazacyclododecane
DMSO	Dimethyl sulfoxide
DNA	Deoxyribonucleic acid
EDTA	Ethylene diamine tetra-acetic acid
EGFR	Epidermal growth factor receptor
ER	Estrogen receptor
ER+	Estrogen receptor positive
ER-	Estrogen receptor negative
ETC	Electron transport chain
FADD	Fas-associated protein with death domain
Fe	Iron
FeS	Iron-sulphur
GAPDH	Glyceraldehyde 3-phosphate dehydrogenase
Gpx	Glutathione peroxidase
GR	Glutathione reductase
GSH	Glutathione
GSSG	Glutathione disulfide
h	Hours
H_2O_2	Hydrogen peroxide
H_3PO_4	Phosphoric acid
HeLa	Cervical cancer cells
HEPES	4-(2-hydroxyethyl)-1-piperazineethanesulfonic acid
HER2	Human epidermal receptor 2
HCl	Hydrochloric acid

HPV	Human papillomavirus
4-HNE	Trans-4-hydroxy-2-nonenal
iNOS	Inducible nitric oxide synthase
IBC	Inflammatory breast cancers
IDC	Invasive Ductal Carcinoma
ILC	Invasive Lobular Carcinoma
JNK	c-Jun N-terminal kinase
LDH	Lactate dehydrogenase
MAPK	Mitogen-activated protein kinase
MDA	Malondialdehyde
MLKL	Mixed lineage kinase domain-like
MOMP	Mitochondrial outer membrane permeabilization
MRI	Magnetic resonance imaging
mRNA	Messenger ribonucleic acid
MTT	3-(4,5-dimethylthiazol-2-yl)-2,5-diphenyltetrazolium bromide
NADPH	Nicotinamide adenine dinucleotide phosphate
NEDD	*N*-(1-Naphthyl)ethylenediamine
NF	Nuclease free
NF-κB	Nuclear factor kappa-light-chain-enhancer of activated B cells
NO	Nitric oxide
NOS	Nitric oxide synthase
NOS2	Nitric oxide synthase 2
$NO_2^{\bullet}$	Nitrogen dioxide radicals
Nrf2	Nuclear factor erythroid 2-related factor 2
$O_2^{\bullet-}$	Superoxide anion
$^{\bullet}OH$	Hydroxyl radical
°C	Degrees celsius
OD	Optical density
OGG1	8-Oxoguanine DNA Glycosylase 1
$ONOO^-$	Peroxynitrite

PALB-2	Partner and localizer of BRCA2
PARP	Poly (ADP-ribose) polymerase
PBS	Phosphate-buffered saline
PI	Propidium iodide
PI3K	Phosphoinositide 3-kinases
PR	Progesterone-receptor
PS	Phosphatidylserine
PUFAs	Polyunsaturated fatty acids
qPCR	Quantitative polymerase chain reaction
RBI	Relative band intensity
RFC	Relative fold change
RIPK1	Receptor-interacting protein kinase1
RIPK3	Receptor-interacting protein kinase3
RLU	Relative light units
RFU	Relative fluorescence units
RNS	Reactive nitrogen species
ROS	Reactive oxygen species
RT	Room temperature
SA	South Africa
SARS-CoV-2	Severe acute respiratory syndrome coronavirus 2
SD	Standard deviation
SDH	Succinate dehydrogenase
SDS-PAGE	Sodium dodecyl sulphate polyacrylamide gel electrophoresis
SMAC	Second mitochondria-derived activator of caspases
SOD2	Superoxide dismutase 2
SULF	Sulfanilic acid
TBA	Thiobarbituric acid
TBARS	Thiobarbituric acid reactive substances
TEMED	N,N,N′,N′-tetramethylethylenediamine
TKIs	Tyrosine kinase inhibitors

TNBC	Triple negative breast cancer
TNF	Tumour necrosis factor
TNFR1	Tumour necrosis factor receptor-1
TRADD	TNF-associated death domain
TRAF2/5	TNF receptor-associated factor 2/5
TRAIL	TNF-related apoptosis-inducing ligand
TTBS	Tris-buffered saline
VCl_3	Vanadium (III) chloride
WHO	World health organization
Zn	Zinc
8-oxoGuo	8-oxo-7,8-dihydro-guanine
8-oxodG	8-oxoGuo and 8-oxo-7,8-dihydro-2′deoxyguanosine

TABLE OF CONTENTS

LIST OF FIGURES

CHAPTER 2

ABSTRACT

Introduction: Breast cancer (BC) is a heterogeneous disease categorised based on the availability of specific female hormone receptors and is thus predominantly associated with female mortality and morbidity globally. The progression of BC and conventional treatments are subtype-specific, producing immunocompromising effects often linked to oxidative stress and cell death pathways, including necroptosis. A promising therapeutic synthetic compound 1,4,7,10-tetraazacyclododecane (cyclen) tetrahydrochloride is a divalent metal chelator that exhibits potential multi-target anti-cancer activities. It harbours high binding affinities toward transition-metal ions or cations, an advantageous pathway to be explored in biomedical research.

Aim: This study aims to determine the anti-proliferative and antioxidant mechanisms of cyclen tetrahydrochloride in MCF-7 and MDA-MB-231 human breast cancer cells.

Methods: The MTT assay assessed the cell viability of MCF-7 and MDA-MB-231 cells following exposure to cyclen tetrahydrochloride (0-1000μM) for 48 hours. Luminometric analysis of ATP and ΔΨm ascertained mitochondrial integrity. Cells were assayed for free radical production (TBARS and NOS assays), while reactive nitrogen species (RNS) were verified by western blotting for iNOS. The antioxidant response was evaluated luminometrically (GSH) and by western blotting (Nrf2 and SOD2). In addition, signalling and cell death pathways activated by oxidative stress (caspases and externalised phosphatidylserine) were evaluated. Cell death by necroptosis was validated by qPCR analysis of *RIPK1, RIPK3, MLKL, TNF-α, NF-κB*, *Gpx-1* and *OGG1* gene expression.

Results: Cell viability decreased with increasing doses of cyclen tetrahydrochloride treatments for MCF-7 (IC_{50} = 168.4μM, IC_{20} = 41.69μM) and MDA-MB-231 (IC_{50} = 561μM, IC_{20} = 302.9μM) cells. This was associated with non-significant changes in CYP34A activity and a dissipated ΔΨm in MCF-7 cells. Although ΔΨm was similar to the control in MDA cells, a corresponding decrease in ATP production was noted for both cell lines (p<0.05). Significant increases in MDA concentration (p<0.05) suggested lipid peroxidation associated with ROS production, particularly in MCF-7 cells. Further evidence of increased ROS was implied by increased *OGG1* gene expression and decreased GSH, suggesting that oxidative

stress was induced. Nitrosative stress was not evident in MCF-7 since iNOS was downregulated, and RNS were decreased. However, cyclen tetrahydrochloride upregulated iNOS to facilitate RNS production in MDA-MB-231 cells ($p<0.05$) and was associated with increased *NF-κB* gene expression ($p<0.05$). An inadequate antioxidant defence was demonstrated by decreased SOD2 and Nrf2 in both cell lines and *Gpx-1* gene expression was upregulated in MCF-7 cells only ($p<0.05$). The prevailing oxidative stress did not initiate apoptosis; caspase-8 and -9 activity were decreased in both cell lines. Although caspase 3/7 was decreased for IC_{20} MCF-7 cells, the IC_{50} induced caspase 3/7 and apoptosis was executed owing to increased PS externalisation. In MDA-MB-231 cells, caspase 3/7 increased in the IC_{20} only, and phosphatidylserine levels were similar to the control. Interestingly, evidence of necrotic cell death in both cell lines was presented by increased DNA fluorescence and LDH leakage ($p<0.05$). Thus, necroptosis was investigated as an alternate mode of cell death. Significant increases in gene expression of *TNF-α* ($p<0.05$), *RIPK1* ($p<0.05$), *RIPK3* ($p<0.05$), and *MLKL* ($p<0.05$) demonstrated that necroptosis was increased.

Conclusion: Cyclen tetrahydrochloride induced ROS-mediated necroptosis in MCF-7 cells, but ROS and RNS facilitated necroptosis in MDA-MB-231 cells.

Keywords: Breast cancer, Cyclen tetrahydrochloride, MCF-7 cells, MDA-MB-231 cells, oxidative stress, nitrosative stress, apoptosis, necrosis, necroptosis

CHAPTER 1: INTRODUCTION

1.1 BACKGROUND

Cancer is a group of life-threatening non-communicable diseases caused by mutations and carcinogens that induce the unregulated replication of genetically abnormal cells in human body tissues and may be promoted by health conditions such as diabetes, obesity and hepatitis (Leal-Esteban and Fajas, 2020). The cancer cells may leave the site of origin via the bloodstream or the lymphatic system and form secondary tumours in other organs in a process known as metastasis (Malik *et al.*, 2022). Despite the efforts of the healthcare systems, the severe acute respiratory syndrome coronavirus 2 (SARS-CoV-2) resulted in the COVID-19 pandemic, which impeded the prognosis, diagnosis and treatment of cancer due to fear of virus exposure, resulting in a 3-year lag of cancer data (Siegel *et al.*, 2023). The secondary consequence of the pandemic confers an upsurge in advanced-stage disease and mortality despite the benefits of modern technologies (Siegel *et al.*, 2023).

According to the World Health Organisation (WHO), cancer accounted for roughly 10 million deaths and an estimated 19.3 million new cases globally in 2020 (World Health Organisation, 2021). The African continent contributed 1.1 million new cases and approximately 711,429 deaths, with South Africa making up 9.8% and 7.9%, respectively (Chhikara and Parang, 2023). Among African females, breast cancer (BC) is the leading malignancy, with 186,598 new cases corresponding with 85,787 deaths and aggressive triple-negative breast cancer (TNBC) being the most prevalent type in 2020 (Chhikara and Parang, 2023). The higher incidences in African females are proportional to the socio-cultural norms and lack of access to appropriate healthcare (Chhikara and Parang, 2023). Breast cancer is a heterogeneous disease characterised by estrogen receptors, progesterone receptors, and expression of human epidermal receptor 2 (HER2) (Malik *et al.*, 2022). Clinical manifestations reveal that BC initially arises within the epithelial cell ducts or lobules of the breast glandular tissue, which can potentially metastasise to surrounding tissue, lymph nodes, and other organs (Feng *et al.*, 2018). Specific factors that increase the risk of breast cancer include increasing age, obesity, harmful use of alcohol, family disease history, history of radiation exposure, reproductive history, tobacco use, and postmenopausal hormone therapy (Momenimovahed and Salehiniya, 2019). Gene mutations are also a risk factor that can be genetically inherited; the most dominant mutations are in the breast cancer gene 1 and 2 (BRCA1, BRCA2), as well as partner and localiser of BRCA2 (PALB-2) genes (World Health Organisation, 2021; Feng *et al.*, 2018).

Breast cancer treatment is sub-type specific, and its management includes surgery, radiation therapy, antibody therapy, and systemic therapy, which consists of anti-cancer medicines for targeted endocrine treatment (Feng *et al.*, 2018). The treatment offered is relatively expensive, with debilitating side effects leading to a decreased survival rate from 90% in high-income countries to 66% in India and 40% in South Africa (World Health Organisation, 2021). Therefore, drug repurposing and metal chelation therapy have sparked much research interest and proven effective in revealing anti-cancer properties. Metal chelators exhibit potential multi-target anti-cancer activities like inducing apoptosis, inhibiting proliferation, blocking metastasis and anti-angiogenic activities (Golbedaghi *et al.*, 2020; Lejault *et al.*, 2019). Ethylene diamine tetra-acetic acid (EDTA) is a metal chelator that shows efficacy as an antioxidant by binding with and removing excess free radicals associated with cancer progression (Timoshnikov *et al.*, 2022). Synthetic metal chelators have been an area of interest in cancer therapy. Therefore, medical research has focused on macrocyclic polyamines' chemical and biological properties to provide a potential anti-cancer therapeutic agent. Macrocyclic polyamines consist of heterocyclic rings with more than two amino groups and a high binding affinity towards transition-metal ions (Lejault *et al.*, 2019). Iron chelators such as deferoxamine and the newer deferasirox, triapine and di-2-pyridylketone-4,4,-dimethyl-3-thiosemicarbazones may inhibit cell proliferation through modulation of ribonucleotide reductase activity (Ibrahim and O'Sullivan, 2020).

The compound 1,4,7,10-tetraazacyclododecane tetrahydrochloride is classified as a macrocycle hydrochloride salt or a macrocyclic polyamine (Chow *et al.*, 2010; Sandnes *et al.*, 1999). This divalent metal chelator is more commonly called cyclen tetrahydrochloride (Tosato *et al.*, 2022; Mcoyi *et al.*, 2020; Lejault *et al.*, 2019). Although the cytotoxic effects of cyclen tetrahydrochloride are relatively unknown, with a sparsity of literature, cyclen forms the backbone of several complexes investigated for their anti-cancer potential (Yang *et al.*, 2007). The synthetic molecule 1,7-dimethyl-1,4,7,10-tetraazacyclododecane (DMC) was the first macrocyclic polyamine shown to induce apoptosis in cervical cancer (HeLa) cells and also inhibit proliferation in HeLa and human alveolar adenocarcinoma (A549) cells (Shen *et al.*, 2017; Yang *et al.*, 2007). In addition, some cyclen compounds demonstrated the potential to decrease oxidative stress by scavenging free radicals (El Safadi *et al.*, 2017).

Under oxidative stress conditions, free radicals produced as by-products of aerobic metabolism tend to become toxic to DNA, proteins, and lipids, which may cause the individual to be susceptible to diseases

such as cancer (Hayes *et al.*, 2020). Reactive oxygen species (ROS) are free radicals produced by the reduction of molecular oxygen within the mitochondrial respiratory chain, and those containing nitrogen are reactive nitrogen species (RNS) (Prasad and Srivastava, 2020). Some important ROS include precursor ROS molecule superoxide anion ($O_2^{\bullet-}$), hydrogen peroxide (H_2O_2), and the cell-damaging hydroxyl radical ($^{\bullet}OH$) molecule (Prasad and Srivastava, 2020). Peroxynitrite ($ONOO^-$) is an RNS free radical derived from the reaction of nitric oxide (NO) with $O_2^{\bullet-}$, which may react with carbon dioxide to form nitrogen dioxide radicals ($NO_2^{\bullet}$) (Timoshnikov *et al.*, 2022; Hayes *et al.*, 2020). An imbalanced level of these free radicals is associated with oxidative stress. It often leads to macromolecule damage by lipid peroxidation processes, protein carbonylation, and DNA oxidation, which results in strand breaks (Arfin *et al.*, 2021). Cells avoid oxidative stress by activating specific signalling pathways and transcription factors, like nuclear factor-like-2 (Nrf2) and the tumour suppressor p53 that play a vital role in maintaining the redox balance or repair of ROS-induced damage (Hayes *et al.*, 2020). The expression of Nrf2 signals the transcription of antioxidant proteins to be released into the cells. Antioxidants function to neutralise free radicals when they have accumulated to toxic levels. Important antioxidant enzymes include superoxide dismutase (SOD), glutathione peroxidase (Gpx) and catalase. Reduced glutathione (GSH) is a vital free radical scavenger and co-factor for the Gpx reaction (Hayes *et al.*, 2020). Failure of the antioxidant mechanism is associated with cell death (Arfin *et al.*, 2021; Hayes *et al.*, 2020).

Cancer influences a loss of apoptotic control, allowing cancer cells to proliferate unchecked, giving rise to invasive mutations, stimulating angiogenesis, and causing cellular stress. Apoptosis is a necessary form of natural cell growth control where cells are programmed to die and is vital to development and homeostasis (Pfeffer and Singh, 2018; Koff *et al.*, 2015). Cellular stress that causes unrepairable DNA damage is a stimulus to apoptosis, leading to molecular changes such as the activation of caspases. Apoptosis also presents morphological changes such as chromatin condensation, nuclear fragmentation, pyknosis, and specific DNA, protein and membrane surface modifications that ensure the apoptotic cell is recognised and engulfed by a phagocytic cell (Koff *et al.*, 2015). Apoptotic initiation is subdivided into the extrinsic and intrinsic pathways that activate the caspase cascade. External death signals activate the extrinsic pathway by binding to the tumour necrosis factor (TNF) death domain receptor family. Binding the respective ligands to the specific death receptors forms a death-inducing complex (DISC) that activates caspases 8/-10 (Pfeffer and Singh, 2018). Activated caspase 8/-10 elicits two mechanisms leading to cell death: direct induction of the executioner caspases-3 and -7 in type I cells or cleavage of Bid (tBID), which engages the intrinsic apoptotic pathway (Pfeffer and Singh, 2018; Koff *et al.*, 2015).

The B-cell lymphoma-2 (Bcl-2) protein family regulates the intrinsic pathway, which consists of pro-apoptotic and anti-apoptotic proteins. BH3-only proteins inhibit the anti-apoptotic Bcl-2proteins. Two pro-apoptotic Bcl-2proteins, Bcl-2-associated X protein (BAX) and Bcl-2 homologous antagonist killer (BAK), migrate to the mitochondria to promote changes to the mitochondrial membrane permeability, leading to the release of cytochrome c and second mitochondria-derived activator of caspases (Smac) in cytoplasm (Pfeffer and Singh, 2018). This, in turn, induces proteolytic cleavage of caspase 9 and the activation of executioner caspases-3 and -7, leading to cell death (Koff *et al.*, 2015).

Past literature also describes other forms of cell death, including autophagy, necrosis, and necroptosis (Yang *et al.*, 2023). Necroptosis is a kind of necrosis that triggers innate immune responses by rupturing dead cells and releasing intracellular components, presenting with morphological features of necrosis. Necroptotic regulated cell death depends on TNF, receptor-interacting serine-threonine kinase 1 (RIPK1), RIPK3 and mixed lineage kinase domain-like (MLKL) (Kim *et al.*, 2019). The metabolic effects of necroptosis may be triggered by an array of signalling consequences like the excessive production of ROS, which induces oxidative stress (Yang *et al.*, 2023). The production of cytotoxic ROS is reported to be promoted by c-Jun N-terminal kinase (JNK), which contributes to TNF-induced necroptosis. Despite the capacity of necroptosis to induce inflammation, emerging evidence suggests that the main pathological role of necroptosis is to initiate defence mechanisms to combat stressors like ROS (Kim *et al.*, 2019).

To date, there is an evident lack of literature regarding the biochemical effects underlying the mechanism of cyclen tetrahydrochloride in BC. Therefore, this study aims to investigate the cytotoxic potential of cyclen tetrahydrochloride by monitoring its impact on the various metabolic pathways mentioned.

1.2 PROBLEM STATEMENT

Although 5th in terms of mortality for both genders, breast cancer currently has the highest mortality, incidence, and prevalence rates among South African women and women globally (Jacobs *et al.*, 2022; World Health Organisation, 2021). Survival rates for BC are relatively high compared to other cancers since the breast tissue is physically not a vital organ for human survival compared to vital organs such as the liver and lungs. However, the mental and emotional trauma from surgeries and the high recurrence rates and metastasis potentially endanger women's health and contribute to mortality (Feng *et al.*, 2018). In addition, the available treatment options are relatively expensive for low-income countries like South

Africa and present debilitating side effects. Therefore, intensive research is ongoing for alternative treatment options, including medicinal compounds, drug repurposing and chelation therapy. Unfortunately, there is insufficient literature available that investigates the antioxidant and anti-proliferative effects of cyclen tetrahydrochloride in MCF-7 and MDA-MB-231 cells.

1.3 SIGNIFICANCE AND IMPLICATIONS

Cancer cells can thrive and evolve under increased ROS concentrations induced by oxidative stress. Cancer also induces a loss of apoptotic control, leading to unchecked abnormal proliferation, giving rise to invasive mutations, stimulating angiogenesis, and causing further cellular stress. Therefore, this research targets the oxidative and apoptotic pathways by a divalent metal chelator. This study will, therefore, be conducted to fill the gap in research for the known antioxidant or anti-proliferative properties of cyclen tetrahydrochloride that may be beneficial towards treating human breast cancer.

1.4 RESEARCH QUESTIONS

Does cyclen tetrahydrochloride attenuate oxidative stress and proliferation within human breast cancer cells?

1.5 HYPOTHESIS

Cyclen tetrahydrochloride modulates oxidative stress and the proliferation of breast cancer cells.

1.6 NULL HYPOTHESIS (H_0)

There is no statistically significant relationship between Cyclen tetrahydrochloride, apoptosis, oxidative stress, and necroptosis in human breast cancer cells.

1.7 ALTERNATIVE HYPOTHESIS (H_1)

Cyclen tetrahydrochloride facilitates a statistically significant relationship between apoptosis, oxidative stress, and necroptosis in human breast cancer cells.

1.8 AIM

To determine cyclen tetrahydrochloride's anti-proliferative and antioxidant mechanisms in MCF-7 and MDA-MB-231 human breast cancer cells.

1.9 OBJECTIVES

The objectives were to evaluate the *in vitro* effects of 1,4,7,10-tetraazacyclododecanetetrahydrochloride (cyclen tetrahydrochloride) in human breast cancer MCF-7 (ER+) and MDA-MB-231 (ER-) cells by

- identifying cytotoxic effects using the
  - 3-(4,5-dimethylthiazol-2-yl)-2-5-diphenyltetrazolium bromide (MTT) assay to calculate cell viability.
  - lactate dehydrogenase assay as a measure of cell membrane integrity.
  - Cell titer glo and JC-10 assays to quantify ATP and mitochondrial membrane potential ($\Delta\Psi m$).
- determining antioxidant mechanisms via
  - spectrophotometric detection of ROS and RNS by quantifying malondialdehyde (TBARS assay) and nitrites (NOS assay), respectively, and western blotting for iNOS.
  - luminometry to quantify reduced glutathione concentration (GSH).
  - western blotting or qPCR for antioxidant expression (Nrf-2, SOD2, Gpx-1, OGG1).
- assessing cell death parameters, including
  - caspases 3/7, 8, and 9 assays to quantify caspase activity to elucidate pathways involved in activating apoptosis.
  - Glo^{TM} Annexin V-propidium iodide (PI) apoptosis and necrosis assay to quantify phosphatidylserine externalisation.
  - gene expression of *RIPK1, RIPK3, MLKL* and *TNF-α* that are linked to necroptosis by qPCR.

CHAPTER 2: LITERATURE REVIEW

2.1 BREAST CANCER

The uncontrolled and unchecked replication of abnormal cells that can metastasise throughout the human body causes a group of life-threatening diseases called cancer (Andele, 2020). Cancer disrupts critical regulatory signalling pathways, leading to genetic and epigenetic mutations (Leal-Esteban and Fajas, 2020; Andele, 2020). They infiltrate and hijack the cell's metabolic processes, targeting key processes like the cell cycle and apoptotic pathway associated with cancer's hallmarks. Cancer cells require oxygen and ATP, which are obtained via pathways of anaerobic glycolysis and the mitochondrial electron transport chain (ETC). Infection with these processes is also a hallmark of cancer (Leal-Esteban and Fajas, 2020).

2.1.1 Breast structure and function

Breast cancer is a collection of different types of malignancies that occur in the mammary glands of breast tissue (World Health Organisation, 2021; Feng *et al.*, 2018). A mammary gland is an essential exocrine gland found within a female mammal, responsible for supporting infant life by manufacturing and secreting nutritional colostrum (Colleluori *et al.*, 2021). It mainly comprises lobules, ducts and adipose tissue (Figure 2.1). The surrounding subcutaneous fatty connective tissue gives the breast its shape and size (Feng *et al.*, 2018). Epithelial cells line the lobules where colostrum (milk) is manufactured and stored; lobules connect to ducts that lead to the nipple (Figure 2.1) through which milk is passed during the lactation process (Colleluori *et al.*, 2021). The major and minor pectoralis (Figure 2.1) are the thick and thin fan-shaped muscles under the breast (Bistoni and Farhadi, 2015). Physical growth, sexual maturation, and hormonal changes during thelarche, menstruation, pregnancy, lactation, and menopause affect the growth of the mammary glands. During pregnancy, hormones like estrogens, progesterone, and prolactin mediate the completion of its development, namely lobuloalveolar maturation during lactation (Feng *et al.*, 2018). The breast also plays a role in lymphatic drainage where the axillary lymph nodes receive approximately 75% of the lymph flowing through the Sappey's plexus from the breast (Colleluori *et al.*, 2021). The lymphatic drainage of the breast is linked to cancer, since cancer cells can metastasise to other organs via the lymphatic system (Colleluori *et al.*, 2021).

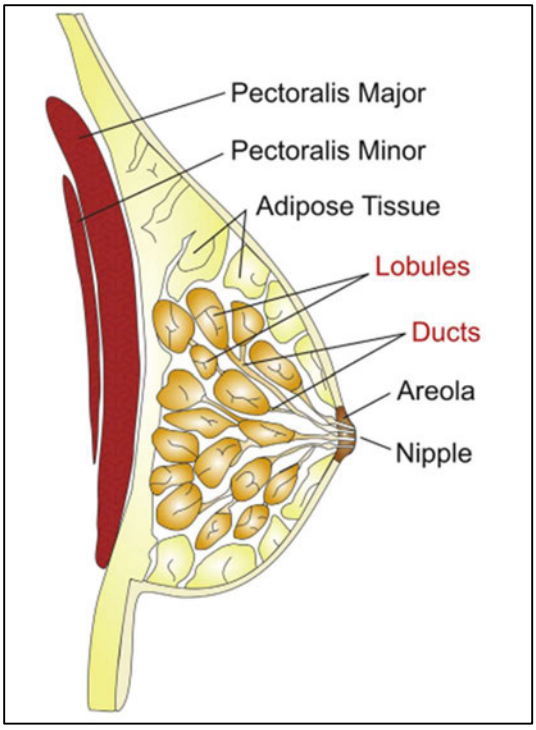

Figure 2.1: The anatomy of the breast (Feng *et al.*, 2018). The structural anatomy of the breast consists of adipose tissue supported by lobules and ducts that converge at the nipple.

2.1.2 Types of breast cancer

Different types of breast cancer are based on pathology, invasiveness, and prevalence. Carcinomas frequently occur, while sarcomas like phyllodes tumours and angiosarcomas rarely manifest (Feng *et al.*, 2018). Carcinomas arise from epithelial cells, while sarcomas arise from connective tissues of the breast that are a part of the musculoskeletal system (Feng *et al.*, 2018). Ductal carcinoma *in situ* is considered a pre-invasive type that develops within normal ducts; it depends on early prognosis and treatment to prevent invasiveness (Feng *et al.*, 2018). The most common type of BC is Invasive Ductal Carcinoma (IDC), which makes up 80% of all cases and is further divided into other carcinoma subtypes such as tubular, medullary, mucinous, papillary, and cribriform carcinoma of the breast (Feng *et al.*, 2018; Bistoni and Farhadi, 2015). The second most common type is Invasive Lobular Carcinoma (ILC), which accounts for 10-15% of BC cases and is more frequent in older women from 50- 60 years. Lobular carcinomas have a distinctive growth pattern where single cells are arranged individually (Feng *et al.*, 2018). Stage IV cancer is an aggressive metastatic type located in the lymph nodes and capable of invading other organs rapidly. Surgical resection of the tumour does not eliminate the spread risk via micro-metastases, allowing BC recurrence. Less common types of BC account for 1-5% of cancer cases, including Inflammatory breast cancers (IBC), BC in men and children and adolescents, Paget breast disease, Papillary carcinoma, Phyllodes tumours, and Angiosarcoma of the breast (Feng *et al.*, 2018).

2.1.3 Molecular or intrinsic subtypes of breast cancer

Breast cancer is known to be heterogeneous and phenotypically diverse, with genetic studies revealing subtypes that have varied prognoses with subtype-specific therapeutic targets within the cancer cell (Feng *et al.*, 2018). Luminal A breast cancer makes up 40% of all BCs and is characterised as being estrogen receptor (ER) and progesterone-receptor (PR) positive while lacking human epidermal growth factor receptor 2 (HER2). Luminal B breast cancer accounts for <20% of all BCs that are characterised by tumours that are ER positive, PR negative and HER2 positive (Feng *et al.*, 2018). The most aggressive subtype is triple-negative/basal-like breast cancer (TNBC), which accounts for 20% of all BCs and is characterised by the lack of all three hormone receptors (Malik *et al.*, 2022). African American Women who present with the breast cancer gene 1 (BRCA1) gene mutation are commonly associated with TNBC (Feng *et al.*, 2018). Evaluation of TNBC tumours revealed an array of abnormally expressed genes related to cell cycle and DNA repair within the basal-like 1 (BL1) category; for example, deletion of the BRAC2 tumour suppressor gene was frequently observed amongst patients (Yin *et al.*, 2020). Its aggressiveness is associated with high metastatic potential, tendency to relapse, and poor prognosis.

Estrogen receptors function by binding to ligands to induce the formation of a homo/heterodimer that regulates the transcription of target genes by activation or suppression (Colleluori *et al.*, 2021; Feng *et al.*, 2018). Target genes such as BRCA1 function as tumour suppressors by preventing the expression of ERα under normal conditions; therefore, they can be subjected to mutations (Feng *et al.*, 2018). ERα may also promote BC growth via its interaction with cyclin D1 and controls the activation of cyclin-dependent kinases (CDKs) 4 and 6, which allows the cell cycle to transition from G1 to the S phase unchecked (Feng *et al.*, 2018). A study by Milne *et al*. (2017) showed that ER-negative breast cancer was associated with an increased risk for BRCA1 gene mutation carriers (Milne *et al.*, 2017). Human epidermal growth factor receptors (HER2) are a family of tyrosine kinase receptors found on cell membranes that are expressed in normal tissues and cancer cells. They play a crucial role in ligand binding, followed by dimerisation, resulting in phosphorylation and the activation of various downstream signalling pathways that promote proliferation, like the mitogen-activated protein kinase (MAPK) and the phosphatidylinositol 4,5-bisphosphate 3-kinase (PI3K) pathways (Feng *et al.*, 2018). Breast cancer with amplified HER2 signalling is associated with the overexpression of HER2 protein that is linked to further tumourigenic activity and an increased likelihood progress to metastasis (Feng *et al.*, 2018).

2.1.4 Estrogen-positive and estrogen-negative BC patterns of growth

Estrogen receptor alpha (ERα) can be associated with estrogen-positive (ER+) BC, whereby the receptor protein mediates the upregulation of cell proliferation by stimulating adaptive proteins, tyrosine kinase (SRC) and PI3K (Miziak *et al.*, 2023). These proteins activate effector molecules like Src homology 2 domain-containing (SHC) transforming protein 1, serine/threonine kinase (AKT) and the extracellular signal-regulated kinase/mitogen-activated protein kinase (Erk/MAPK) signalling cascade. This stimulates the transcription of growth factors like epidermal growth factor receptor (EGFR), thereby increasing cell proliferation, migration, drug resistance or apoptotic inhibition (Miziak *et al.*, 2023). Estrogen receptor -β (ERβ) opposes the actions of ERα, but the metabolic effect is unclear; some studies reveal a regulatory pathway that decreases the migration of cancer cells (Miziak *et al.*, 2023; Feng *et al.*, 2018).

2.1.5 Breast cancer incidence and mortality

According to the WHO, BC is the leading cause of death amongst women globally (World Health Organisation, 2021). In incidence and mortality compared to all cancers (Figure 2.2), BC is ranked 2nd and 5^{th,} respectively (Arnold *et al.*, 2022; World Health Organisation, 2021). Breast cancer accounted for approximately 2.3 million new cases with an 11.7% incidence rate and 685000 deaths with a 6.9% mortality rate (World Health Organisation, 2021). Globally, the incidence rates are higher in more developed countries like the United States, with approximately 252,710 new cases of invasive BC in 2017 (Momenimovahed and Salehiniya, 2019). In South Africa, BC has an age-standardised rate of 49 per 100 000 women and a mortality rate of 16.3 per 100 000 women in 2018 (Jacobs *et al.*, 2022). Incidence rates are greatly dependent on ethnicity, race, and age. According to a study conducted in Southern Asia, women of colour, namely Malay and Indian women, were more susceptible to unfavourable characteristics like ER-positive and hormone receptor-negative tumours with decreased survival rates (Bhoo-Pathy *et al.*, 2012). Asian Pacific Islanders account for 24% of all BC cases and are commonly associated with HER2-positive subtype, while Japanese women are more susceptible to ER-positive tumours (Jacobs *et al.*, 2022). According to Momenimovahed *et al.* (2019), BC is estimated to reach approximately 3.2 million new cases by 2050 (Momenimovahed and Salehiniya, 2019).

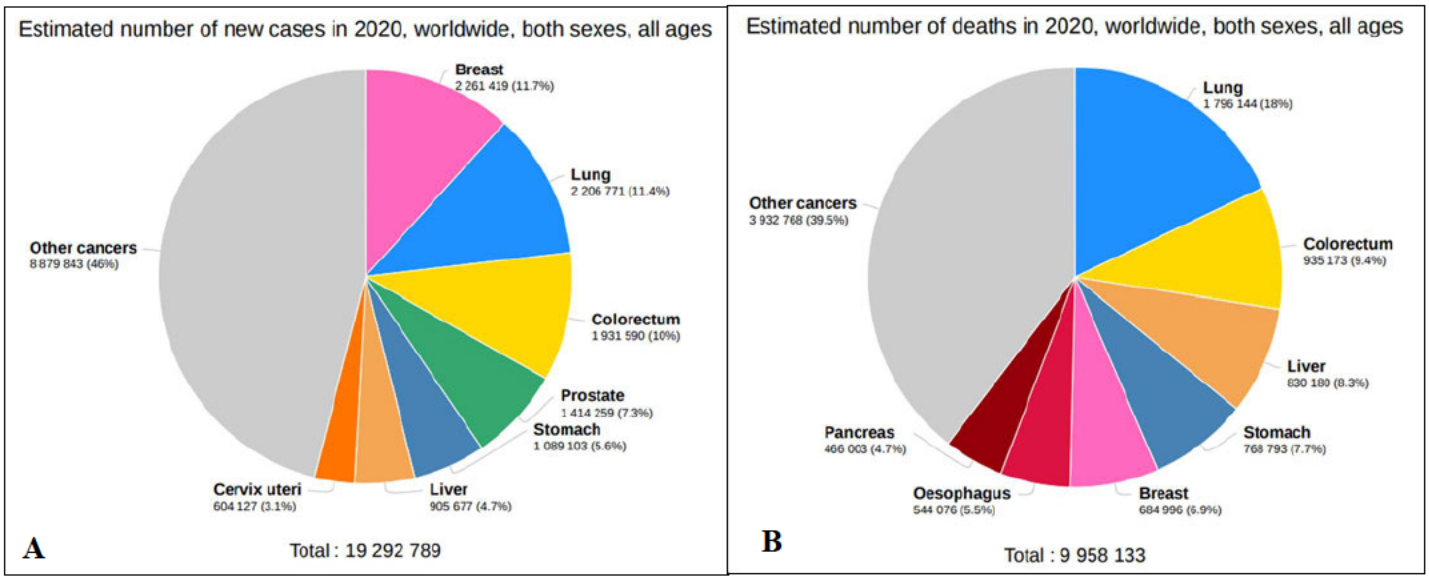

Figure 2.2: Breast cancer incidence and mortality rates in 2020 for both sexes and all ages amongst all cancers (World Health Organisation, 2021)**.** The graphical statistics for comparative analysis of breast cancer and other types of cancers globally with an estimate of 11.7% and 6.9% for BC incidence **(A)** and mortality **(B),** respectively.

2.1.6 Risk factors

Breast cancer is a non-communicable disease and lacks infection-related causes, unlike cancers that are linked to viral infections like human papillomavirus (HPV) infection and cervical cancer. Breast cancer risk factors can be subdivided into two groups, namely, inherent factors and extrinsic factors (Momenimovahed and Salehiniya, 2019). Intrinsic factors include age, sex, race, and genetic inheritance (Figure 2.3), promoting neoplastic disease or benign proliferative mammary gland lesions. There is an increased incidence rate of BC amongst older women within the menopause threshold, and breast tumours observed in younger women seem to be bigger, advanced stages positive lymph nodes and are associated with weaker survival outcomes (Momenimovahed and Salehiniya, 2019). Women are most susceptible to the disease, and it's rarely present in men. Genetic factors with deleterious mutations have an increased risk and account for 40% of BC cases. Mutations occur in the BRCA1 and BRCA2 genes inherited through the dominant autosomal manner (Sun *et al.*, 2017). The second group consists of extrinsic factors, which include lifestyle choices, diet, or long-term medical usage of oral hormonal contraceptives (Figure 2.3) (Feng *et al.*, 2018; Sun *et al.*, 2017). Westernised lifestyles promote excessive alcohol consumption, smoking, and too much dietary fat intake. Alcohol consumption can elevate the level of estrogen-related hormones in the blood and trigger the ER pathways. Cigarette smoke consists

of mutagens that have been found within the breast fluid of non-lactating women. Excessive intake of saturated fats is related to obesity and obstructs efficient BC prognosis. Many birth control methods use hormones, which may increase BC risk. Studies have shown a correlation with medroxyprogesterone acetate with BC (Momenimovahed and Salehiniya, 2019). However, the risk decreases 5-10 years after the discontinuation of contraception pills (Momenimovahed and Salehiniya, 2019).

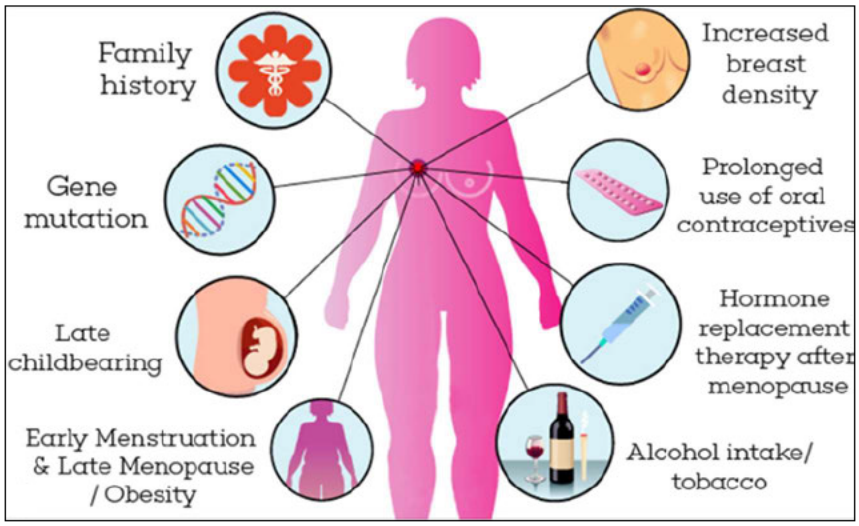

Figure 2.3: Breast cancer risk factors (Feng *et al.*, 2018). Image depicting factors that influence the risk of developing BC, such as genetic inheritance, hormonal imbalances, genetic mutations and alcohol or tobacco abuse.

2.1.7 Breast cancer treatment

Early prevention and prognosis are associated with an above 80% 5-year relative survival rate for breast cancer patients (World Health Organisation, 2021). Studies conducted by Wang *et al.* (2018) revealed that even though hormonal therapy via tamoxifen or aromatase inhibitors is the preferred treatment for estrogen-positive BCs, only 70% of patients respond well to treatment (Wang *et al.*, 2018a). According to Wang *et al.* (2018) tamoxifen, a common ERα inhibitor, showed adverse effects on ERα36, by promoting the progression of disease instead of inhibiting it by the increased transcription of ALDH1A1 gene that can give rise to differentiated cells (Wang *et al.*, 2018a). Hormone receptor-negative and HER2 positive BC can be effectively treated with antibodies like Herceptin or trastuzumab that target the HER2 protein (Swain *et al.*, 2023; Malik *et al.*, 2022). However, these monoclonal antibodies or tyrosine kinase inhibitors (TKIs) are relatively expensive and inaccessible to lower-income countries (Malik *et al.*, 2022). These therapies can be combined with chemotherapy to increase efficacy. For late-stage cancers like TNBC, possible therapeutic drugs for the BL1 subtype include poly (ADP-ribose) polymerase (PARP) inhibitors and genotoxic agents such as cisplatin have shown efficacy (Yin *et al.*, 2020). Radiotherapy has been proven to reduce the recurrence risk for late-stage cancers in combination with

other treatments (World Health Organisation, 2021). Despite the effectiveness of the different cancer therapies, the outcome is dependent the complete course of treatment to achieve a better chance of survival. For this reason, the research is intended to identify an alternative avenue in cancer treatment research that will effectively address the shortfalls of currently available treatment.

2.2 1,4,7,10-TETRAAZACYCLODODECANE TETRAHYDROCHLORIDE

1,4,7,10-Tetraazacyclododecane tetrahydrochloride (Figure 2.4) is a macrocyclic polyamine and divalent metal chelator that is more commonly referred to as cyclen tetrahydrochloride (Tosato *et al.*, 2022; Mcoyi *et al.*, 2020; Lejault *et al.*, 2019). Macrocyclic polyamines are excellent ligands with high binding affinities toward transition-metal ions or other cations (Lejault *et al.*, 2019). According to Sigma-Aldrich the compound is commonly used as a ligand with certain chemicals used in Magnetic resonance imaging (MRI) contrast agents that improve the sensitivity of the images produced (Aldrich, 2020). Cyclen derivatives like lanthanide, zinc and cobalt complexes are synthesised for MRIs, DNA recognition and DNA-cleavage, respectively. The parent compound of cyclen tetrahydrochloride is cyclododecane (Figure 2.4), a naturally occurring compound found in the *Terminalia chebula* tree; however, most cyclododecane derivatives like this compound are synthetic or manufactured by Sigma-Aldrich and other laboratories (Pubchem, 2024; Sultan *et al.*, 2023; Aldrich, 2020). According to Reddy *et al*. (2022), the fruit of the *Terminalia chebula* tree contains phytochemicals like flavonoids, polyphenols, tannins, alkaloids, and terpenoids in the ethanolic extracts of the plant materials (Reddy *et al.*, 2022). These phytoconstituents represent molecules with several bioactivities such as antidiabetic, anti-cancer, anti-inflammatory, antimicrobial and hepatoprotective properties (Reddy *et al.*, 2022). Other constituents harbour anti-cancer properties, like anti-proliferative and apoptotic activity conferred by manganese oxide nanoparticles (MNOs) against MCF-7 BC cells with 86% inhibition of the cells at 320µg/ml concentration (Reddy *et al.*, 2022). Therefore, the cyclen tetrahydrochloride derivative investigated in this study may have promising anti-cancer discoveries to be explored.

Polyamines affect numerous processes in carcinogenesis (Damiani and Wallace, 2018). Some studies show that incredibly high polyamine content can cause apoptosis and consequent ulcerations, while other studies contradict these findings (Golbedaghi *et al.*, 2020; Lejault *et al.*, 2019; Damiani and Wallace, 2018). Polyamines can be associated with normal growth, development, and tissue repair (Damiani and Wallace, 2018). According to Damiani and Wallace (2018), some cancers have been shown to have an upregulated polyamine transport system, and polyamines naturally bind to DNA (Damiani and Wallace,

2018). Therefore, polyamine analogues and polyamine-like structures are being synthesised to target epigenetic regulators, with promising biomedical research results (Damiani and Wallace, 2018).

2.2.1 Description

Cyclen tetrahydrochloride is derived from the organic heteromonocyclic parent compound, cyclododecane, and is characterised as an azacycloalkane with an orthorhombic crystal structure (Figure 2.4). The azacycloalkane aspect means the compound consists of hydrogen and carbon atoms arranged in a structure containing a single ring around the nitrogen's; cyclen tertrahydrochloride consists of ten carbon atoms in which four nitrogen atoms are at corner positions 1, 4, 7 and 10 (Lejault *et al.*, 2019; Pubchem, 2024). It is classified as a polyamine due to its functional groups; polyamines contain two or more nitrogens (Golbedaghi *et al.*, 2020). Aside from its primary structure, the compound is bound with four hydrochlorides (HCl), which is an acid salt (Lejault *et al.*, 2019; Reibenspies and Anderson, 1990). These salts are commonly used in creams with antifungal properties that treat eczema and athletes' feet (Dwiecki *et al.*, 2021).

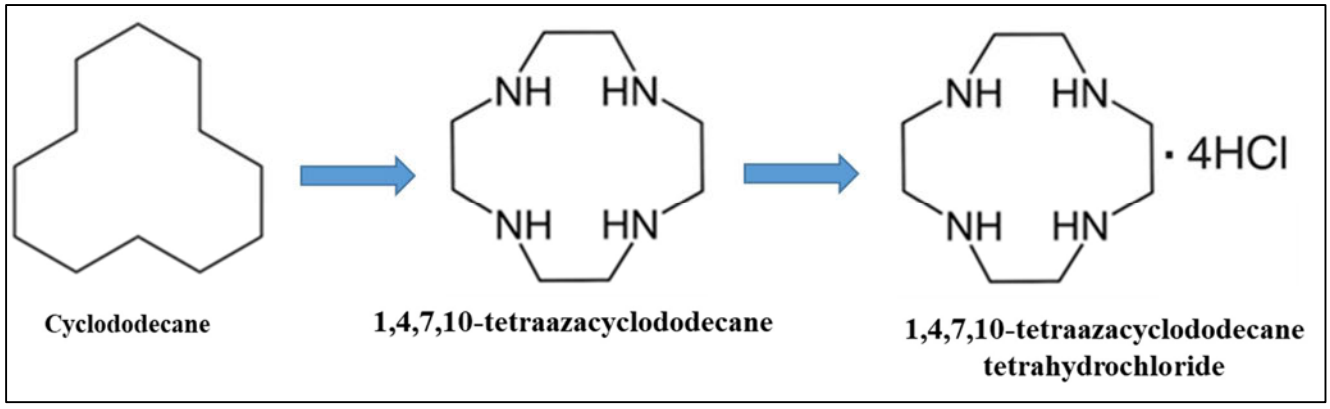

Figure 2.4: Chemical structure of 1,4,7,10-tetraazacyclododecane tetrahydrochloride (Pubchem, 2024) (Modified by Author). Parent compound cyclododecane from which 1,4,7,10-tetraazacyclododecane and 1,4,7,10-tetraazacyclododecane tetrahydrochloride is synthesised, characterised by four nitrogen bonds bound to hydrochloric acid.

2.2.2 Other cyclen derivatives

Recognised derivatives of cyclen include 1,7-dimethyl-1,4,7,10-tetraazacyclododecane (DMC), 1,4,7-Triazacyclononane (TACN) and 1,4,7,10-tetraazacyclododecane-1,4,7,10-tetraacetic acid (DOTA) of which their biochemical effects or properties have been elucidated in previous literature (Tosato *et al.*, 2022; Mcoyi *et al.*, 2020; Yang *et al.*, 2007). According to Yang *et al* (2007), DMC is described as a macrocyclic polyamine that can hydrolyse double-stranded DNA under physiological conditions and harbours anticancer properties (Yang *et al.*, 2007). Cytotoxic investigations by Yang et al (2007) on

HeLa and A459 cancer cells concluded that DMC induced apoptotic cell death in HeLa cells and inhibited growth in both cell lines (Yang *et al.*, 2007). Hiller *et al* (2019), stated in Mcoyi *et al* (2020), describes TACN as a cyclic organic tridentate inhibitor that harbours strong metal-chelating abilities inhibits β-lactamase enzymes and forms metal complexes that catalyse oxidative transformation (Hiller *et al.*, 2019; Mcoyi *et al.*, 2020). Studies conducted by Mcoyi *et al* (2020), concluded that TACN has tolerable cytotoxicity in HepG2 cells and may aid in the treatment of drug-resistant bacterial strains as a potential metallo β-lactamase inhibitor since it does not induce oxidative stress (Mcoyi *et al.*, 2020). 1,4,7,10-tetraazacyclododecane-1,4,7,10-tetraacetic acid (DOTA) is a macrocyclic polyamine that has been widely used for its ability to chelate metal ions, its four nitrogen atoms and four surrounding carboxylic moieties plays a role in attracting ions (Lejault *et al.*, 2019).

2.3 OXIDATIVE STRESS

Redox homeostasis is the naturally occurring balance between oxidants and antioxidants; the imbalance is oxidative stress (Hayes *et al.*, 2020). Reactive oxygen and nitrogen species are produced due to aerobic cell metabolic processes, which damage essential macromolecules, leading to chromosomal abnormalities (Hayes *et al.*, 2020; Liguori *et al.*, 2018). The body becomes susceptible to lethal cardiovascular diseases, liver cancer, diabetes, and neurodegenerative disorders like Alzheimer's disease (Liguori *et al.*, 2018).

2.3.1 Free radicals

Free radicals are defined as species capable of harbouring independent existence. These molecules consist of one or more unpaired electrons in their outer orbital that are highly reactive towards oxygen, specifically creating toxic compounds (Liguori *et al.*, 2018). Reactive oxygen species (ROS) include superoxide ($O_2^{\bullet-}$), singlet oxygen ($^1O_2$), the three-fated hydrogen peroxides (H_2O_2), and the highly reactive hydroxyl radicals ($^{\bullet}OH$) (Figure 2.5, 2.6) (Hayes *et al.*, 2020). The mitochondrial ETC complex I and III generate electrons necessary to initiate ROS production (Figure 2.6); therefore, $O_2^{\bullet-}$ is formed from the uncoupling of oxidative phosphorylation (Liguori *et al.*, 2018). Non-mitochondrial sources of ROS are located intracellularly in the cytoplasm, such as cytochrome p450 (CYP) and nicotinamide adenine dinucleotide phosphate (NADPH) oxidase (Figure 2.5) (Liguori *et al.*, 2018). They can also produce $O_2^{\bullet-}$ by reducing the molecular oxygen by one electron and leaving it in a reactive state with an unpaired electron; the electrons involved in these reactions are obtained from NADPH during cellular respiration (Liguori *et al.*, 2018). More sources of ROS (Figure 2.5, 2.6) include xanthine oxidase,

lipoxygenase, and during respiratory bursts where oxygen can render an infectious species less harmful, or the excess oxygen can lead to ROS production (Liguori *et al.*, 2018).

The superoxide anion is considered the precursor free radical and plays the role of the initiator in the formation of other ROS like H_2O_2 by superoxide dismutase 2 (SOD2) (Figure 2.6) (Liguori *et al.*, 2018). Hydrogen peroxide has three fates in many reactive pathways (Figure 2.6). The reaction of H_2O_2 with transition metals in the Fenton reaction produces $^{\bullet}OH$, which inevitably damages macromolecules by reacting with the phospholipids in cell membranes and proteins (Arfin *et al.*, 2021; Hayes *et al.*, 2020; Liguori *et al.*, 2018). Superoxide is also an endogenous source of reactive nitrogen species (RNS); $O_2^{\bullet-}$ reacts with nitric oxide ($NO^{\bullet}$) to produce peroxynitrite ($ONOO^-$) (Figure 2.5, 2.6). Nitric oxides are formed from L-arginine in a reaction catalysed by nitric oxide synthase 2 (NOS2), inducible NOS, and NAPDH oxidase (Wang *et al.*, 2016).

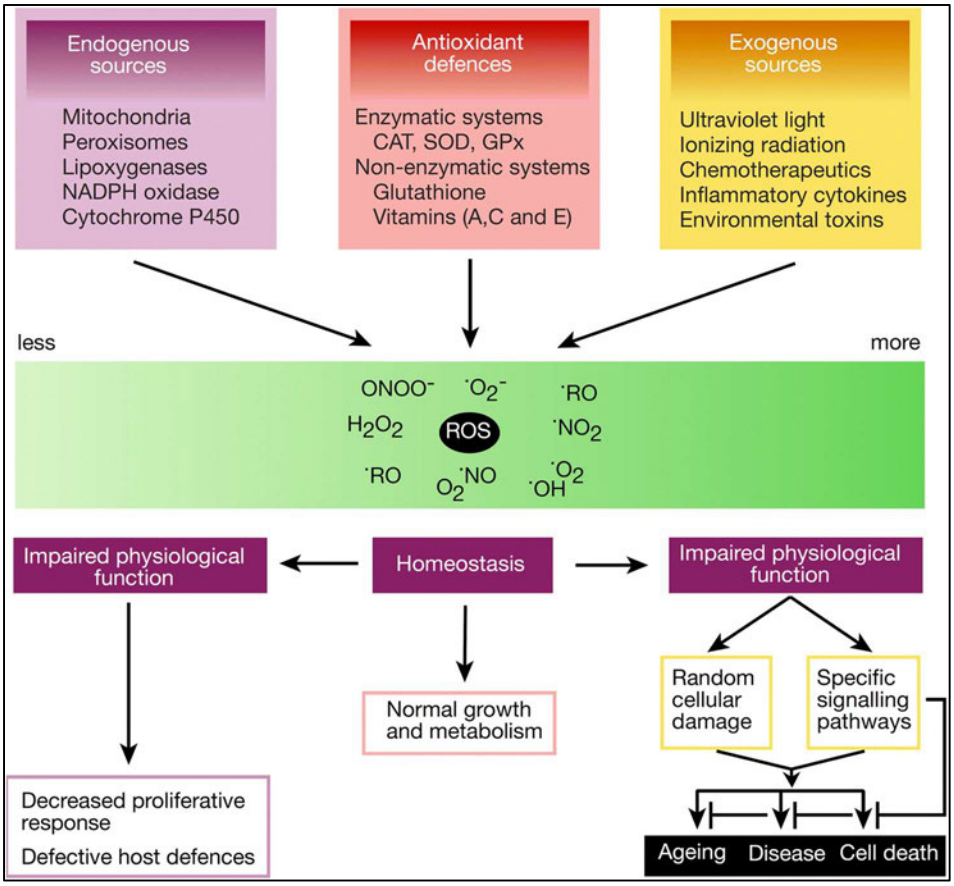

Figure 2.5: Image that includes the endogenous and exogenous sources of ROS, combated with antioxidant defences in normal conditions but promote aging, disease, and cell death under oxidative stress (Finkel and Holbrook, 2000).

2.3.2 Antioxidant response

Cancer cells can thrive and evolve under increased ROS concentrations. Normal cells depend on signalling its endogenous antioxidants pathway, including SOD, reduced glutathione (GSH), glutathione peroxidase (Gpx), and catalase, and nuclear factor-erythroid 2-related factor 2 (Nrf2) (Hayes *et al.*, 2020). As mentioned, the $O_2^{\bullet-}$ is dismutated by SOD to H_2O_2, which stimulates cellular protective defences where catalase detoxifies the H_2O_2 into water and oxygen (Figure 2.6). The alternative fate is mediated by Gpx and GSH that will continue to neutralise ROS to water; GSH is oxidised to glutathione disulfide (GSSG), and its replenishment is NADPH dependent (Figure 2.6) (Arfin *et al.*, 2021; Hayes *et al.*, 2020). The Nrf2 is tightly regulated by Keap1, which keeps it inactive and needs to be phosphorylated and translocated to mediate a defence response (Prasad and Srivastava, 2020). The translocation of Nrf2 results in the production of antioxidant response element genes (AREs), including SOD, GSH, and catalase (Prasad and Srivastava, 2020). Usually, when endogenous Nrf2 is activated, it regulates the expression of these antioxidant genes to scavenge free radicals and has claims to prevent carcinogenesis (Cervello *et al.*, 2020).

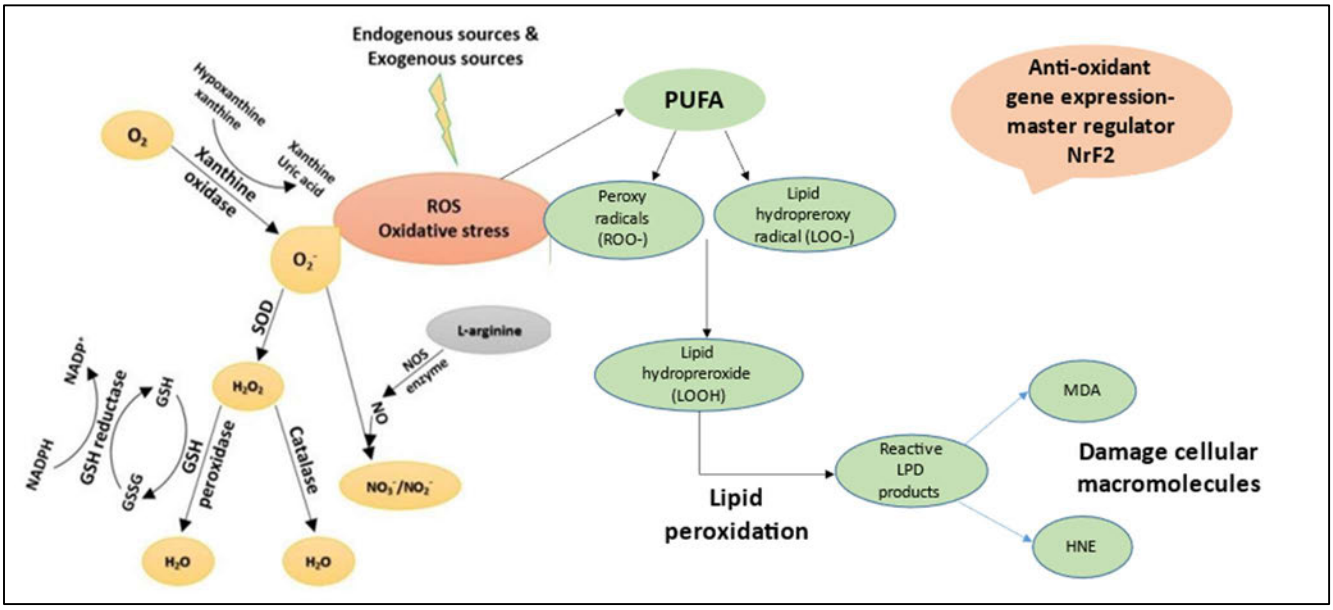

Figure 2.6: The interrelationship between oxidants and antioxidants (Prepared by author, 2024). The neutralisation reactions needed to overcome ROS-induced oxidative stress to prevent macromolecular damage, such as lipid peroxidation, facilitated by antioxidants, namely, SOD, catalase, Gpx, and GSH.

2.3.3 Effects of oxidative stress on cellular macromolecules

When antioxidants cannot overcome endogenous and exogenous ROS overproduction, extensive cytotoxic damage to cellular components such as DNA, protein and lipids can occur (Hayes *et al.*, 2020).

Oxidative damage to DNA tends to target the guanine residues, primarily forming 8-oxo-7,8-dihydro-guanine (8-oxoGuo). Under normal conditions, guanine pairs with cysteine; therefore, 8-oxoGuo and 8-oxo-7,8-dihydro-2′deoxyguanosine (8-oxodG) lesions are the most frequent base damage. However, under oxidative stress conditions, there is a mispairing with adenine, thereby inducing mutations that may facilitate the onset of cancer if appropriate repair systems are not initiated (Rose Li *et al.,* 2020, cited in (Hayes *et al.*, 2020; Liguori *et al.*, 2018). The base excision repair (BER) pathway is responsible for executing repair to damaged DNA bases (Wang *et al.*, 2018b). 8-Oxoguanine DNA glycosylase1 (OGG1) carries out BER by recruiting chromatin remodelers, modifiers and modulates gene transcription (Wang *et al.*, 2018b). Specifically, OGG1 removes 8-oxoG as well as its open-ring product 2,6-diamino-4-hydroxy-5-formamidopyrimidine thereby inducing an allosteric transition of G-quadruplex structure and triggers transcriptional activation of genes associated with inflammation (Wang *et al.*, 2018b).

The ˙OH targets proteins, forming protein carbonyls via the oxidation of the amino acids, mainly methionine and cysteine. If they develop a disulfide bridge, the damage is repairable, but if the sulfur is further oxidised, an irreversible sulfonic acid compound is formed (Liguori *et al.*, 2018; Barreiro, 2016). The reactions between RNS and tyrosine residuals within polypeptide sequences produce nitrotyrosine (Liguori *et al.*, 2018). Nitrotyrosine can be measured and indicates nitrosative stress (Liguori *et al.*, 2018). Low-density lipoproteins undergo oxidation that affects proteins and lipids, causing cholesterol accumulation. Lipids undergo a process of lipid peroxidation that targets the poly-unsaturated fatty acids, mainly linoleic and arachidonic acids (De Leon and Borges, 2020). During initiation, the ˙OH abstracts allylic hydrogen, forming a lipid radical that reacts with oxygen in the propagation phase, producing lipid peroxyl radicals and lipid hydroperoxide. The termination products of lipid peroxidation (Figure 2.6) are trans-4-hydroxy-2-nonenal (4-HNE), malondialdehyde (MDA), and isoprostanes (F2-IsoPs) (Kaur *et al.*, 2019; Liguori *et al.*, 2018).

2.4 APOPTOSIS

Cell death or apoptosis is a programmed strategy that the body uses to remove unwanted or damaged cells that cannot be repaired, and its regulation is critical to homeostasis (Krasovec *et al.*, 2022). It is also recognised as a mechanism to prevent cancer, and evasion of apoptosis by various mechanisms is a hallmark of cancer (Pfeffer and Singh, 2018; Hanahan and Weinberg, 2011). Two main pathways are associated with apoptosis: extrinsic and intrinsic. The loss of apoptotic control is related to disturbances

in either or both of these pathways. It allows for prolonged survival, resulting in highly mutagenic and invasive cancer cell proliferation (Pfeffer and Singh, 2018).

2.4.1 The extrinsic pathway

On the cell surface, ligands from the TNF family, such as Fas/Apo1 (Figure 2.7) and TNF-related apoptosis-inducing ligand (TRAIL) (Figure 2.8), bind with associated death receptors and undergo trimerisation to recruit Fas-associated death domain protein (FADD) or TNF receptor-associated death domain (TRADD). Pro-apoptotic pathways are triggered with the recruitment of FADD, while TRADD induces anti-apoptotic signals (Pfeffer and Singh, 2018; Koff *et al.*, 2015). These death domains dimerise with adapter proteins to amplify the apoptotic signal. This includes the death effector domain (DED) proteins that attract pro-caspase-8 and -10 and promote the formation of the death-inducing signalling complex (DISC) (Figure 2.7) (Koff *et al.*, 2015). Anti-apoptotic protein TRADD facilitates the formation of complex I with receptor-interacting protein kinase 1 (RIPK1), TNF receptor-associated factor-2 (TRAF2), TRAF5 and the inhibitor of apoptosis protein-1 and -2 (cIAP1/2) (Figure 2.8). Complex I promotes the expression of pro-survival signals mediated by nuclear factor kappa B (NF-κB) and members of the mitogen-activated protein kinase (MAPK) pathway, including Jun N-terminal kinase (JNK) and p38 (Koff *et al.*, 2015). Suppose the path is interrupted by the deubiquitination of RIPK1 by the enzyme cylindromatosis (CYLD), complex II forms with RIPK1, TRADD, FADD and caspases-8 and -10 (Figure 2.8) (Mezzatesta and Bornhauser, 2019). Active caspase-8 and -10 emerge after the cleavage of pro-caspase 8 in the DISC, which may activate the executioner caspases and the intrinsic apoptotic pathway (Pfeffer and Singh, 2018).

2.4.2 The intrinsic pathway

The intrinsic pathway is stimulated by internal cytotoxicity, DNA damage, cell damage, growth factor deprivation, surplus Ca^{2+}, and oncogenes' overexpression (Pfeffer and Singh, 2018). This pathway is usually regulated by B-cell lymphoma 2 (Bcl-2) proteins and tumour suppressor gene p53. When the intrinsic pathways are stimulated, it activates BH3-only Bcl-2 proteins that trigger Bcl-2-associated X protein (BAX) and Bcl-2 homologues antagonist/killer (BAK) activity; BAX and BAK are inhibited by binding to anti-apoptotic Bcl-2 and Bcl_{XL} (Figure 2.7) (Jan, 2019; Pfeffer and Singh, 2018). Upon migration to the mitochondria, BAK and BAX homodimerise, which exposes cryptic dimer-dimer binding sites located on the surface of the mitochondria, resulting in increased outer membrane permeabilisation (MOMP) (Pfeffer and Singh, 2018; Koff *et al.*, 2015). The opened membrane pores

allow for the intermembrane proteins to be released, such as cytochrome c, the second mitochondria-derived activator of caspase (SMAC) and Omi, amongst others (Figure 2.7) (Pfeffer and Singh, 2018). The release of these proteins triggers the apoptosome formation when cytochrome c binds the caspase adaptor molecule apoptotic protease activating factor-1 (Apaf-1) and ATP (Figure 2.7), stimulating oligomerisation of Apaf-1 to expose its caspase activation and recruitment domains (CARDs). The apoptosome is consequently formed when Apaf-1 CARD domains bind to pro-caspase-9, resulting in its cleavage and activation (Figure 2.7). Caspase 9 then activates executioner caspases-3/-7 to enact cell death (Mhlanga *et al.*, 2019; Pfeffer and Singh, 2018).

2.4.3 Execution of apoptosis

The execution phase of apoptosis is triggered by the cleavage of caspase 3, which cleaves the DNase inhibitor and proteins of the cytoskeleton, facilitating the process of cellular fragmentation (Pfeffer and Singh, 2018). Caspase 3 activates the endonuclease caspase-activated DNase (CAD), which results in chromatin condensation by degrading chromosomal DNA within the nuclei (Jan, 2019). Caspase-3 also causes cytoskeletal reorganisation and disintegration of the cell into apoptotic bodies called blebs (Koff *et al.*, 2015). Later-stage damage to the cell causes the phosphatidylserine to become externalised on apoptotic cells (Jan, 2019; Pfeffer and Singh, 2018). This facilitates non-inflammatory phagocytic recognition. The final event of apoptosis is the phagocytosis of the apoptotic bodies by phagocytic cells (Jan, 2019).

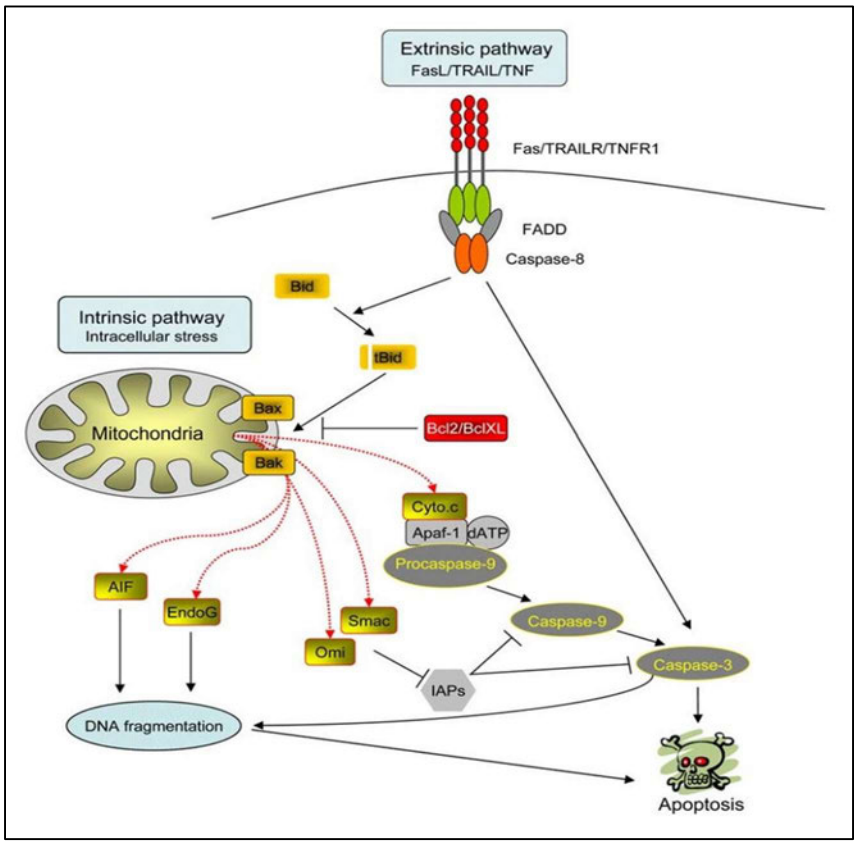

Figure 2.7: The execution of apoptosis carried out by the extrinsic and intrinsic pathways (Gonzalvez, 2008). The intercalated relationship between the extrinsic and intrinsic pathways involving the caspase 3/7, 8, 9 and Bcl-2 related proteins used to carry out programmed cell death.

2.5 NECROPTOSIS

Necroptosis is a form of programmed necrosis that is regulated by RIPK1, RIPK3, and Mixed Lineage Kinase Domain Like (MLKL). Upon activation, RIPK1 and RIPK3 bind to each other to form a necrosome and promote RIPK3 autophosphorylation and subsequent activation, allowing RIPK3 to recruit and phosphorylate MLKL (Figure 2.8). This results in oligomerisation of MLKL, membrane insertion of MLKL oligomers, which disrupts the plasma membrane integrity and carries through necroptotic death (Kim *et al.*, 2019). Therefore, RIPK1, RIPK3 and MLKL are specific markers of necroptotic death (Berghe *et al.*, 2010). RIPK1, RIPK3, and MLKL activation in necroptosis can be detected by changes in their phosphorylation status or membrane accumulation. This triggers the innate immune system with an inflammatory response by rupturing dead cells and releasing intracellular components such as lactate dehydrogenase (LDH), that initiates the recruitment of extracellular damage-associated molecular patterns (DAMPs) and cytokines that affect neighboring cells (Kim *et al.*, 2019; Berghe *et al.*, 2010).

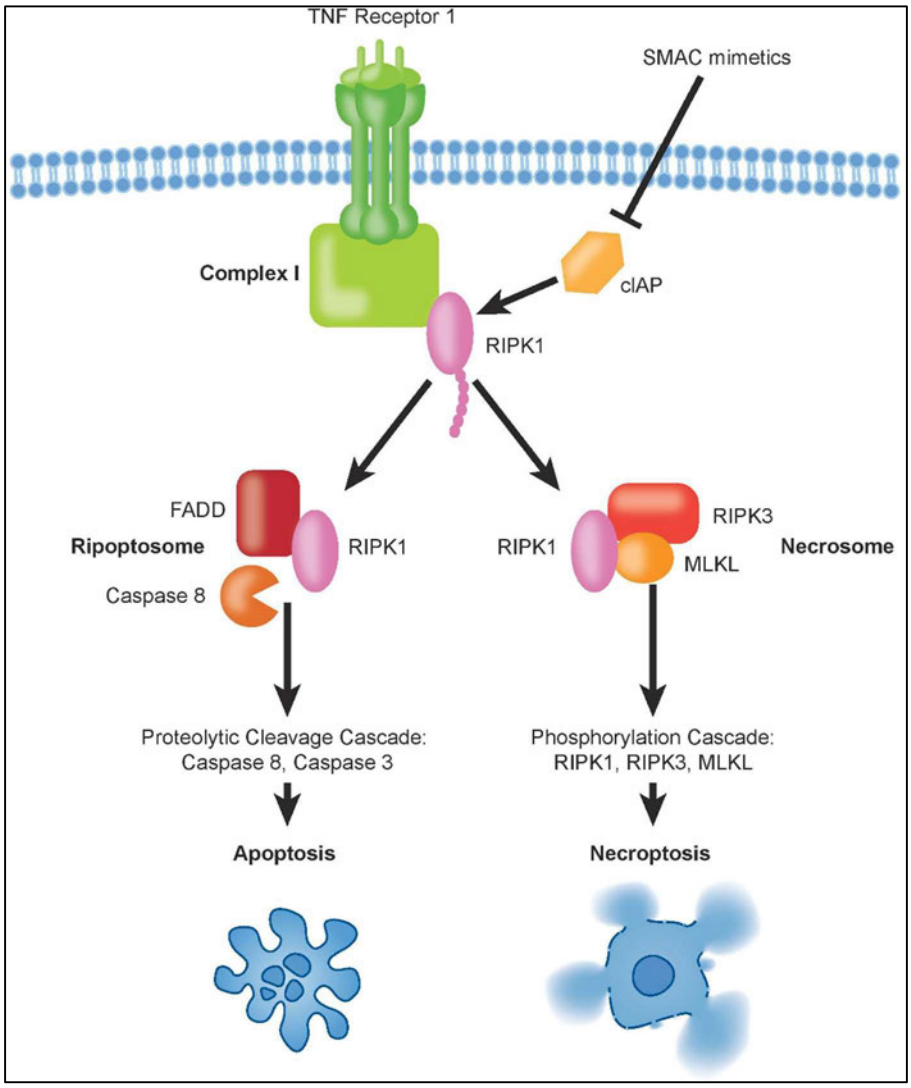

Figure 2.8: The necroptotic pathway (Mezzatesta and Bornhauser, 2019). The schematic comparison of a cell undergoing apoptosis and necroptosis depending on the recruitment and availability of certain proteins. Under necroptosis complex I allows for the formation of a necrosome in the absence of caspase 8, whereas apoptosis relies on caspase 8 for its execution.

CHAPTER 3: METHODOLOGY

3.1 MATERIALS

Cyclen tetrahydrochloride (1,4,7,10-Tetraazacyclododecanetetrahydrochloride) was procured from Sigma Aldrich (St. Louis, Missouri, USA), and the MCF-7 and MDA-MB-231 cells were obtained from Cellonex (Johannesburg, South Africa (SA)). Cell culture reagents [Eagles Minimum Essential Medium (EMEM), L-glutamine, penstrep-fungizone] were procured from Whitehead Scientific, Cape Town, SA). Tissue culture plates, test tubes, micro-centrifuge tubes, 75cm² flasks and luminometer plates were purchased from Lasec SA (Pty) Ltd. Foetal bovine serum and Pierce™ protease/phosphatase inhibitor was acquired from Thermofisher Scientific (Johannesburg, SA), methylthiazol tetrazolium (MTT) salt and phosphate-buffered saline (PBS) from Sigma (St. Louis, Missouri, USA), and dimethylsulfoxide (DMSO) and β-actin (#A3854) from Merck (Johannesburg, SA). Cytobuster™ protein extraction reagent, bicinchoninic acid (BCA), thiobarbituric acid (TBA), malondialdehyde (MDA), butylated hydroxytoluene (BHT), copper sulphate, sodium nitrate, vandium (III) chloride (VCl_3), sulfanilamide, N-1-Naphthyl ethylenediamine dihydrochloride (NEDD) and JC-10 were purchased from Sigma (St. Louis, Missouri, USA). Western blot reagents were procured from Bio-Rad (Hercules, California, USA), while Cell Signalling Technology (CST, Danvers, Massachusetts, USA) antibodies and Promega products (Madison, Wisconsin, USA) were obtained from Anatech (Johannesburg, SA). The phosphoric acid (H_3PO_4), ethanol, hydrochloric acid (HCl) and butanol were from Merck (Darmstadt, Germany). Bovine serum albumin (BSA) was obtained from Inqaba Biotech (Johannesburg, SA). Unless stated otherwise, all salts and solvents/acids were purchased from Lasec SA (Pty) Ltd.

3.2 CELL CULTURE

3.2.1 Principle

Biomedical scientists use cell culture as a crucial tool to conduct routine laboratory experiments pertaining to mammalian research. Cancer cell culture stems from human tumours or tissue, whereby a primary culture undergoes many passages or sub-cultures within culture serum media containing additives to promote growth and produce a cell line (Cree, 2011). Aseptic techniques should be strictly followed to maintain a controlled environment supported by incubation with optimal temperature, pH, CO_2, and O_2 levels, and routine media changes to ensure cells reach confluency without contamination (Cree, 2011).

The MCF-7 cell is an adhesive, epithelial luminal cell line, useful for *in vitro* breast cancer studies because it retains specific characteristics of mammary epithelium. These include the ability of MCF-7 cells to process estrogen in the form of oestradiol via estrogen (ER) receptors and progesterone receptors (PR) in the cell cytoplasm. The MDA-MB-231 cell line is commonly used to mimic late-stage or triple-negative breast cancer. This cell line is ER, PR, and E-cadherin negative and expresses mutated p53 (Momenimovahed and Salehiniya, 2019; Feng *et al.*, 2018).

3.2.2 Procedure

Cell culture was performed under the laminar flow hood using cryopreserved MCF-7 and MDA-MB-231 cell lines provided by the UKZN Medical Biochemistry laboratory. The MCF-7 and MDA-MB-231 cells were cultured in two labelled 75 cm^2 flasks with complete culture medium (CCM) that consisted of 500ml EMEM supplemented with 10% foetal calf serum, 1% L-glutamine, 1% penstrep-fungizone, and was incubated at 37°C in an atmosphere of 5% CO_2 to grow in a monolayer until confluent. The following was conducted for each cell line: At 80-100% confluency, the adherent cells were trypsinised; the contents of the 75 cm^2 flasks were discarded, and under strict aseptic techniques, the cells were rinsed with 10ml PBS three times, then 2 ml trypsin was added for cell detachment. Cells were viewed using an inverted phase-contrast microscope to observe the initial morphological characteristics. Trypsin was then discarded. To deactivate the trypsin and resuspend cells, 2 ml of CCM was added to the 75 cm^2 flasks. The flask was then tapped against the palm, and the resulting cell suspension was counted using the trypan blue method. A cell counting solution was prepared by adding 150 µl of CCM, 50 µl of cell suspension and 50 µl of trypan blue dye into a micro-centrifuge tube. The cell counting solution was vortexed, and 10 µl was transferred to a haemacytometer counting grid. Cells were counted using the inverted phase-contrast microscope, and the cell number was calculated:

$$\frac{Number\ of\ cells}{5}\ x\ 5\ x\ 10^4$$

As required, a calculated mixture of CCM and the cell suspension was prepared for subculturing.

3.3 PREPARATION OF THE TREATMENT

The cyclen tetrahydrochloride compound was purchased in a powdered form. Treatment stock solution was then prepared (3143.57 µM) by dissolving 5 mg of cyclen tetrahydrochloride powder in 5 ml of CCM. The required treatment concentrations were then prepared from the stock solution. Treatment stock

was prepared freshly when required for investigative assays due to unpredictable compound alterations when stored for long periods.

3.4 THE 3-(4,5-DIMETHYLTHIAZOL-2-YL)-2-5-DIPHENYLTETRAZOLIUM BROMIDE (MTT) ASSAY

3.4.1 Principle

The 3-(4,5-dimethylthiazol-2-yl)-2-5-diphenyltetrazolium bromide (MTT) assay is a colourimetric assay used to determine the percentage of viable cells by detecting the presence of metabolic activity within living cells of mammals, fungi, and bacteria (Grela *et al.*, 2018). Cell cytotoxicity can be associated with this assay since certain chemical compounds, such as drugs and synthetic compounds, can induce cell death, thereby inflicting a change measured by percentage cell viability. The principle of this assay depends on NAD-dependent reduction enzymes such as succinate dehydrogenase located in the mitochondria of viable cells to reduce yellow MTT salt to a purple formazan crystal by-product (Figure 3.1) (Dhanalakshmi and AnandaThangadurai, 2020). An intensified purple colour represents a greater proportion of viable cells.

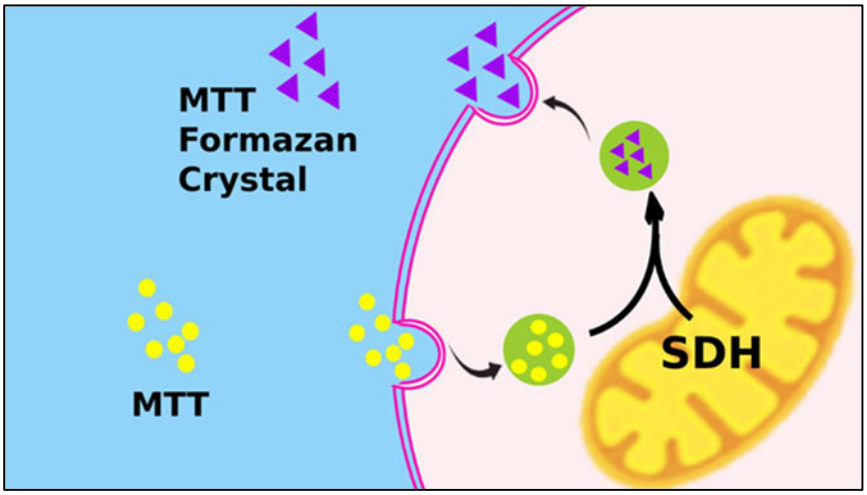

Figure 3.1: Reduction of the yellow MTT salt to purple formazan by-product in the presence of succinate dehydrogenase (https://tribioscience.com/wp-content/uploads/2021/06/MTT.png).

3.4.2 Procedure

Since certain chemical compounds, such as synthetic drugs, can induce cytotoxicity, the MTT assay was used to determine cell viability following exposure to cyclen tetrahydrochloride treatment concentrations. Confluent MCF-7 and MDA-MB-231 cell line flasks were trypsinised in preparation for the MTT assay. The resuspended cells were counted and plated for each cell line in a 96-well microtiter plate (20000 cells/well in 200 µl CCM) in triplicate per treatment. After allowing the cells to adhere

overnight, the CCM was discarded, and the cells were treated with 0-1000 µM cyclen tetrahydrochloride dilutions for 48 hours. The treatment supernatant in the 96 plate wells was removed, then 100µl fresh CCM and 20 µl of yellow MTT salt (5 mg/ml in 0.1 M PBS) were added to each well and incubated for 4 hours in 5% CO_2 atmosphere at 37°C. The MTT solution was discarded, and 100 µl of DMSO was added to each well, which can dissolve the purple formazan crystals. The absorbance values were obtained at 570 nm with a reference wavelength of 690 nm using the SPECTROstar Nano (BMG Labtech, Ortenberg, Germany) spectrophotometer. The absorbance values were used to calculate cell viability relative to the untreated control [% cell viability = $\frac{\text{Absorbance sample}}{\text{Absorbance control}}$*100] and were analysed using Graph Pad v5.1 software (GraphPad Software Inc., La Jolla, CA, USA). A non-linear regression analysis was used to derive a half-maximum inhibitory concentration (IC_{50}) of 168.4 µM for MCF-7 cells; the concentration producing 20% cell death or IC_{20} of 41.69 µM was extrapolated from the dose-response curve. The MDA-MB-231 cell line IC values were as follows: IC_{50}, 561 µM and IC_{20}, 302.9 µM. The IC_{20} and IC_{50} concentrations were used for subsequent assays.

3.5 SAMPLE PREPARATION

Confluent cells (80%) in a 75 cm^2 flask were treated with IC_{20} and IC_{50} concentrations of cyclen tetrahydrochloride for 48 hours. Cells treated with CCM only served as the control. Cells were then washed with 0.1 M PBS, trypsinised and suspended before counting, and volumes were adjusted for luminometric assays, western blotting, and qPCR. To perform a non-waste investigation, the treatment medium was preserved, stored at -20ºC and used for the LDH, TBARS and NOS assays.

3.6 LACTATE DEHYDROGENASE (LDH) ASSAY

3.6.1 Principle

When there is an interruption of a cell's metabolic function, it causes cellular damage that affects the integrity of the cell membrane. A weakened plasma membrane allows enzymes like LDH to leak from the cytoplasm into the extracellular matrix or the cell culture medium (Parhamifar *et al.*, 2013). The LDH assay detects cellular membrane damage and can verify cellular cytotoxicity by quantifying the released LDH in two serial enzymatic reaction steps (Figure 3.2). In the first step, LDH catalyses conversion of lactate to pyruvate and results in NAD being reduced to $NADH/H^+$, then a catalyst (diaphorase) transfers H/H^+ from $NADH/H^+$ to the tetrazolium salt 2-(4-iodophenyl)-3-(4-nitrophenyl)-5-phenyltetrazolium chloride (INT) in a second step, causing it to be reduced to purple formazan (Aslantürk, 2018). The

amount of formazan is quantified at 490 nm and is directly proportional to the number of damaged cells in the sample (Kamiloglu *et al.*, 2020).

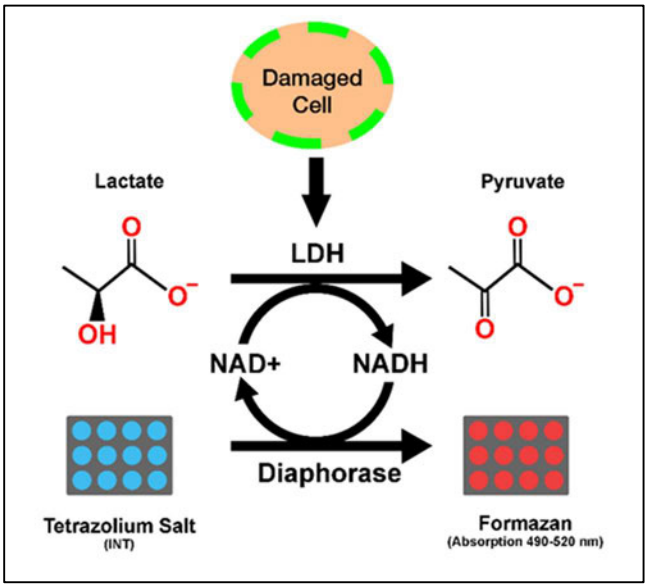

Figure 3.2: The quantification of lactate via conversion to pyruvate by LDH and diaphorase to assess cell damage proportional to colour end-product (Parhamifar *et al.*, 2013).

3.6.2 Procedure

The LDH cytotoxicity detection kit (Roche, Mannheim, Germany) evaluated plasma membrane integrity by quantifying LDH released into the treatment medium. Sample supernatants were retained from treated and untreated flasks of MCF-7 and MDA-MD-231 cells, after which 50 µl was transferred into a 96-well plate in triplicate according to treatment concentration (control CCM only, IC_{50}, IC_{20}). A working solution that consisted of substrate (diaphorase/NAD^+) and dye solution (INT/sodium lactate) was prepared according to the manufacturer's specifications. After that, 25 µl of the working solution was added to each well. The plate was then incubated for 30 minutes at room temperature (RT). Following incubation, 12.5 µl of stop solution was added to each well, and absorbance was read at 490 nm with a reference wavelength of 600 nm using a spectrophotometer (BMG Labtech, Ortenberg, Germany). Results were presented as mean optical density (OD).

3.7 THIOBARBITURIC ACID REACTIVE SUBSTANCES (TBARS) ASSAY

3.7.1 Principle

The TBARS assay detects and measures the amount of oxidative stress within the cells of interest when exposed to treatments. It specifically quantifies the by-product of lipid peroxidation, malondialdehyde (MDA). The cells sensitivity to antioxidants or oxidants is also detectable with this assay. In the presence

of heat and low pH, thiobarbituric acid (TBA) can react with the MDA present in the sample to form a red end-product that absorbs light at 530-540nm (Figure 3.3) (De Leon and Borges, 2020). Butylated hydroxytoluene (BHT) is added during sample preparation to prevent further reaction peroxidation (Boligon *et al.*, 2014). The reaction requires heat to facilitate peroxide breakdown, and acid induces colour development (De Leon and Borges, 2020; Boligon *et al.*, 2014). The colour development intensifies with the level of lipid peroxidation. Butanol is added for adduct separation and extraction from the sample.

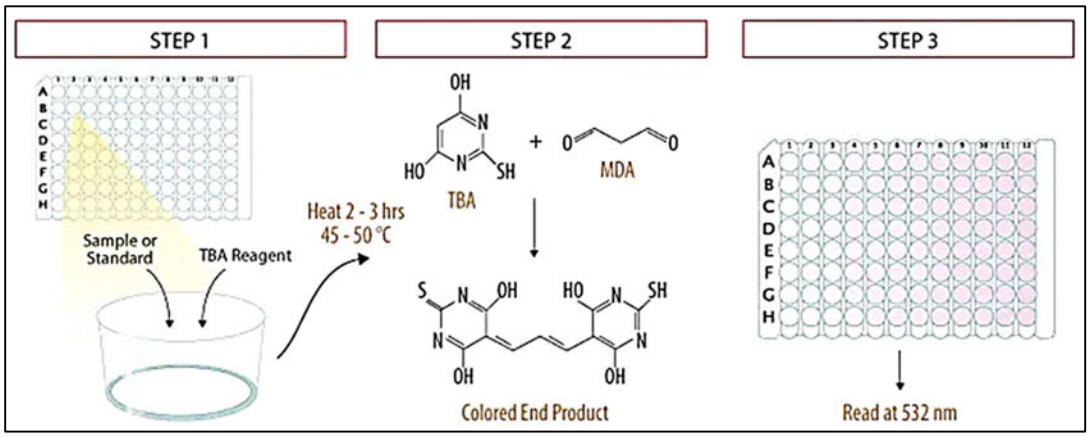

Figure 3.3: The quantification of MDA by reaction with TBA/BHT to measure lipid peroxidation (Boligon *et al.*, 2014).

3.7.2 Procedure

The TBARS assay was used to detect the cell sensitivity to antioxidants or oxidants. Samples were prepared using the collected supernatant from treated MCF-7 and MDA-MB-231 cell lines, a positive control (1 µl MDA in CCM) and a negative control (CCM only). The samples and controls (200 µl) were transferred to clean labelled glass test tubes. Thereafter, 200 µl of 7% H_3PO_4 and 400 µl TBA/ BHT were sequentially added to the test tubes containing treated samples and positive control. 200 µl of 7% H3PO4 and 400 µl of 3 mM HCl were added for the negative control. All tubes were vortexed, and 200 µl of 1 M HCl was added to each test tube. Tubes were vortexed, placed in a water bath at 100ºC for 15 minutes, and then cooled to RT. Under the fume hood, 1500 µl of butanol was added to each test tube and vortexed for 30 seconds each, then samples were allowed to settle to view two distinct phases. The upper butanol phase (500µl) was transferred into a labelled micro-centrifuge tube, and 100 µl of each sample was transferred into a 96-well microtitre plate in triplicate. Absorbance values were obtained at 532 nm with a reference wavelength of 600 nm using a SPECTROstar Nano (BMG Labtech, Ortenberg, Germany)

spectrophotometer. Absorbance values were converted to MDA (µM) using the following equation [MDA concentration = $\frac{\text{Absorbance}}{156\text{mM}^{-1}}$*1000].

3.8 NITRIC OXIDE SYNTHASE (NOS) ASSAY

3.8.1 Principle

Nitrate concentrations are detected and measured by the NOS assay due to the short half-life of nitric oxide (NO); therefore, the increase in concentrations of its degraded by-products, nitrate and nitrite, indicates nitrosative stress (Vishwakarma *et al.*, 2019). Nitric oxide synthase (NOS) catalyses arginine and oxygen reactions to produce NO and release citrulline depending on NAD(P) H-reducing equivalents (Vishwakarma *et al.*, 2019). The principle of the NOS assay (Figure 3.4) relies on the ability of VCl_3 to reduce nitrate to nitrite, which is detected by the two-step Griess reaction that uses sulfanilamide and NEDD to produce an azo dye-coloured end product at 540 nm (Vishwakarma *et al.*, 2019).

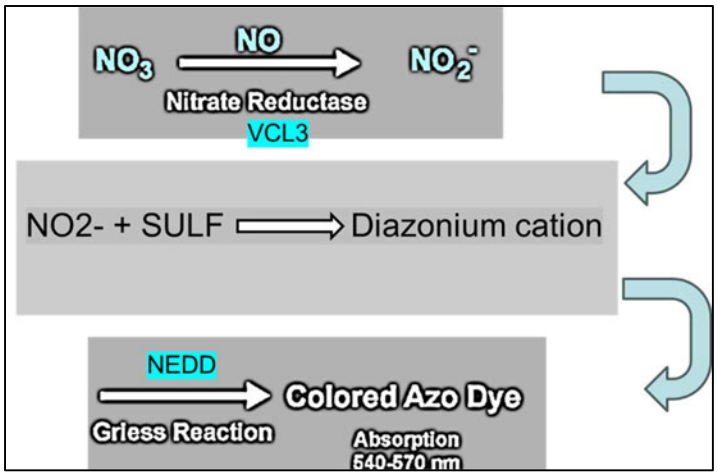

Figure 3.4: The reduction of NO_3^- to NO_2^- catalysed by VCl_3, which further reacts with sulphanilamide and NEDD in the Griess reaction to form an azo dye product (Prepared by author, 2024).

3.8.2 Procedure

The NOS assay was used to detect the effects of cyclen tetrahydrochloride on NO production in MCF-7 and MDA-MB-231 cells. Sodium nitrate standards (0-200 µM) and treatment supernatant were used as samples. The samples (50 µl) were dispensed into a 96-well microtiter plate in triplicate. After that, 50 µl VCl_3, 25 µl of sulfanilimide and 50 µl of NEDD were added to each well. The plate was incubated for 45 minutes at 37°C. Absorbance values were obtained using a spectrophotometer (SPECTROstar Nano,

BMG Labtech, Ortenberg, Germany) at 540 nm with a reference wavelength of 690 nm. A standard curve was drawn, and nitrite/nitrate (µM) concentration was derived from the trendline equation.

3.9 LUMINOMETRY

Confluent MCF-7 and MDA-MB-231 cells were trypsinised, counted, and seeded in triplicate into a white opaque 96-well luminometer microtiter plate capable of blocking unwanted fluorescence (20000 cells/200 µl CCM/well). After overnight incubation, the CCM was removed, and control, IC_{20} and IC_{50} treatments were added for 48 hours at 37ºC. The treatment medium was replaced with 50 µl of PBS, and the respective reagents per assay were added as required. This was repeated for each assay.

3.9.1 Cytochrome P450 3A4 assay

3.9.1.1 Principle

Cytochrome P450 (CYPs) is a family of enzymes containing haem co-factors that oxidise or metabolise steroids, fatty acids, and xenobiotics (Kehinde *et al.*, 2021). Cytochrome P450s play a major role in drug detoxification, and inhibition of CYP-mediated metabolism may lead to the accumulation of toxic drug levels in the plasma (Cali *et al.*, 2009). New drug candidates are routinely tested for their ability to inhibit these enzymes to prevent adverse drug-drug interactions. The cytochrome p450 3A4 (CYP3A4) assay (Figure 3.5) depends on converting inactive D-luciferin derivatives by CYPs to an active form that emits light; the reaction is catalysed by luciferase. The light intensity measured by a luminometer reflects proportionality to CYP activity (Cali *et al.*, 2009).

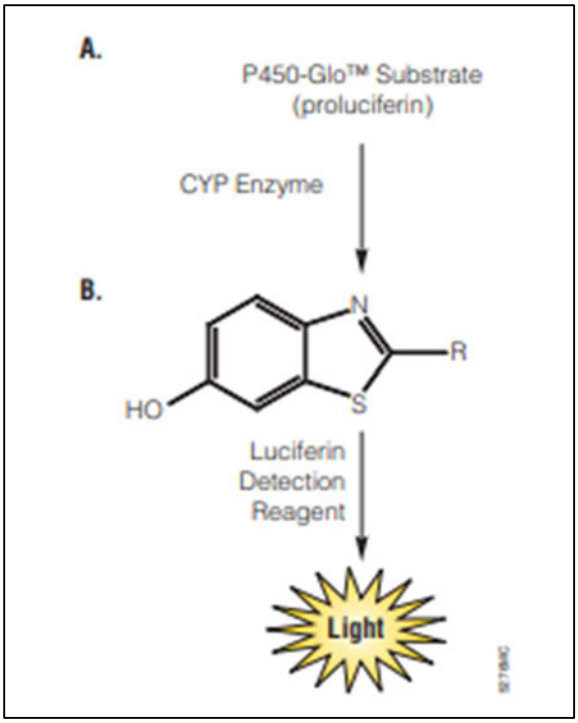

Figure 3.5: Conversion of inactive D-luciferin derivatives to oxyluciferin by CYP3A4 that can produce light (Cali *et al.*, 2006; Promega, 2016).

3.9.1.2 Procedure

The P450-Glo™ assay kit (#G8201) was used to quantify the activity of CYP3A4 (Promega, Madison, USA). The reagents were prepared according to the manufacturer's guidelines, and 25 µl was added to the treated cells in the white 96-well luminometer plate. After incubation at RT for 30 minutes in the dark, the luminescent signal was measured and recorded using the Modulus^{TM} microplate luminometer (Turner Bio-systems, Sunnyvale, California, USA). Data was expressed in relative light units (RLU).

3.9.2 The adenosine triphosphate (ATP) assay

3.9.2.1 Principle

The ATP assay can be performed to verify the findings of the MTT assay. Adenosine triphosphate is a nucleoside triphosphate produced in the mitochondria through oxidative phosphorylation. It is an energy reservoir for metabolically active cells to perform cellular functions (Aslantürk, 2018). When cells perform metabolic activities like biological synthesis, signalling and transport, they take the stored energy from the chemical bonds of ATP to fuel these metabolic reactions, thereby releasing adenosine diphosphate (ADP) and a free phosphate molecule as by-products (Aslantürk, 2018). The ATP assay evaluates cell viability by quantifying the intracellular ATP levels of drug-exposed cells and untreated

controls by luminometric detection. The assay depends on the successful reaction of luciferin to oxyluciferin catalysed by luciferase in the presence of Mg^{2+} ions and ATP (from lysed cells), yielding a luminescent signal (Figure 3.6) (Kamiloglu *et al.*, 2020). A directly proportional relationship can be identified between the luminescent signal intensity and the cells' ATP concentration (Aslantürk, 2018).

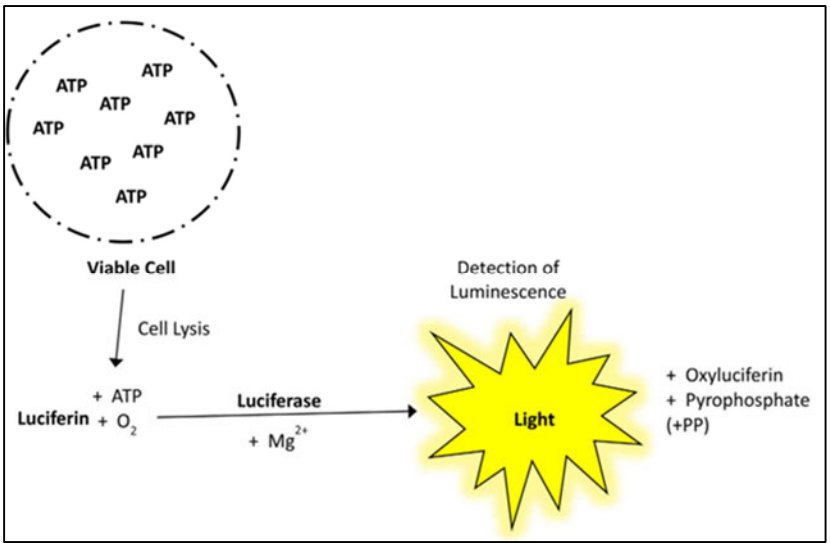

Figure 3.6: Schematic illustration of the principle of the ATP luminometric assay (Kamiloglu *et al.*, 2020).

3.9.2.2 Procedure

The amount of intracellular ATP was measured using the Promega Cell Titre-Glo® kit (#G7570). After preparing the reagent working solution according to the manufacturer's instruction, 25 µl of reagent was added to each treatment well and incubated at RT for 30 minutes in the dark. The ModulusTM microplate luminometer measured the luminescent signal (Turner Bio-systems, Sunnyvale, California, USA). Data was expressed as average RLU.

3.9.3 Mitochondrial Membrane Potential assay (JC-10 assay)

3.9.3.1 Principle

The mitochondria are an integral part of the cell responsible for energy synthesis (Kamiloglu *et al.*, 2020). Some dyes target the mitochondria so that its status and other essential parameters can be evaluated. A common parameter that can indicate cell death is mitochondrial membrane potential ($\Delta\Psi m$). A downstream of signals associated with the apoptotic cascade is triggered by a collapsed mitochondrial membrane that has opened mitochondrial permeability transition pores that allow cytochrome c to be released from the cytosol and activate apoptotic caspase signalling (Kamiloglu *et al.*, 2020). The assay depends on detecting cells' mitochondrial membrane potential changes by the cationic, lipophilic JC-10

dye (Figure 3.7). Normal cells emit a red fluorescent since the JC-10 dye is concentrated within the mitochondrial matrix. However, in dying cells affected by apoptosis or necrosis, the JC-10 dye can be released out of the mitochondria and stain the cells with a green fluorescence. Therefore, membrane potentials increase, becoming more polarised as the JC-10 dye changes its colour from green to red due to shifts in emitted light 520 nm/570 nm (Kamiloglu *et al.*, 2020).

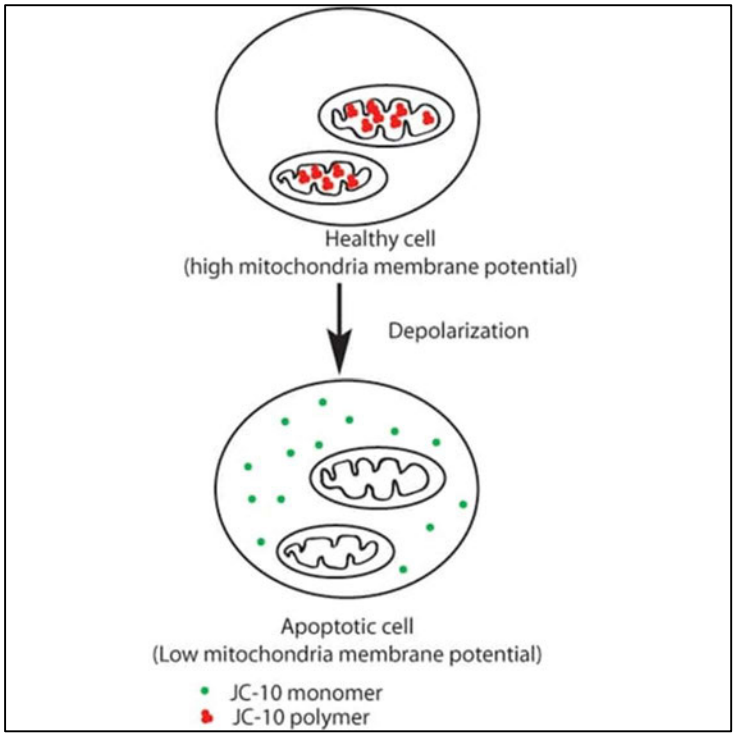

Figure 3.7: Quantification of mitochondrial membrane potential changes measured by a color shift from red to green in mitochondria of cells by lipophilic JC-10 dye (Miyai *et al.*, 2018).

3.9.3.2 Procedure

The JC-10 assay (#MAK 159) was used to evaluate changes in mitochondrial membrane polarity. The JC reagent was prepared per the manufacturer's instructions, and 25 µl of JC-10 loading dye solution was added to each well containing untreated and treated cells. After 30 minutes of incubation at RT protected from light, the green fluorescence intensity (490/525 nm) and red fluorescence intensity (540/590 nm) were recorded using a Modulus^{TM} microplate luminometer (Turner Bio-systems, Sunnyvale, California, USA). The data was recorded as relative fluorescence units (RFU), and the calculated red/green ratio determined the ΔΨm.

3.9.4 The glutathione (GSH) assay

3.9.4.1 Principle

Reactive oxygen species can induce a decrease in reduced glutathione (GSH) concentrations through their reactions with its thiol group or via oxidative pathways. This can ultimately promote oxidative stress, and the failure to repair DNA damage initiates apoptosis transcribed by p53; therefore, cell death occurs (Townsend *et al.*, 2003). The GSH luminescence assay can quantify and detect the presence of GSH (GSH-Glo™ Glutathione Assay Promega protocol) (Rocha *et al.*, 2016). The principle of the GSH assay (Figure 3.8) depends on the ability to convert the luciferin derivative into luciferin catalysed by glutathione S-transferase in the presence of GSH. The reaction requires ATP to produce luciferin (Townsend *et al.*, 2003). The final step is dependent on the luciferin detection reagent to emit light. The amount of light released is proportional to the concentration of reduced GSH in the cells (MURPHY *et al.*, 2008).

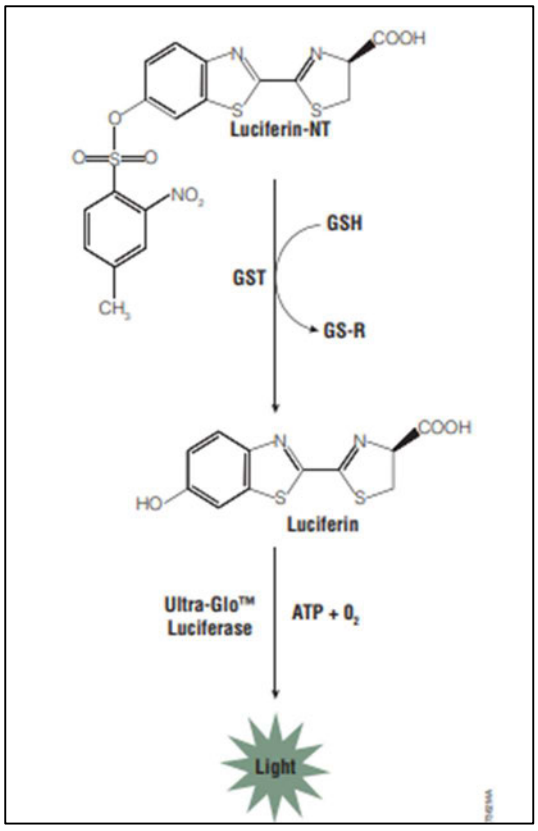

Figure 3.8: In the presence of Luciferin-NT substrate and glutathione S-transferase, GSH in the cells acts as a co-factor to form luciferin. Thereafter, luciferin reacts with oxygen, catalysed by luciferase, and light is emitted (MURPHY *et al.*, 2008).

3.9.4.2 Procedure

The Promega GSH-Glo™ Glutathione Assay (#V6911) was used to quantify GSH in the treated MCF-7 and MDA-MB-231 cell lines. The GSH working solution was prepared as instructed by the manufacturer, then 25 µl was added to each well and incubated at RT for 30 minutes in the dark. Finally, 12.5 µl of luciferin detection reagent was added to each well and set for 15 minutes more. Light emitted was measured with a Modulus^{TM} microplate luminometer (Turner Bio-systems, Sunnyvale, California, USA). Data was reported in RLU.

3.9.5 Caspase assays

3.9.5.1Principle

Caspases are cysteine-aspartate proteases that play a vital role in initiation (caspase-8 and -9) and execution (caspase-3/7) of apoptosis (Yadav *et al.*, 2021; Butterick *et al.*, 2014). The luminometric caspase assay (Figure 3.9) is based on luminogenic substrate-conjugated pro-luciferin cleavage by the caspases, which release aminoluciferin. Aminoluciferin reacts with luciferase in the presence of ATP, Mg^{2+} and molecular oxygen to produce a luminescent signal directly proportional to cell caspase activity (Butterick *et al.*, 2014).

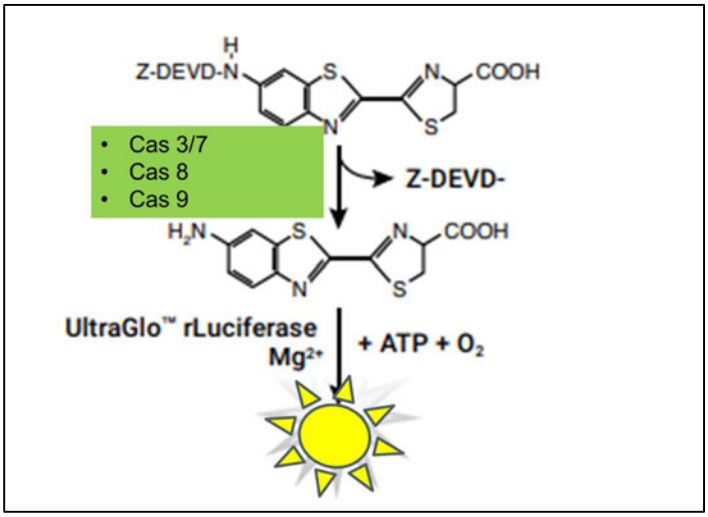

Figure 3.9: When caspases are cleavage from the proluciferin DEVD substrate, aminoluciferin is released. The enzyme luciferase is present with ATP and results light production (Promega, 2016) (Modified by author).

3.9.5.2 Procedure

Caspase-Glo® 8 (G8200), Caspase-Glo® 9 (G8210) and Caspase-Glo® 3/7 (G8090) was used to quantify caspase activity and to elucidate pathways involved in the activation of apoptosis. After

preparing the caspase working solution according to the manufacturer's instruction, 25 µl of the caspase 8 reagent was added to each well containing untreated and treated cells. This was repeated for the caspase 9 and caspase 3/7 reagents, into the respective treated cells. Following incubation at RT for 30 minutes in the dark, the luminescent signal was measured and recorded using the Modulus™ microplate luminometer (Turner Bio-systems, Sunnyvale, California, USA). Data was presented in RLU.

3.9.6 Apoptosis and necrosis assay

3.9.6.1 Principle

The assay counts the number of cells that have undergone apoptosis by staining the cells with Annexin V and propidium iodide dye mixture followed by luminometric analysis (Figure 3.10). The principle depends on the ability of normal cells to express inner membrane phosphatidylserine due to their hydrophobic nature. Therefore, when cells undergo apoptosis, the phosphatidylserine becomes exposed on the outer membrane. The exposed phosphatidylserine becomes detectable by Annexin V, and propidium iodide stains DNA of necrotic cells characterised by their leaky cell membrane. Therefore, it can differentiate between apoptotic and necrotic cells. The RealTime-Glo™ Annexin V Apoptosis Assay kit comprises of two Annexin V fusion proteins, namely Annexin V-LgBiT and Annexin V-SmBiT these proteins contain complementary subunits of NanoBiT® Luciferase (Kupcho *et al.*, 2019; Promega, 2017; Lakshmanan and Batra, 2013). Therefore, luminescence emission remains low until PS exposure can attract subunits into complementing proximity, which allows the detection dyes to stain the exposed PS.

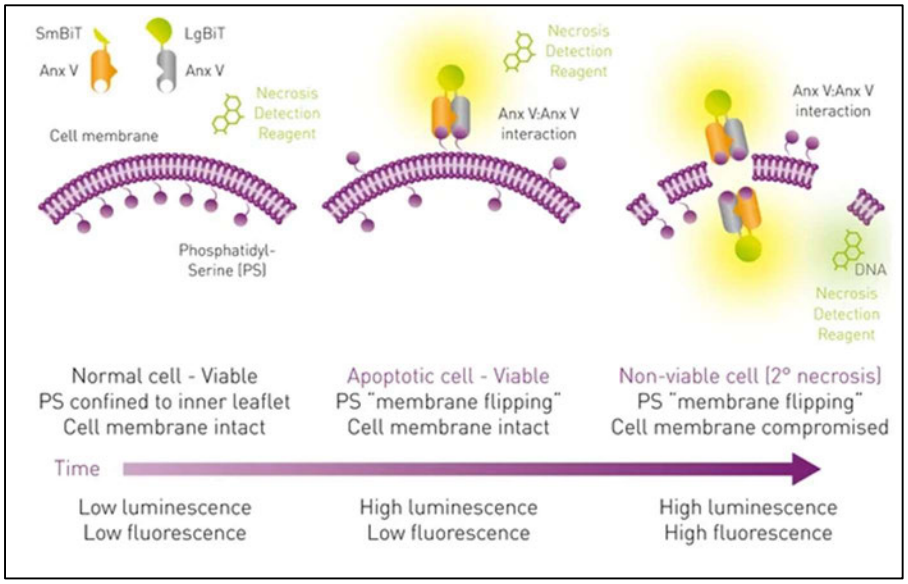

Figure 3.10: Externalisation of phosphatidylserine (PS) on the cytoplasmic membrane, which is detectable and stainable by Annexin V and PI, respectively (Kupcho *et al.*, 2017; Promega, 2017).

3.9.6.2 Procedure

The Glo™ Annexin V-propidium iodide (PI) apoptosis and necrosis assay was conducted to quantify phosphatidylserine externalisation. The working solution was prepared according to the manufacturer's instruction, and then 25 µl of annexin/necrosis reagent was added to each well and incubated at RT for 30 minutes in the dark. Both luminescence and fluorescence were measured using the Turner BioSystems Modulus™ microplate luminometer (Sunnyvale, California, USA). Data was presented in RLU and RFU, respectively.

3.10 WESTERN BLOTTING

3.10.1 Principle

The western blot immunoassay involves detecting specific proteins by separation based on molecular weight within a sample via gel electrophoresis. The principle depends on the proteins of interest in a gel to be electrophoretically transferred to a hydrophobic membrane after SDS-PAGE and detected using primary and secondary antibodies (Liu *et al.*, 2014). A single protein can be identified from a mixture of proteins (Mahmood and Yang, 2012).

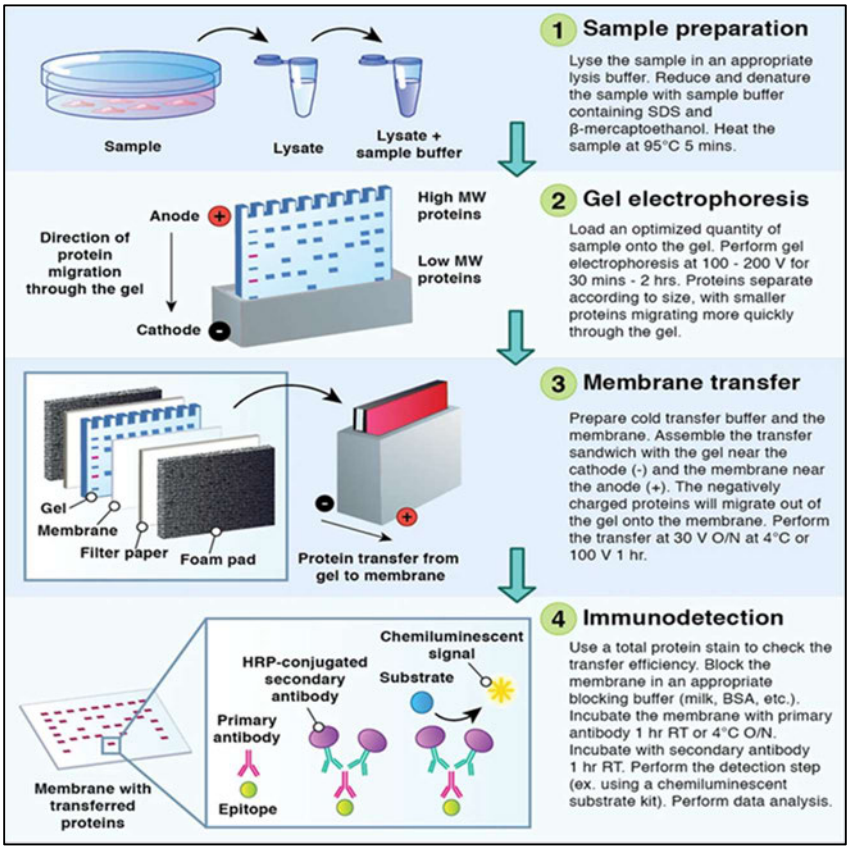

Figure 3.11: The steps involved in the western blot assay, namely sample preparation, gel electrophoresis, membrane transfer and immunodetection (Moore, 2009).

3.10.2 Procedure

Western blotting was utilised to evaluate the protein expression of iNOS, SOD2, and Nrf2. Treated and untreated flasks of MCF-7 and MDA-MB-231 cells were rinsed with 0.1M PBS (3 times), then 200 µl Cytobuster™ protein extraction reagent (#71009) supplemented with protease and phosphatase inhibitors (#A32961) was added to induce cell lysis to isolate the protein. Flasks were then placed on ice for 30 minutes to preserve proteins. The flasks were scraped to dislodge cells, and the cell suspension was transferred into a micro-centrifuge tube. After centrifugation (10000 rpm, 4ºC, 10 minutes) the crude protein supernatant was transferred into a new micro-centrifuge tube.

The BCA assay was used to quantify and standardise proteins. A 1mg/ml BSA stock solution was used to prepare standards (0, 0.2, 0.4, 0.6, 0.8 and 1 mg/ml BSA). First, 25 µl of each sample and the relevant standards were dispensed into a 96-well plate in triplicate. Thereafter, 200 µl BCA working solution (4 µl $CuSO_4$ and 198 µl BCA) was added to each well and then incubated at 37ºC for 30 minutes. Plates were read on a SPECTROstar Nano (BMG Labtech, Ortenberg, Germany) to determine the absorbance at 562 nm. The absorbances of the standards were used to construct a standard curve, from which the protein concentration of each sample was calculated. Sample protein concentration was standardised to 1mg/ml, and 5x Laemmli sample buffer (3.55 ml distilled water [dH_2O], 2 ml 10% sodium dodecyl sulphate, 500 µl β-mercaptoethanol, 2.5 ml glycerol, 1.25 ml 0.5 M Tris (pH 6.8), 0.2 ml 0.5% (w/v) bromophenol blue) was added to each standardised sample (1:4). Protein samples were then boiled for 5 minutes (100ºC) to activate β-mercaptoethanol and SDS for the unfolding of proteins to take place, and for a uniform negative charge to be obtained.

The Mini-PROTEAN 3 SDS-PAGE gel casting apparatus was set up to prepare a 10% resolving gel (3.95 ml dH_2O, 2.5 ml 1.5 M Tris-HCl [pH 8.8], 100 µl 10% SDS, 3.35 ml 30% bis-acrylamide, 50 µl 10% ammonium persulphate, 5 µl tetramethylethylenediamine); dH_2O was used to make sure the interface was smooth and set for one hour. The prepared 4% stacking gel [dH_2O, 0.5 M Tris-HCl (pH 6.8), 10% (w/v) SDS, 30% bis-acrylamide, 10% APS, TEMED] was added with a 10-well comb and allowed to set for 40 minutes. The prepared protein samples were loaded into the prepared gels, and the gel cassettes were placed into an electrophoresis tank containing cold electrophoresis buffer (dH_2O, SDS, glycine, Tris, kept at 4ºC). Electrophoresis proceeded for 1 hour at 150 volts until the tracker dye reached the bottom of the gel. An electrotransfer to equilibrate gel and nitrocellulose in transfer buffer (dH_2O, Tris, glycine, methanol, pH 8.3, kept at 4ºC) was conducted for 10 minutes. A gel sandwich was prepared and

placed into a Transblot®Turbo^{TM} Transfer system (Bio-Rad, Hercules, California, USA) to transfer proteins to the membrane at 25 V for 30 minutes. The nitrocellulose membrane was removed carefully using forceps and blocked with 5 ml of 2% BSA in Tris-buffered saline (TTBS) [100 ml; Tris-buffered saline (dH_2O, Tris-HCl [pH 7.4], NaCl) with 0.05% Tween-20] for 2 hours on a shaker at RT.

The membranes were subsequently immunoprobed with primary antibodies SOD2 (#13141), Nrf2 (#12721) and iNOS (#2982) diluted in 2% BSA-TTBS (1:1000) and incubated with the membrane overnight at 4°C. After incubation, the primary antibody was removed and washed with TTBS 5 times for 10 minutes each time. The membrane was subsequently immunoprobed with horseradish peroxidase conjugated (HRP-conjugated) secondary antibody [anti-rabbit IgG (#7074) for SOD2, Nrf2, and anti-mouse IgG (#7076) for iNOS] in 2% BSA-TTBS (1:5000) for 2 hours. After incubation, the secondary antibody was discarded, and the membrane was washed with TTBS 5 times for 10 minutes. Protein bands were then viewed using the Clarity Western ECL substrate kit (Bio-Rad, Hercules, California, USA) by mixing the reagent in 1:1 ratio, and 200 µl of the mixture was added to the nitrocellulose membrane. Images of protein bands were viewed and captured using the Molecular imager GelDoc XRS imaging system (Bio-Rad imaging system, Hercules, California, USA).

To normalise the protein expression, the membrane was immunoprobed with β-actin, which was used as a loading control. Briefly, the membrane was stripped with 5 ml H_2O_2 (32% solution) at 37^{o}C for 30 minutes. After washing in TTBS to remove H_2O_2, the membrane was blocked (2% BSA in TTBS) for 1 hour, then incubated for 1 hour with β actin (1:5000 in 2% BSA-TTBS). After incubation, the membrane was washed and viewed. Analysis was done using the Image Lab V6.0.1 (Bio-Rad Laboratories Inc. software, Hercules, California, USA). The band intensity was measured for the respective protein, and data were expressed as relative band intensity (RBI).

3.11 QUANTITATIVE POLYMERASE CHAIN REACTION (QPCR)

3.11.1 Principle

The polymerase chain reaction (PCR) is a sensitive and specific assay for amplifying deoxyribonucleic acid (DNA) sequences. In the process, the target DNA strands are denatured, and strands are bound to the complementary sequences of the DNA. New DNA strands are formed by DNA polymerase attaching free nucleotides to the DNA templates. This occurs in a series of steps known as denaturation, annealing, and elongation. In quantitative polymerase chain reaction (qPCR) (Figure 3.12), complementary DNA

(cDNA) is transcribed by reverse transcriptase from messenger RNA (mRNA). This method involves repeated cycles of different alternate temperature incubations, including denaturation (95°C) to separate double-stranded DNA, annealing of primers at specific temperatures, and elongation using Taq polymerase, primers of interest and iTaq Universal SYBR® Green Supermix (#172-5271).

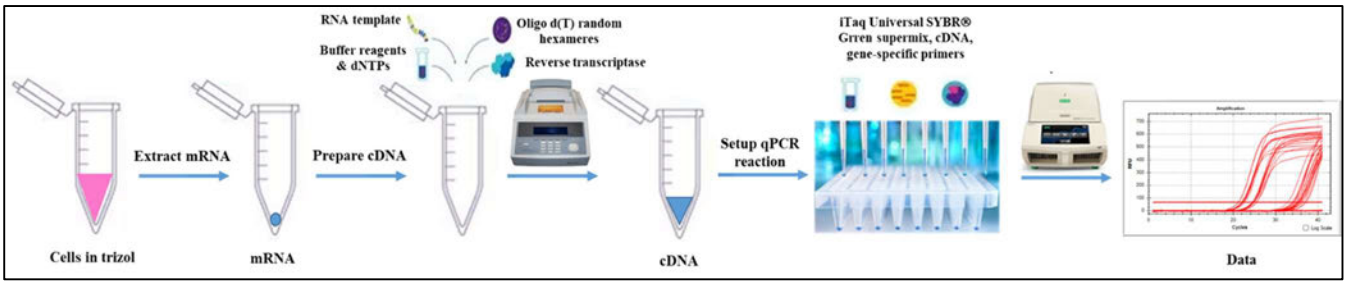

Figure 3.12: Simplified procedure for qPCR that starts with sample preparation, lysis in trizol, mRNA isolation and standardisation, cDNA synthesis and finally the qPCR reaction to generate Cq values for analysis (Cirera and Busk, 2014) (Modified by author).

3.11.2 Procedure

The RNA isolation includes cell lysis, separation, precipitation, and solubilisation of the RNA from the cell sample. Firstly, treated, and untreated cultured cells were washed with 0.1 M PBS, then 500 µl of Trizol (#15596026) and 500 µl of 0.1M PBS were added to each flask and incubated at RT for 5 minutes. Following incubation, cells were scraped from the flasks, collected in labelled 1.5 ml microcentrifuge tubes and stored at -80ºC. The samples were thawed and 100 µl of chloroform was added, followed by vigorous shaking for 30 seconds. Thereafter, samples were centrifuged (12000xg/ 4ºC/ 15 minutes). The aqueous phase containing RNA was transferred to a new microcentrifuge tube and placed on ice, followed by the addition of 250 µl isopropanol to precipitate the RNA in the sample. The sample was stored at -80℃ overnight, then thawed and centrifuged (12000xg, 4ºC, 20 minutes). The resulting supernatant was discarded, the pellet was washed with 500 µl ice-cold 75% ethanol. The sample was centrifuged again at 7400xg (4ºC for 15 minutes). Excess ethanol was carefully discarded, and pellet was left to air-dry for 1 hour. The dry pellet was solubilised in 15 µl nuclease-free (NF) water at RT for 3 minutes. The RNA was quantified using the nanodrop 2000 spectrophotometer (Thermo-Scientific, Johannesburg, SA), and purity of RNA was assessed using the A260/A280 ratio. The RNA samples stored at -80ºC.

The cDNA was prepared with the standardised RNA (1000 ng/ml) using the Bio-Rad iScript™ cDNA synthesis kit (#170-8890). The reaction mixture was prepared as per product instructions. The reaction mixture had a total volume of 20 µl which consisted of 4 µl 5X iScript™ reaction mix, 1 µl iScript reverse

transcriptase, 11 µl nuclease-free water and 4 µl of the RNA template. The sample was placed into the thermocycler and reverse transcribed at the following temperatures 25ºC for 5 minutes, 42ºC for 30 minutes, 85ºC for 5 minutes, and was placed on hold at 4ºC using the GeneAmp PCR System 9700 (Applied Biosystems). The cDNA was then diluted with 80 µl of NF water to obtain a final volume of 100µl and stored at -80ºC for further use.

Working stock solutions of forward and reverse primers (Table 3.1) were prepared separately according to manufacture guidelines (25 µl primer, 75 µl NF water) in a master mix with a total volume of 11 µl which consisted of SYBR green (6.25 µl), forward primer (0.5 µl), reverse primer (0.5 µl), NF water (3.75 µl) and cDNA template (1 µl); GAPDH was used as the housekeeping gene. The master mix and the cDNA sample were plated in triplicate and placed into the CFX96 Touch™ Real-Time PCR Detection System (Bio-Rad) and run under specified temperatures. The reaction was subjected to initial denaturation (95ºC, 4 minutes), followed by the annealing phase (per primer, 40 seconds) (Table 3.1), and finally the extension phase (72ºC for 30 seconds). The data acquired was analysed using the Livak & Schmittgen (2001) method and presented as relative fold change in mRNA expression (Livak and Schmittgen, 2001).

Table 3.1: Forward and reverse primer sequences with respective annealing temperatures.

Gene	Primer sequence	Annealing temperature (°C)
OGG1	F (5′-GCATCGTACTCTAGCCTCCAC-3′) R (5′-AGGACTTTGCTCCCTCCAC-3′)	58
GPX1	F (5′-GACTACACCCAGATGAACGAGC-3′) R (5′-CCCACCAGGAACTTCTCAAAG-3′)	58
NF-κB	F (5′-GACCTGAATGCTGTGCGGC-3′) R (5′-ATCTTGAGCTCGGCAGTGTT-3′)	58
TNFα	F (5′-CAGAGGGAAGAGTTCCCCAG-3′) R (5′-CCTTGGTCTGGTAGGAGACG-3′)	60
RIPK1	F (5′-AGGTACAGGAGTTTGGTATGGGC-3′) R (5′-GGTGGTGCCAAGGAGATGTATG-3′)	60
RIPK3	F (5′-TAGTTTATGAAATGCTGGACCGC-3′) R (5′-GCCAAGGTGTCAGATGATGTCC-3′)	60
MLKL	F (5′-CTGAGGGAACTGCTGGATAGAG-3′) R (5′-CGAGGAAACTGGAGCTGCTGAT-3′)	60
GAPDH	F (5′-TCCCTGAGCTGAACGGGAAG-3′) R (5′-GGAGGAGTGGGTGTCGCTGT-3′)	Temperature of gene of attention

3.12 Statistical analysis

Statistical analysis of all data obtained was performed using GraphPad Prism v5.0 software (GraphPad Software Inc., La Jolla, California, USA). Experiments were performed in triplicate and repeated for verification. Statistical significance was determined by performing the unpaired students *t*-test with Welch's correction (data expressed as mean ± standard deviation (SD)). Statistical significance was determined with a 95% confidence interval and with the p-value < 0.05. For the MTT assay, a non-linear regression log inhibitor versus normalised response graph was generated to obtain an IC_{50} value and the IC_{20} value was extrapolated from the graph.

3.13 Ethics

Ethical approval was sought from the Biomedical Research Ethics Administration and exemption from ethics granted (Protocol reference number: BREC/00005021/2022).

CHAPTER 4: RESULTS

4.1 METABOLISM

The CYP3A4 activity was quantified to identify if cyclen tetrahydrochloride was metabolised in MCF-7 (Figure 4.1A) and MDA-MB-231 (Figure 4.1B) cells. The CYP3A4 activity was similar to the control when MCF-7 cells were treated with IC_{20} (3026±448.1 RLU, p = 0.7616), compared to the control (2804±344.1 RLU). Still, cyclen tetrahydrochloride decreased CYP3A4 activity by 0.8-fold compared to control to 2430±12.01 RLU (p = 0.4736) for the IC_{50} treatment. The CYP3A4 activity in untreated MDA-MB-231 cells was 3453±400 RLU and remained similar to the control for the IC_{20} treatment (3531±350.1 RLU, p = 0.9072), with a non-significant 0.6-fold reduction compared to the control at the IC_{50} (2160±12.01 RLU, p = 0.1912) (Figure 4.1B).

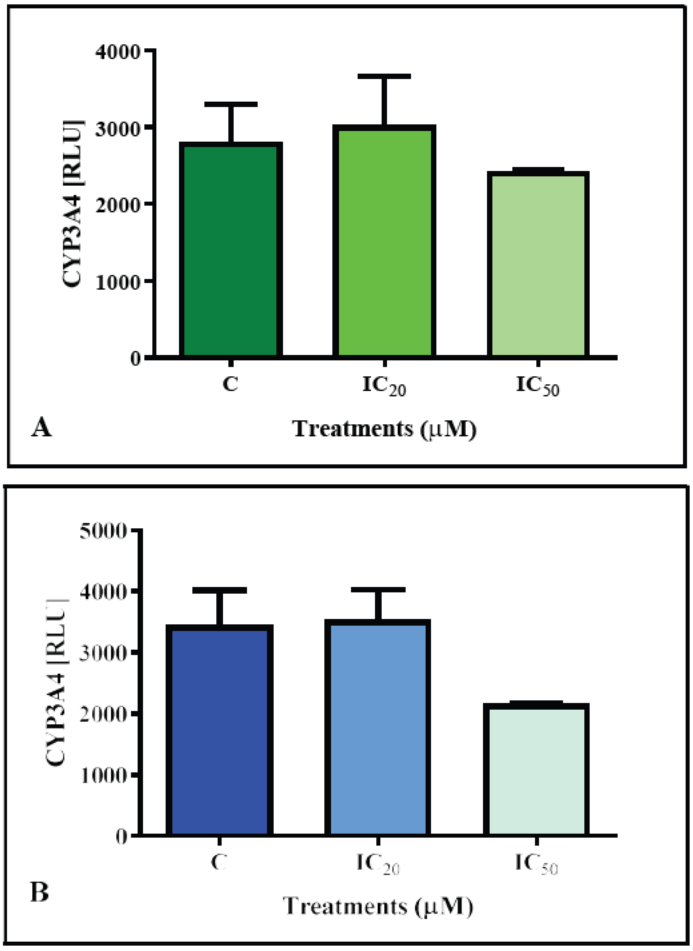

Figure 4.1: The CYP3A4 levels were non-significantly increased in both cell lines at for IC_{20} cyclen tetrahydrochloride treatments and decreased for the IC_{50} after 48-hour treatment, RLU: relative light units.

4.2 CELL VIABILITY (MTT) ASSAY

Cell viability was measured to determine the cytotoxic effects of cyclen tetrahydrochloride on MCF-7 and MDA-MB-231 cells at concentrations of 0–1000µM. Cyclen tetrahydrochloride inhibited the metabolic activity of MCF-7 and MDA-MB-231 cells (Figure 4.2 A and B). In the MCF-7 cells, the cell viability was similar to the control (99%) for the 12.5µM treatment, then decreased with increasing doses (Figure 4.2A). Cell viabilities above 70% were recorded for the 25µM and 50µM treatments. Cell viabilities decreased sequentially for subsequent therapies, with the lowest cell viability of 6% documented at 1000µM (Figure 4.2). The 48-hour treatment of MCF-7 cells yielded an IC_{50} value of 168.7µM (Log concentration = 2.226), and IC_{20} of 41.7µM was extrapolated (Figure 4.2A). The cyclen tetrahydrochloride increased cell viability of MDA-MB-231 cells for 12.5µM–100µM treatments, and 81% and 56% cell viability were recorded for the 250µM and 500µM treatment (Figure 4.2B). The lowest cell viability of 24% was observed for the 1000µM treatment; an IC_{50} value of 561µM (Log concentration = 2.749) and IC_{20} of 302.9µM were derived. These concentrations were used in all the upcoming assays to understand the pathways contributing to cyclen tetrahydrochloride effects in MCF-7 and MDA-MB-231 cells.

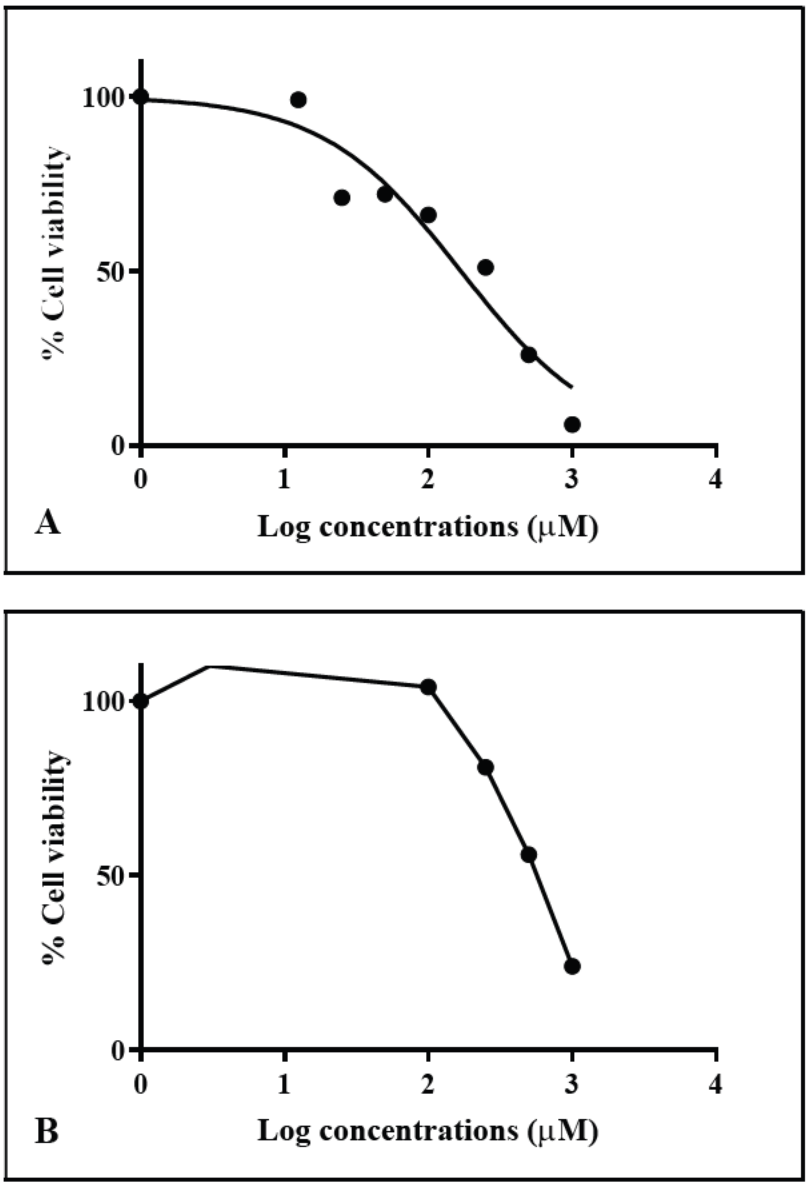

Figure 4.2: The dose-response curves for cell viability used to calculate the cyclen tetrahydrochloride 48-hour treatment concentrations in MCF-7 and MDA-MB-231 cells. (A) An increase in compound treatment concentration showed lower cell viability in MCF-7 cells. **(B)** Decreased cell viability in MDA-MB-231 cells after treatment with concentrations of cyclen tetrahydrochloride above 250μM.

4.3 MITOCHONDRIAL INTEGRITY

Mitochondrial integrity was assessed by determining ΔΨm and ATP production. Cyclen tetrahydrochloride decreased intracellular ATP MCF-7 (Figure 4.3A) and MDA-MB-231 (Figure 4.3C) cells. The ATP concentration decreased to 0.8-fold from 6094000±23980 RLU in control MCF-7 cells to 5461000±94240 RLU (p = 0.0970) for IC_{20}-treated cells and a significant decrease to 0.2-fold (1677000±208500 RLU, p = 0.0302) for the IC_{50} treatment. A statistically significant decrease to 0.7-fold in ATP was observed in MDA-MB-231 cells for the IC_{20} cyclen tetrahydrochloride treatment

(2517000±52390 RLU, $p = 0.0277$) and to 0.3-fold at the IC_{50} to 1114000±179900 RLU ($p = 0.0438$) when compared to the control (3724000±4435 RLU) (Figure 4.3B). The MCF-7 cells decreased ΔΨm to 0.8-fold when the cells were treated with IC_{20} (0.05531±0.002739, $p = 0.1386$) and to 0.7-fold (0.04814±0.01052, $p = 0.3098$) for the IC_{50}, compared to the control (0.06807±0.0006772) (Figure 4.3B). The ΔΨm in MDA-MB-231 cells was similar to the control (0.09315±0.005025) for both treatments; 0.08867±0.01325 when the cells were treated with IC_{20} (0.95-fold, $p = 0.8051$) and a 0.9-fold decrease to (0.08696±0.001778, $p = 0.4527$) for the IC_{50} (Figure 4.3D).

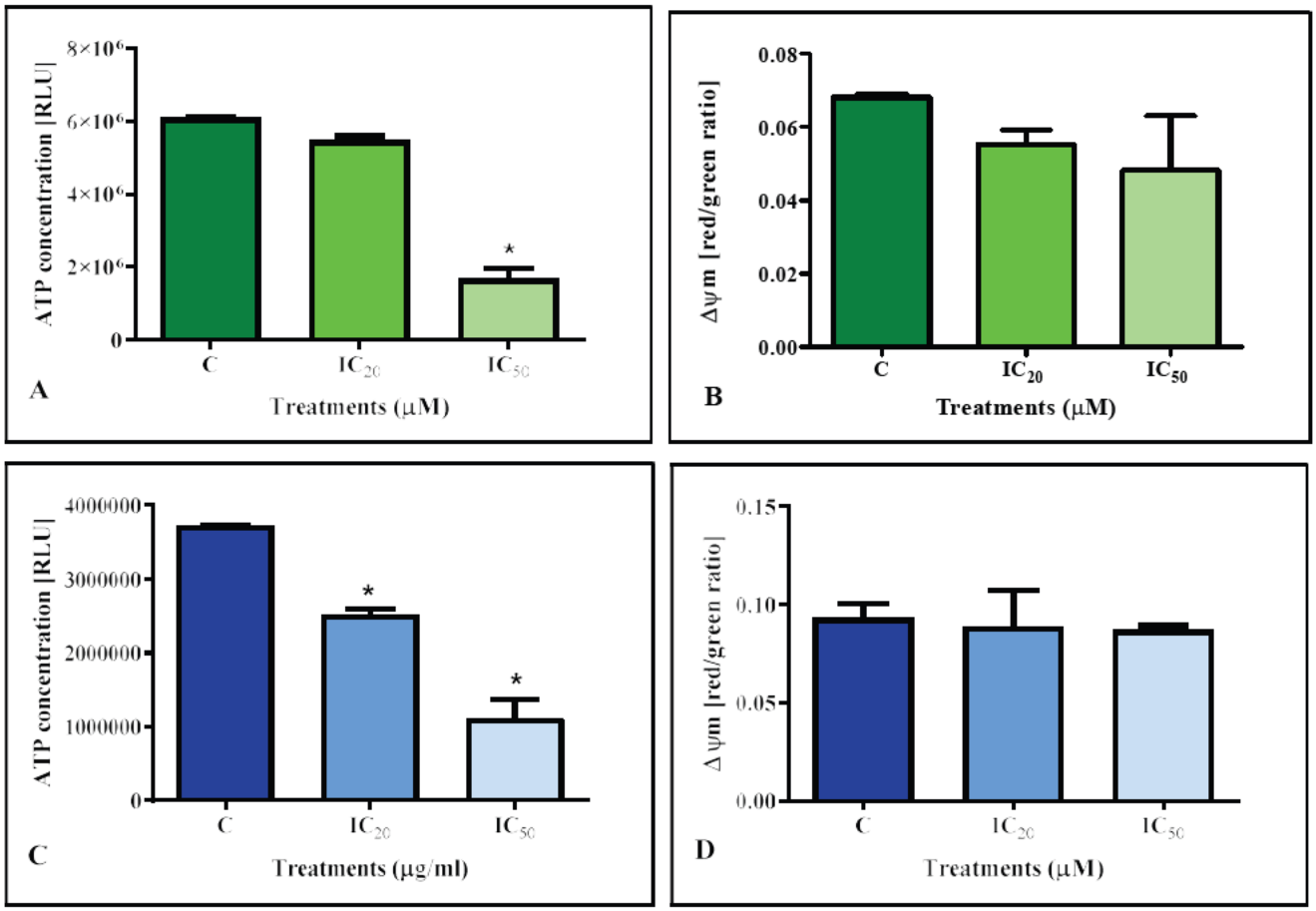

Figure 4.3: Cylen tetrahydrochloride effects on mitochondrial integrity following 48-hour treatment. (A) After exposure to cyclen tetrahydrochloride treatment, the intracellular ATP concentration significantly decreased in MCF-7 cells at IC_{50}. **(B)** Mitochondrial membrane potential measured by JC-10 was reduced for both concentrations in MCF-7. **(C)** The expression of intracellular ATP after exposure to Cyclen tetrahydrochloride treatment significantly decreased in MDA-MB-231 cells at IC_{20} and IC_{50}. **(D)** In MDA-MB-231 cells, the JC-10 expression decreased non-significantly for both concentrations. [*, unpaired students *t*-test with Welch's correction]

4.4 REACTIVE OXYGEN SPECIES-ASSOCIATED MACROMOLECULAR DAMAGE

The ROS was determined by measuring the MDA concentrations using the TBARS assay (Figure 4.4A, C), and DNA damage marker OGG1 was quantified using qPCR (Figure 4.4B, D) respectively to assess the effects of cyclen tetrahydrochloride. Lipid peroxidation in cyclen tetrahydrochloride treated MCF-7 cells (Figure 4.4A) increased significantly for IC_{20} and IC_{50} to 0.1432±0.007704 µM (1.97-fold, p = 0.0051) and 0.1816±0.005653 µM (2.5-fold, p = 0.0009) respectively, compared to the untreated control (0.07265 ± 0.005653 µM). Cyclen tetrahydrochloride treatment increased lipid peroxidation for MDA-MB-231 cells (Figure 4.4C) from 0.1047±0.005653 µM in control cells to 0.1838±0.005653 µM for the IC_{20} treatment (1.76-fold, p = 0.0006) and was similar to the control for the IC_{50}-treated cells (0.1080±0.003819 µM, p = 0.6586). In MCF-7 cells, the *OGG1* gene expression (Figure 4.4B) induced by cyclen tetrahydrochloride was significantly increased (4.337±0.5966 RFC, p = 0.0305 and 8.696±0.4516 RFC, p = 0.0373 respectively), compared to the untreated control. The *OGG1* gene expression induced by cyclen tetrahydrochloride was significantly increased for IC_{20} and IC_{50} to 7.369±0.4255 RFC (p = 0.0044) and 68.44±0.5684 RFC (p < 0.0001), respectively, compared to the untreated control for MDA-MB-231 cells (Figure 4.4D).

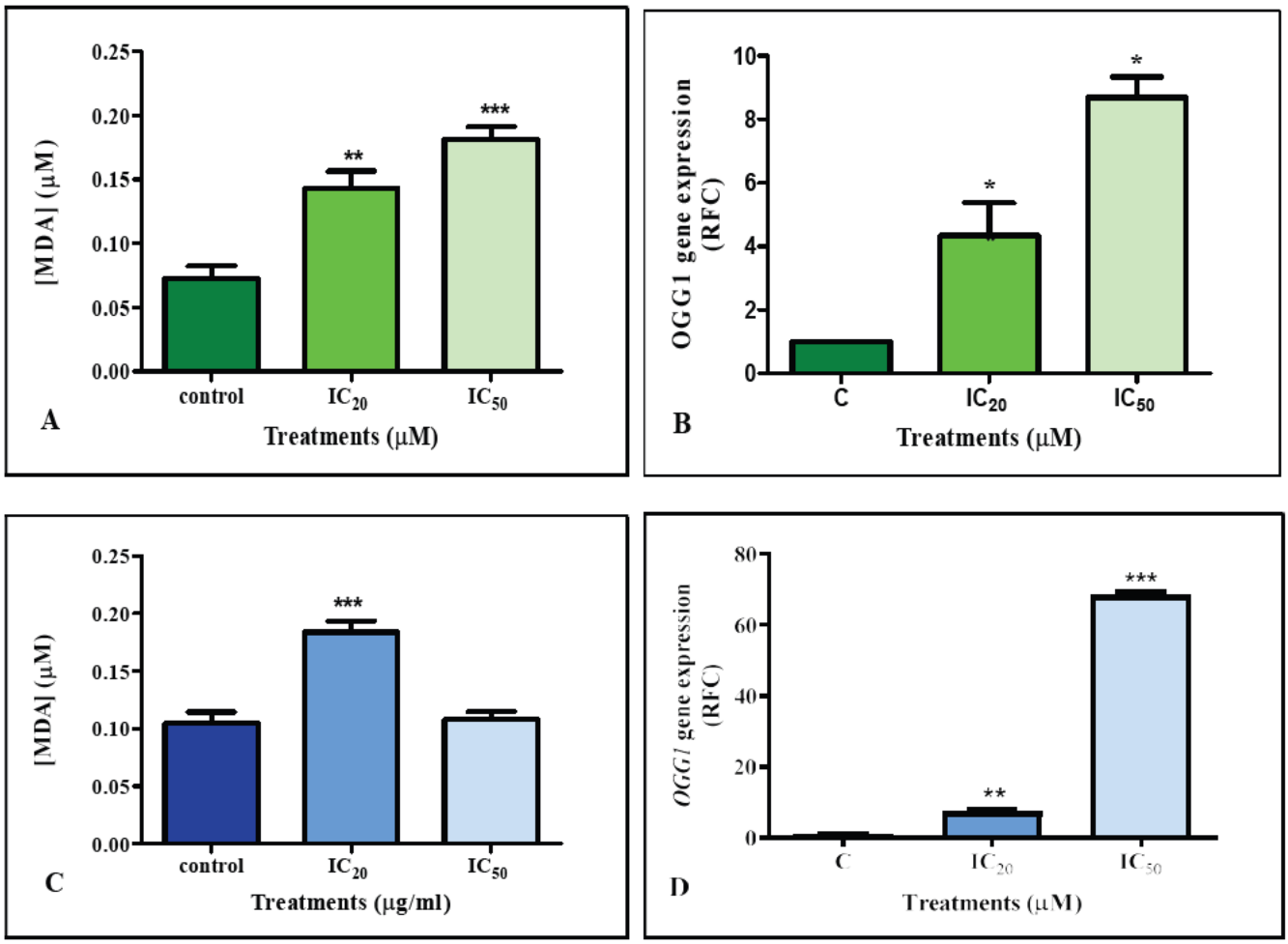

Figure 4.4: ROS-associated macromolecular damage induced by 48-hour exposure to cyclen tetrahydrochloride in MCF-7 and MDA-MB-231 cells (A) The concentration of MDA was significantly increased for all cyclen treatments in MCF-7 cells. **(B)** The *OGG1* gene expression was significantly increased for both treatments in MCF-7 cells. **(C)** In MDA-MB-231 cells MDA concentration was significantly increased at IC_{20} treatment, followed by a non-significant decrease at IC_{50}, similar to the control. **(D)** In MDA-MB-231 cells, the *OGG1* gene expression was significantly increased for both treatments. [**/***, unpaired students *t*-test with Welch's correction]

4.5 NITROSATIVE STRESS

Nuclear factor kappa B (NF-κB) transcriptionally regulates the expression of iNOS, which is associated with large amounts of nitric oxide production. Therefore, *NF-κB* gene expression, iNOS protein expression and nitrate/nitrite concentrations were measured to assess the effects of cyclen tetrahydrochloride on RNS. Cyclen tetrahydrochloride non-significantly increased the gene expression of *NF-κB* at IC_{20} (2.389±1.109 RFC, $p = 0.4288$) and IC_{50} (19.05±6.584 RFC, $p = 0.2227$) relative to the control MCF-7 cells (Figure 4.5A). In Figure 4.5D, cyclen tetrahydrochloride treatment induced significant increases in *NF-κB* gene expression to 3.321±0.4209 RFC at IC_{20} ($p = 0.0313$) and

7.051±1.225 RFC at the IC_{50} (p = 0.0386) compared to the untreated control. The iNOS protein expression was non-significantly decreased for both IC_{20} (0.1133±0.01453 RBI, p = 0.0663) and IC_{50} (0.2367±0.03712 RBI, p = 0.1675) to 0.26-fold and 0.54-fold respectively, relative to the control (0.4367±0.08647 RBI) in MCF-7 cells (Figure 4.5B). The MDA-MB-231 cells showed a statistically significant increase to 18.53-fold in iNOS protein expression when the cells were treated with IC_{20} (4.693±0.3667 RBI, p = 0.0068) and to 11.14-fold for the IC_{50} (2.823±0.2140 RBI, p = 0.0071), compared to the control (0.2533±0.04333 RBI) (Figure 4.5E). The RNS in MCF-7 cells was similar to the control (53.70±1.266 μM) for the IC_{20}-treated (55.57±0.333 μM, p = 0.2901) and IC_{50}-treated cells (49.07±0.9821 μM, p = 0.0629) (Figure 4.5C). However, RNS in MDA-MB-231 cells was increased from 41.20±0.4583 μM in the control cell to 1.3-fold for the IC_{20} treatment (53.93±0.8819 μM, p = 0.0010) and to 1.1-fold in IC_{50}-treated cells (46.17±0.5364 μM, p = 0.0059) (Figure 4.5F).

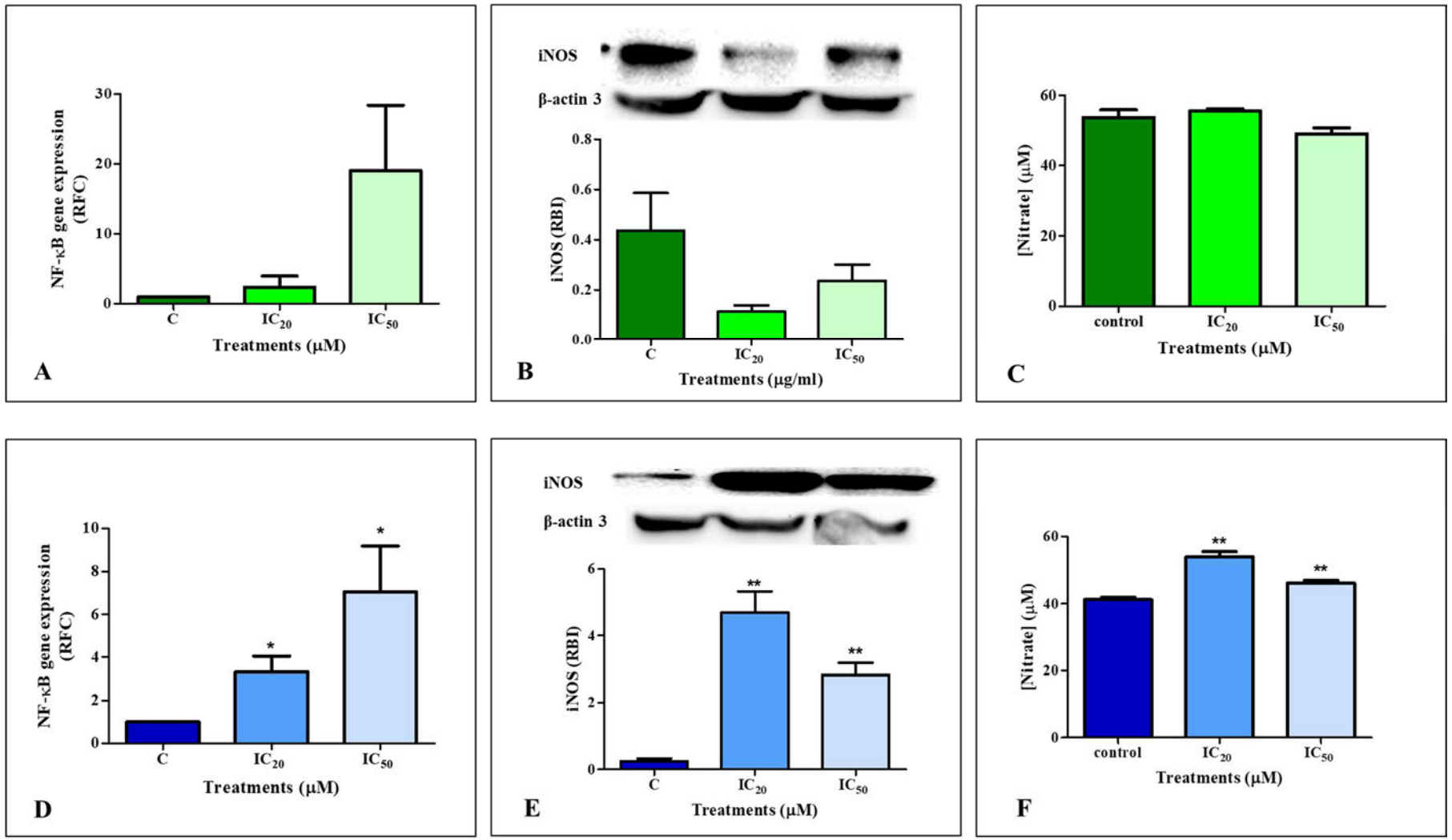

Figure 4.5: The effects of cyclen tetrahydrochloride on nitrosative stress following 48-hour treatment (A) Cyclen tetrahydrochloride induced non-significant increases in *NF-κB* gene expression for both IC_{20} and IC_{50} treatments. **(B)** The iNOS expression was decreased for both treatments in MCF-7 cells. **(C)** The nitrate concentration for MCF-7 IC_{20}-treated cells was similar to the control, followed by a decrease for the IC_{50} treatment. **(D)** The *NF-κB* gene expression was increased for both treatments. **(E)** In MDA-MB-231 cells, iNOS was significantly increased for IC_{20} and IC_{50} treatments. **(F)** Nitrate concentrations were increased significantly for both treatments in MDA-MB-231 cells. [*/**, unpaired students *t*-test with Welch's correction]

4.6 ANTIOXIDANT RESPONSE

Antioxidant response was assessed by quantifying SOD2, *Gpx1*, GSH and Nrf2 following 48-hour treatment to determine the effects of cyclen tetrahydrochloride and its ability to modulate oxidative stress. In Figure 4.6A, the protein expression of SOD2 in MCF-7 cells revealed non-significant changes in expression in IC_{20}-treated (0.8533±0.08876 RBI, p = 0.5176) and IC_{50}-treated cells (0.8500±0.06807 RBI, p = 0.4283)) that were similar to the control (0.7767±0.04256 RBI). The SOD2 protein expression decreased to 0.81-fold in IC_{20}-treated MDA-MB-231 cells (0.6033±0.04372 RBI, p = 0.1099) and 0.61-fold for the IC_{50} treatment (0.4567±0.02728 RBI, p = 0.0125), relative to the control (0.7467±0.04631 RBI) (Figure 4.7A). The gene expression of *Gpx1* was significantly upregulated in MCF-7 cells at IC_{20} (1.113±0.02541 RFC, p = 0.0473) and IC_{50} treatments (4.153±0.4777 RFC, p = 0.0222), compared to the control (Figure 4.6B). In contrast, the MDA-MB-231 cells revealed statistically significant downregulation at IC_{20} (0.2906±0.003488 RFC, $p < 0.0001$) and IC_{50} (0.3312±0.02968 RFC, p = 0.0020), relative to the control (Figure 4.7B). There was a non-significant decrease in GSH concentration for MCF-7 cells from 305200±10370 RLU in the control to 200700±24670 RLU (0.66-fold, p = 0.1595) in the IC_{20} treatment and 269500±81780 RLU (0.88-fold, p = 0.7397) for the IC_{50} treatment (Figure 4.6C). Results were similar for MDA-MB-231 cells with a non-significant decrease in GSH concentration from 200800±61340 RLU in control cells to 81320±81100 RLU (0.4-fold, p = 0.4489) in the IC_{20} treatment and 115500±12010 RLU (0.58-fold, p = 0.4027) for the IC_{50} treatment (Figure 4.7C). In Figure 4.6D, Nrf2 exhibited significantly reduced expression in MCF-7 cells to 0.6-fold at IC_{20} (0.1833±0.008819 RBI, p = 0.0040) and to 0.75-fold at IC_{50} (0.2267±0.01764 RBI, p = 0.0370) compared to the control 0.3033±0.01202 RBI. Similarly, in MDA-MB-231 cells the Nrf2 expression decreased for both treatments to 0.58-fold and to 0.86-fold for IC_{20} (0.1500±0.005774 RBI, p = 0.0135) and IC_{50} (0.2233±0.01202 RBI, p = 0.1152) respectively, compared to the control (0.2600±0.01155 RBI) (Figure 4.7D).

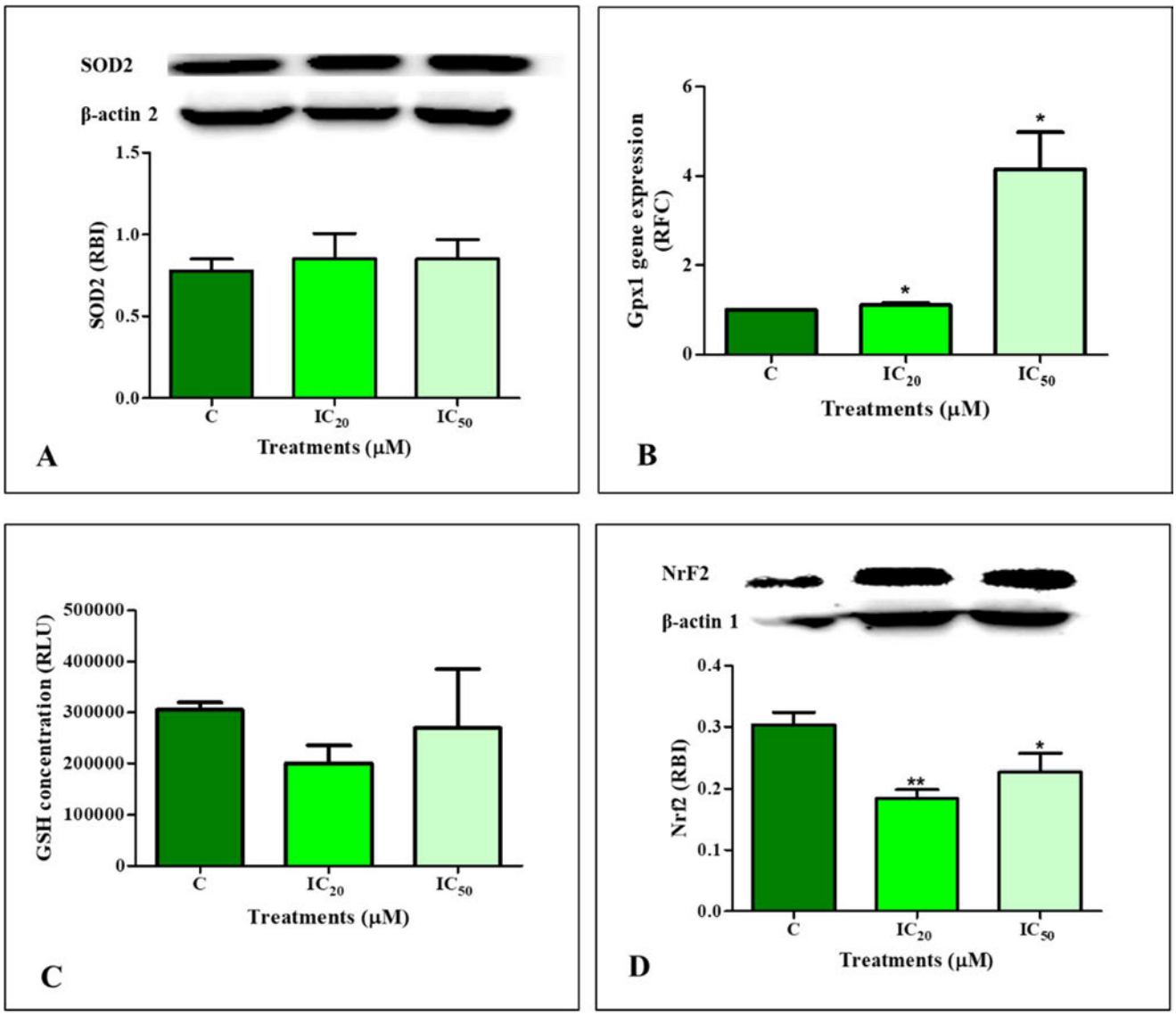

Figure 4.6: Protein expression of antioxidants in MCF-7 cells following 48-hour treatment at IC_{20} and IC_{50} with cyclen tetrahydrochloride compared to the control. (A) The SOD2 expression was similar to the control for IC_{20} and IC_{50} treatments. **(B)** *Gpx1* gene expression increased in cells exposed to cyclen tetrahydrochloride. **(C)** The concentration of GSH was decreased for both treatments relative to the control. **(D)** The Nrf2 expression was significantly decreased for IC_{20} and IC_{50} treatments compared to the control. [*/**, unpaired students *t*-test with Welch's correction]

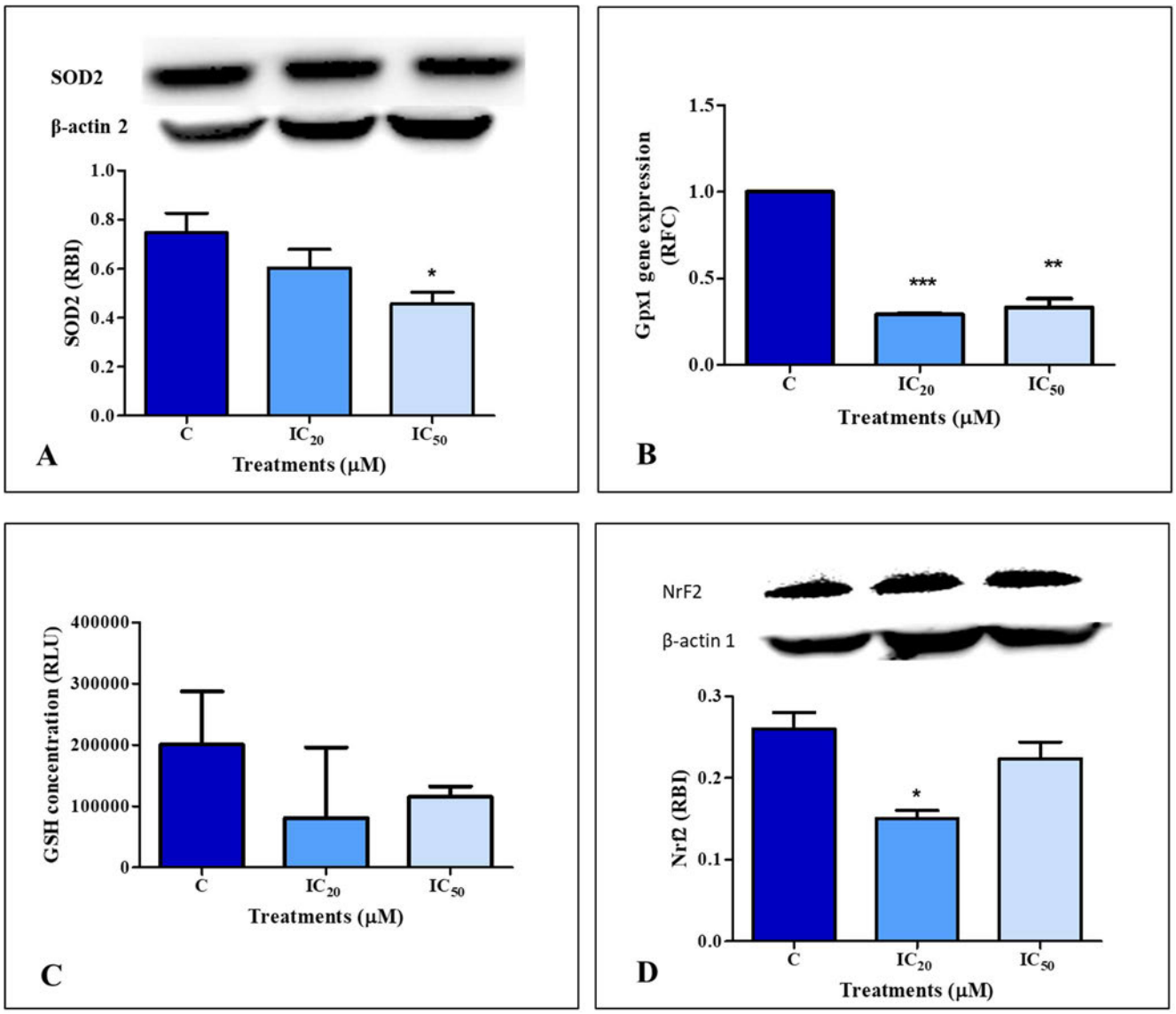

Figure 4.7: Protein expression of antioxidants in MDA-MB-231 cells following 48-hour exposure to cyclen tetrahydrochloride at IC_{20} and IC_{50} treatments, relative to the control. (A) The SOD2 expression was decreased in IC_{20} and IC_{50} treated cells. **(B)** Statistically significant reduction in *Gpx1* gene expression for both IC_{20} and IC_{50} treatments, compared to the control. **(C)** The concentration of GSH was non-significantly decreased for both treatments, relative to the control. **(D)** The Nrf2 expression decreased for IC_{20} and IC_{50} treatments, compared to the control. [*/**/***, unpaired students *t*-test with Welch's correction]

4.7 EXTRINSIC APOPTOSIS

The activity of caspase 8 was quantified using luminometry, and the gene expression of TNF-α was measured using qPCR following 48-hour treatment with cyclen tetrahydrochloride to assess its effects on the extrinsic apoptosis pathway. Cyclen tetrahydrochloride non-significantly downregulated caspase 8 activity in MCF-7 cells to 0.74-fold at IC_{20} (494100±8437 RLU, $p = 0.0911$) and to 0.62-fold for the IC_{50} (413700±38460 RLU, $p = 0.1113$) treatments, compared to the control (670100±23920 RLU) (Figure 4.8A). In MDA-MB-231 cells, the caspase 8 activity was non-significantly downregulated from 587200±221600 RLU in the control to 301100±18430 RLU and 257000±7175 RLU in the IC_{20} (0.51-fold, $p = 0.4206$) and IC_{50} (0.44-fold, $p = 0.3764$) respectively (Figure 4.8C). The gene expression of *TNF-α* was significantly decreased for both treatments at IC_{20} (0.4667±0.07474 RFC, $p = 0.0191$) and IC_{50} (0.4123±0.05053 RFC, $p = 0.0073$) treated MCF-7 cells respectively (Figure 4.8B). In contrast, the gene expression of *TNF-α* in MDA-MB-231 cells was significantly increased for both treatments at IC_{20} (12.88±0.2678 RFC, $p = 0.0143$) and IC_{50} (15.58±1.453 RFC, $p = 0.0633$) treatments respectively, compared to the control (Figure 4.8D).

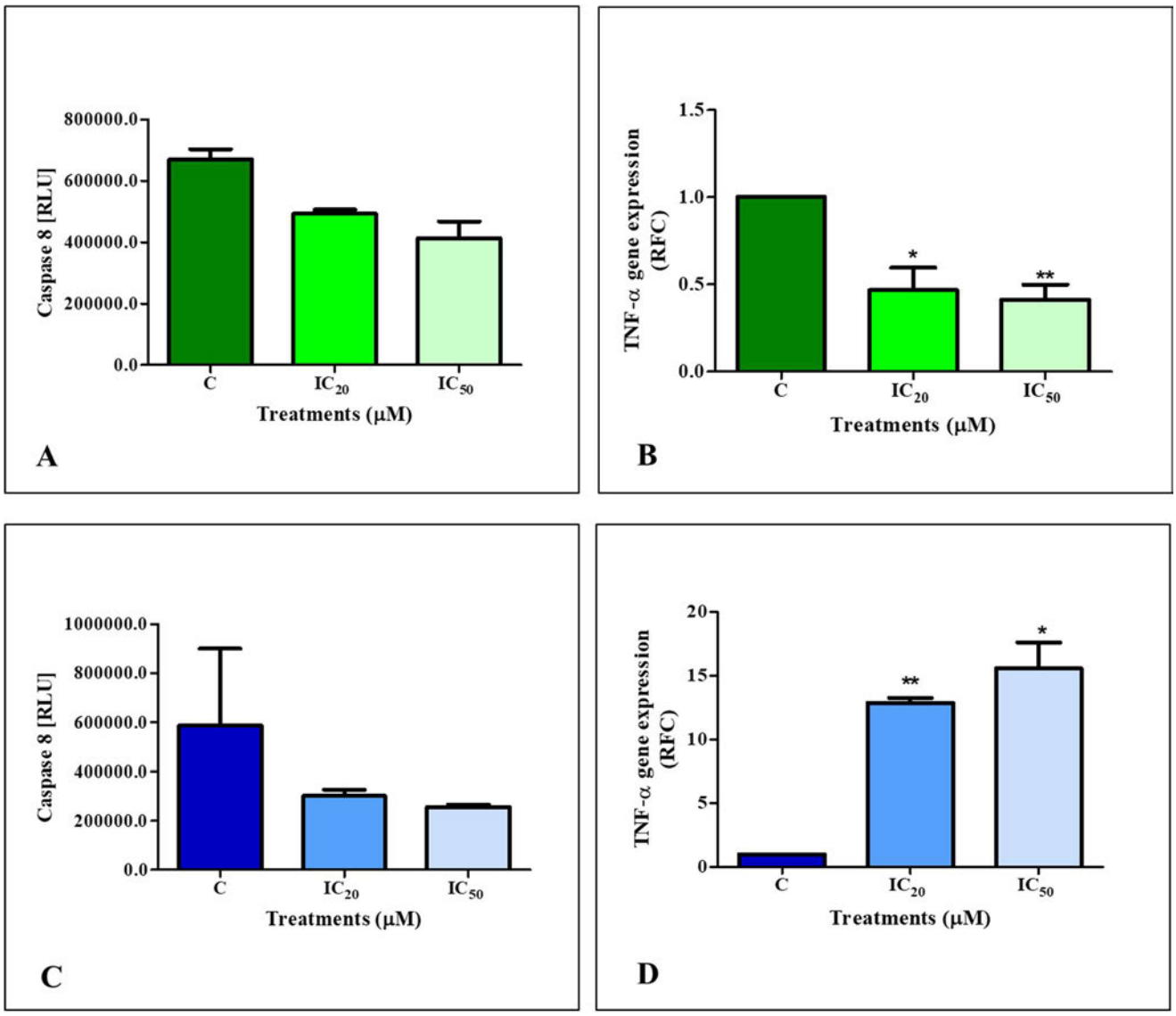

Figure 4.8: The effects of cyclen tetrahydrochloride on the extrinsic pathway of apoptosis induced by 48-hour treatment in MCF-7 and MDA-MB-231 cells. (A) Compared to the control, caspase 8 activity was downregulated in MCF-7 cells for IC_{20} and IC_{50} treatments. **(B)** Compared to the control, a reduction in TNF-α gene expression was observed in MCF-7 cells for both IC_{20} and IC_{50} treatments. **(C)** Cyclen tetrahydrochloride decreased caspase 8 activity in MDA-MB-231 cells for both treatments. **(D)** Upregulation of *TNF-α* gene expression was observed for both IC_{20} and IC_{50} treatments, compared to the control in MDA-MB-231 cells. [*/**, unpaired students *t*-test with Welch's correction]

4.8 INTRINSIC APOPTOSIS

The activity of caspase 9 was quantified using luminometry following 48-hour treatment with cyclen tetrahydrochloride to assess its effects on the intrinsic apoptosis pathway. The caspase 9 activity (Figure 4.9A) did not decrease significantly in any treatments in MCF-7 cells, IC_{20} 737700±3670 RLU (0.82-fold, p = 0.1671) and IC_{50} 765700±19220 RLU (0.85-fold, p = 0.2145), compared to the control (904500±44670 RLU). Similarly, when compared to the control 737400±86830 RLU, the caspase 9 activity decreased non-significantly in both treatments to 0.65-fold at IC_{20} (478800±73050 RLU, p = 0.2632) and to 0.42-fold at IC_{50} (308500±38010 RLU, p = 0.1385) in MDA-MB-231 cells (Figure 4.9B).

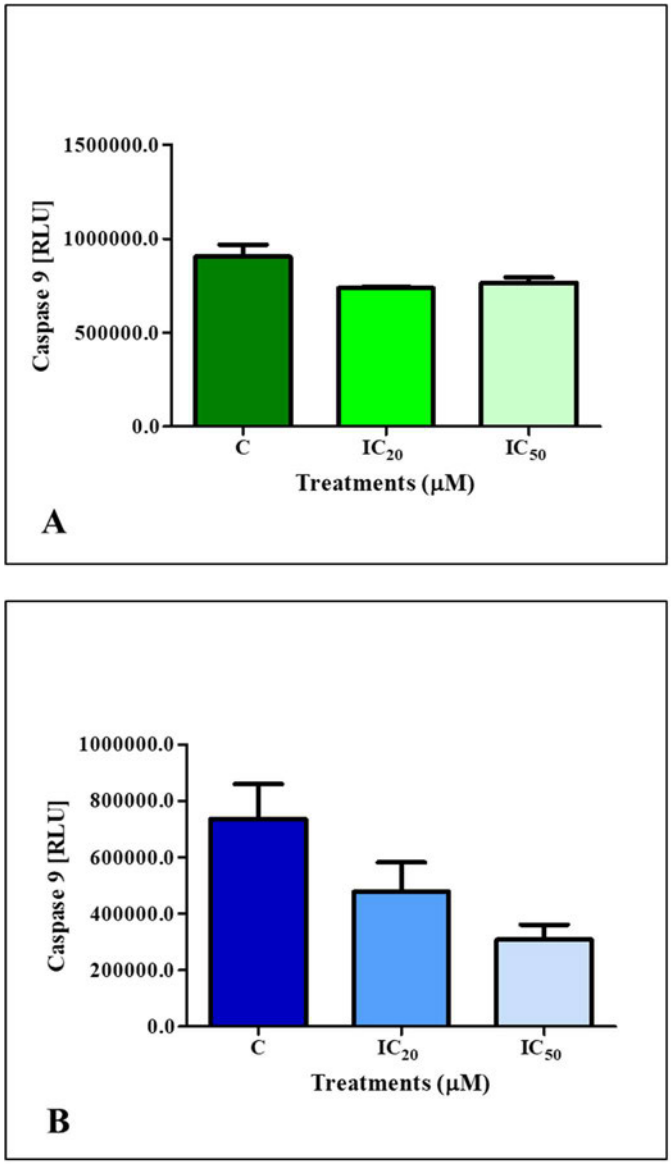

Figure 4.9: The effects of cyclen tetrahydrochloride on the intrinsic pathway of apoptosis induced by 48-hour treatment in MCF-7 and MDA-MB-231 cells. (A) A non-significant downregulation of caspase 9 activity was observed in MCF-7 cells for IC_{20} and IC_{50} treatments. **(B)** Caspase 9 activity decreased for both treatments, relative to the control in MDA-MB-231 cells.

4.9 EXECUTION OF APOPTOSIS

Caspase 3/7 activity and phosphatidylserine (PS) externalisation were quantified as an indication of apoptotic execution when exposed to cyclen tetrahydrochloride for 48 hours. The caspase 3/7 activity (Figure 4.10A) decreased non-significantly in IC_{20}-treated MCF-7 cells (0.51-fold, 89500±3999 RLU, p = 0.0594) but was increased to 1.36-fold in IC_{50}-treated cells (239400±107600 RLU, p = 0.6601), compared to the control (175600±6991 RLU). In MDA-MB-231 cells, the caspase 3/7 activity in both treatments remained relatively similar to the control (57260±5605 RLU), with only slight non-significant changes observed for IC_{20}-treated (1.1-fold, 62130±7811 RLU, p = 0.7015) and at IC_{50}-treated (0.95-fold, 54440±11600 RLU, p = 0.8627) cells (Figure 4.10C). In MCF-7 cells, PS externalisation was increased non-significantly for both IC_{20} (329400±49150 RLU, p = 0.2888) and IC_{50} (404900±83870 RLU, p = 0.2805) treatment, to 1.47-fold and 1.80-fold respectively, compared to control (224500±14130 RLU) (Figure 4.10B). The PS externalisation in MDA-MB-231 for both IC_{20} (132400±3994 RLU, p = 0.8262) and IC_{50} (119300±1456 RLU, p = 0.6372) treatments remained relatively close to the control (128400±14040 RLU).

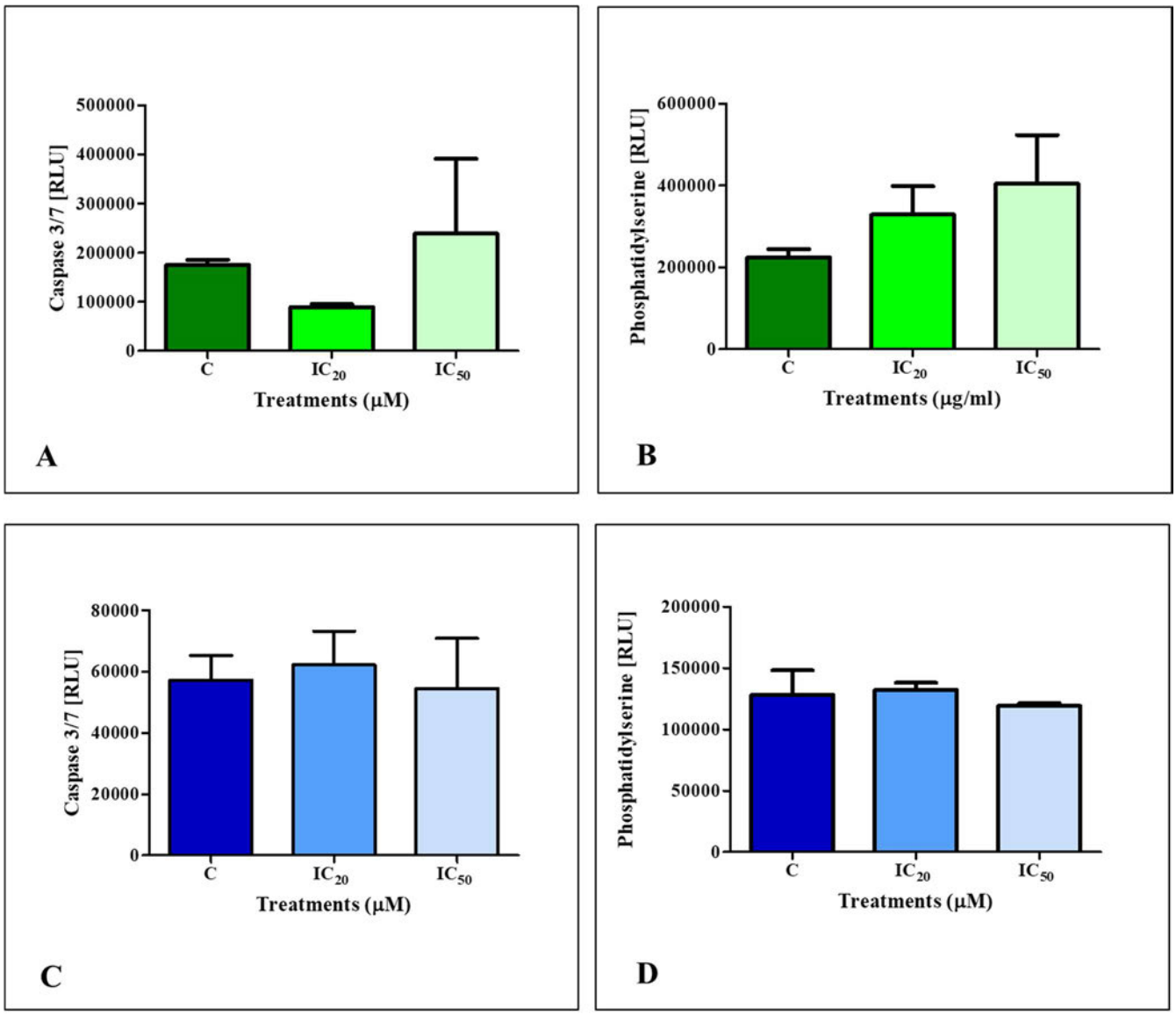

Figure 4.10: The effects of cyclen tetrahydrochloride on the execution of apoptosis induced by 48-hour treatment in MCF-7 and MDA-MB-231 cells. (A) Compared to the control, there was a non-significant downregulation of caspase 3/7 activity in MCF-7 cells for IC_{20} and a non-significant increase for IC_{50} treatments. **(B)** Compared to the control, there was a non-significant increase in PS externalisation in MCF-7 cells for IC_{20} and IC_{50} treatments. **(C)** Non-significant changes in caspase 3/7 activity for both treatments were similar to the control in MDA-MB-231 cells. **(D)** In MDA-MB-231 cells, the PS externalisation was non-significant and remained similar to control values.

4.10 CELL MEMBRANE DAMAGE ASSOCIATED CELL DEATH

Extracellular lactate dehydrogenase (LDH) was measured as an indicator of membrane integrity in both cell lines following 48-hour treatment with cyclen tetrahydrochloride using spectrometry. The Annexin V assay was used to quantify propidium iodide (PI), a DNA-binding dye, to determine the number of cells undergoing necrosis when exposed to cyclen tetrahydrochloride in both cell lines. In MCF-7 cells (Figure 4.11A), the LDH concentration was significantly increased in all treatments to 1.5-fold increments at IC_{20} (0.2347±0.01659 OD, p = 0.0391) and to 1.99-fold at IC_{50} (0.3017±0.01761 OD, p = 0.0140) respectively, compared to control (0.1517±0.003333 OD). The results for MDA-MB-231 showed a slight increase in LDH (Figure 4.11C) to 1.5-fold for IC_{20}-treated cells (0.2407±0.02206 OD, p = 0.0682) and a significant increase to 1.80-fold for the IC_{50} (0.2823±0.006119 OD, p = 0.0008) treatment, compared to the control (0.1570±0.006658 OD). The amount of propidium iodide dye detected in MCF-7 cells decreased non-significantly to 0.77-fold for the IC_{20} (269500±10600 RFU, p = 0.4379), but increased to 1.66-fold for IC_{50}-treated cells (584700±50480 RFU, p = 0.2189), compared to the control (351500±66530 RFU) (Figure 4.11B). In contrast, the amount of propidium iodide dye detected in MDA-MB-231 cells increased significantly for both IC_{20} (197800±16830 RFU, p = 0.0871) and IC_{50} (268400±9086 RFU, p = 0.0333) treatments, to 2.81-fold and 3.82-fold respectively when compared to the control (70310±4983 RFU) (Figure 4.11D).

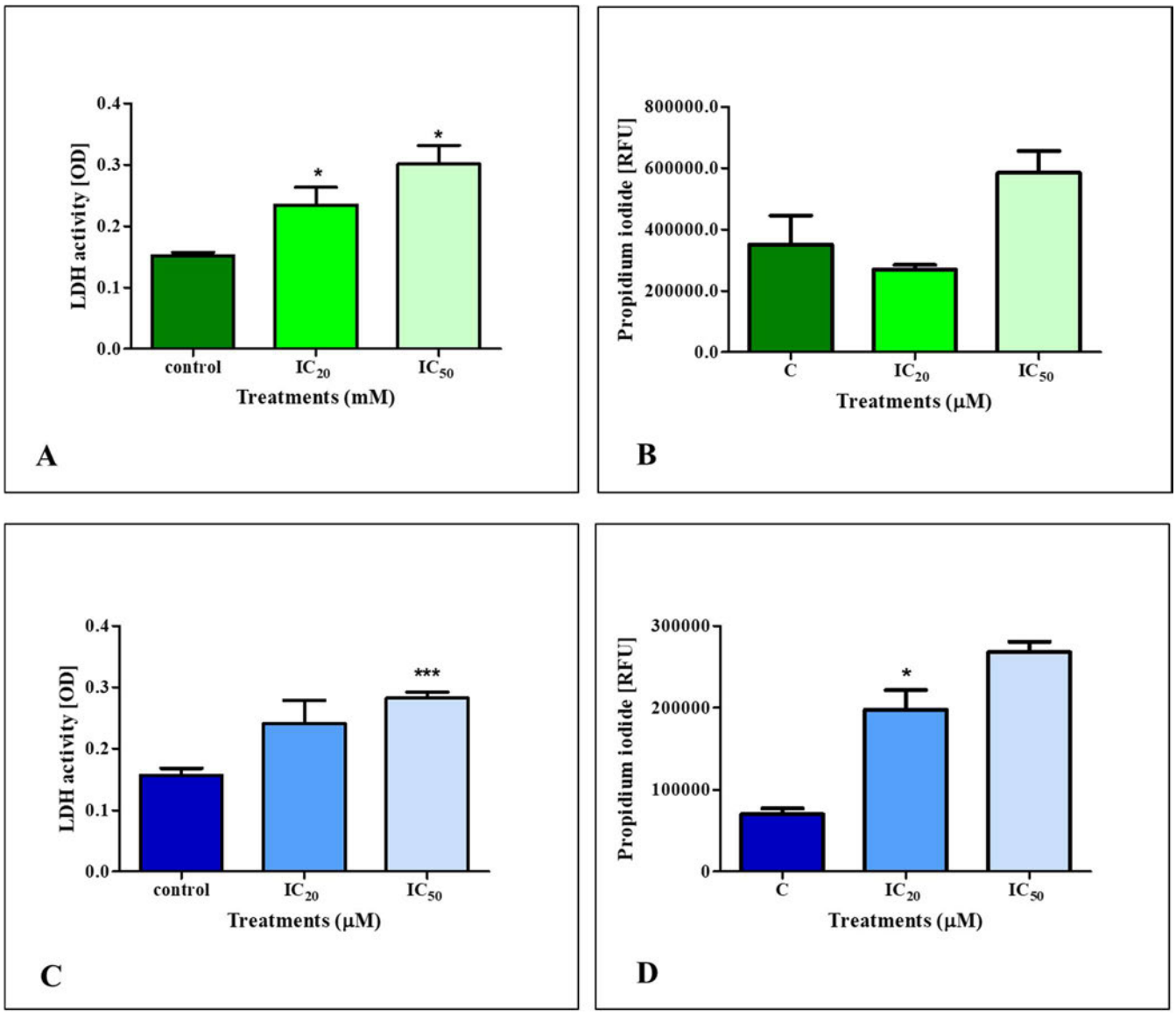

Figure 4.11: The effects of cyclen tetrahydrochloride on the cell membrane integrity in MCF-7 and MDA-MB-231 cells after 48-hour treatment. (A) The LDH concentration in MCF-7 cells increased for both treatments, compared to the control. **(B)** The amount of PI dye detected decreased in IC_{20}-treated cells, but increased for the IC_{50} treatment compared to control MCF-7 cells. **(C)** In MDA-MB-231 cells, the LDH activity increased in the IC_{20} and IC_{50} treatments compared to the control. **(D)** The amount of PI dye detected in MDA-MB-231 cells increased significantly for the IC_{20} and IC_{50} treatments relative to the control. [*/***, unpaired students *t*-test with Welch's correction]

4.11 NECROPTOSIS

The necroptotic elucidation was quantified by evaluating gene expression of necroptotic-associated proteins, *receptor-interacting serine-threonine kinase 1 (RIPK1), RIPK3*, and *mixed lineage kinase domain-like (MLKL)* using qPCR to determine the effects of cyclen tetrahydrochloride after 48-hour treatment. In Figure 4.12A in MCF-7 cells, *RIPK1* was significantly increased to 1.343±0.05371 RFC for the IC_{20} treatment ($p = 0.0237$) and non-significantly decreased to 0.5834±0.1430 RFC for the IC_{50} treatment ($p = 0.1002$), compared to the control. In MDA-MB-231 cells, *RIPK1* gene expression increased for IC_{20} (6.306±0.04371 RFC, $p = 0.0052$) and IC_{50} (6.744±0.1402 RFC, $p = 0.0155$) treatments, relative to the control (Figure 4.12D). The gene expression of *RIPK3* in MCF-7 cells was non-significantly increased for both treatments at IC_{20} (1.501±0.1965 RFC, $p = 0.2380$) and IC_{50} (1.338±0.1157 RFC, $p = 0.2097$) respectively, compared to the control (Figure 4.12B). In contrast, the gene expression of *RIPK3* in MDA-MB-231 cells significantly increased compared to the control for both treatments at IC_{20} (9.264±0.8243 RFC, $p = 0.0098$) and IC_{50} (28.52±2.006 RFC, $p = 0.0053$) treatments respectively (Figure 4.12E). In MCF-7 cells, cyclen tetrahydrochloride non-significantly increased the gene expression of *MLKL* at IC_{20} (3.344±0.8066 RFC, $p = 0.2110$) and IC_{50} (2.868±0.03976 RFC, $p = 0.0135$) treated cells relative to the control (Figure 4.12C). In Figure 4.12F, cyclen tetrahydrochloride treatment induced significant increases in *MLKL* gene expression relative to control levels, to 5.734±0.4561 RFC at the IC_{20} ($p = 0.0612$) and 12.19±0.3868 RFC at the IC_{50} ($p = 0.0012$).

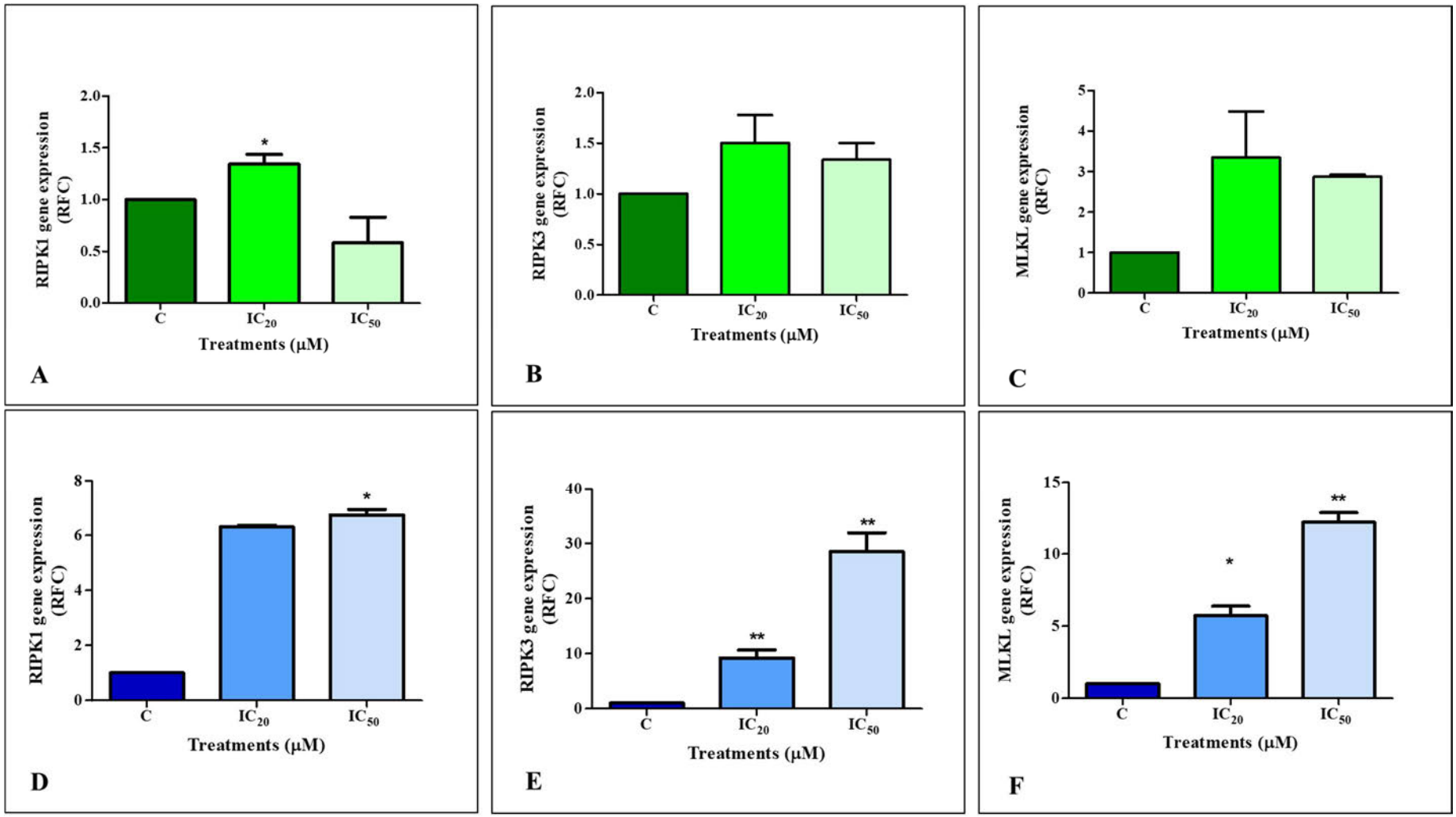

Figure 4.12: The expression of necroptosis-related genes induced by cyclen tetrahydrochloride in MCF-7 and MDA-MB-231 cells after 48-hour exposure. (A) The *RIPK1* gene expression increased for IC_{20}, but decreased for IC_{50} treatments, compared to the MCF-7 control. **(B)** Upregulated *RIPK3* gene expression was observed for both treatments in MCF-7 cells relative to the control. **(C)** Non-significant increases in *MLKL* gene expression were noted in MCF-7 cells for both treatments compared to the control. **(D)** Compared to the control, the RIPK1 gene expression increased for IC_{20} and IC_{50}-treated MDA-MB-231. **(E)** Upregulated *RIPK3* gene expression was observed in MDA-MB-231 cells for both treatments relative to the control. **(F)** Increased *MLKL* gene expression was observed in MDA-MB-231 cells for both treatments, compared to the control [*/**, unpaired students *t*-test with Welch's correction]

CHAPTER 5: DISCUSSION

Globally, cancer remains a clinical burden, mainly due to the unpredictable nature of the disease (Feng *et al.*, 2018). Breast cancer (BC) is a heterogeneous disease, and its pathogenesis and treatments are subtype-specific depending on the presence of female hormone receptors (Feng *et al.*, 2018). Breast cancer is ranked 2nd and 5th in terms of incidence and mortality, respectively, worldwide (Arnold *et al.*, 2022). By 2040, the projected rates are expected to increase to approximately 3 million diagnosed cases and 1 million deaths (Arnold *et al.*, 2022; Momenimovahed and Salehiniya, 2019). The breast cancer statistics are not much better in South Africa, where a 3-5% increase in incidence is recorded each year (Arnold *et al.*, 2022; Momenimovahed and Salehiniya, 2019). The survival rates associated with BC are higher compared to other cancers; however, due to the proximity of the breast tissue and lymphatic system, the risk for recurrence and metastasis potential is increased (Feng *et al.*, 2018). These risk factors, amongst other intrinsic/extrinsic factors, contribute to unforeseeable disease prognosis and progression despite many advances in conventional therapies such as surgery, radiation, antibodies, and systemic therapy (Malik *et al.*, 2022; Feng *et al.*, 2018). Therefore, research towards novel and conservative treatment is necessary. Recently, metal chelators have shown efficacy for the treatment of cancer. Cyclen tetrahydrochloride has shown promise as a ligand with a high binding affinity towards transition metals like iron (Fe), cobalt (Co), copper [Cu(II)] and zinc [Zn(II)], and may therefore exert anti-proliferative effects in cancer cells (Pubchem, 2024; Timoshnikov *et al.*, 2022; Aldrich, 2020; Lejault *et al.*, 2019; Reibenspies and Anderson, 1990). This is the first study to investigate the biochemical mechanism of cyclen tetrahydrochloride on human ER-positive (MCF-7) and ER-negative (MDA-MB-231) BC cells.

To prevent adverse drug-drug interactions, new drugs or treatment candidates are routinely tested for their ability to inhibit cytochrome p450 3A4 (CYP3A4), due to its critical function in drug metabolism (Promega, 2016; Basheer and Kerem, 2015; Cali *et al.*, 2009). Metabolic transformation predominantly occurs in the liver once the intestine has digested and absorbed compounds. The overexpression of CYP3A4 limits the bioavailability, increases toxicity, and reduces the therapeutic effect of the treatment compounds (Kehinde *et al.*, 2021; Promega, 2016). In this study, cyclen tetrahydrochloride decreased the activity of CYP3A4 in both cell lines (Figure 4.1 A and B), suggesting downregulation of phase I oxidative metabolism and limiting biotransformation or bioactivation. However, cyclen tetrahydrochloride is a chelator, and binding divalent metal cations in the bloodstream or by phase 2 detoxification involving GSH and glutathione-S-transferase could facilitate its filtration through the kidneys and excretion via urine (Sun *et al.*, 2021). Nevertheless, downstream data suggests that cyclen

tetrahydrochloride remained as its active parent compound at a concentration that enabled it to exert its biochemical effects in the BC cells; there is evidence to suggest that this would ultimately improve the drug's therapeutic effects (Kehinde *et al.*, 2021). In addition, combination therapy with known chemotherapeutics could result in enhanced outcomes since optimal drug plasma concentrations could be maintained (Kehinde *et al.*, 2021).

The metabolic viability of cells is dependent on mitochondrial integrity and energy metabolism. The mitochondria house the centre of oxidative phosphorylation to ensure that ATP is produced to promote cell viability and survival (Yong *et al.*, 2019). This study observed a loss of cell viability for both MCF-7 and MDA-MB-231 cell lines (Figure 4.2 A and B), with IC_{50} concentrations of 169µM and 561µM, respectively. The lower IC_{50} in MCF-7 cells suggests that these cells were more sensitive to the cyclen tetrahydrochloride treatment. It's important to note that the loss of cell viability occurred even though MCF-7 cells are ER-positive, and binding of estrogen would stimulate growth; phenol red in the culture medium is a weak estrogen which could bind ER in MCF-7 cells to increase proliferation (Berthois *et al.*, 1986). Previous research indicates that the two ERs have contrasting metabolic effects (Miziak *et al.*, 2023). Estrogen positive (ER+) BC mimics the characteristics of ERα and allows for increased cell proliferation by promoting the actions of adaptive proteins, tyrosine kinase (SRC) and phosphoinositide 3-kinases (PI3K), which trigger growth factor transcription (Miziak *et al.*, 2023). Estrogen receptor -β (ERβ) opposes the actions of ERα, but the metabolic pathway affected is inconclusive thus far (Miziak *et al.*, 2023; Feng *et al.*, 2018).

Loss of cell viability reflects decreased MTT reduction to formazan, usually accomplished by mitochondrial succinate dehydrogenase (SDH) and NADPH-dependent oxidoreductases in the cytosol (Yong *et al.*, 2019). Thus, decreased cell viability (Figure 4.2 A and B) could imply decreased SDH, consequently minimising the oxidation of succinate to fumarate in the Krebs cycle and the flow of electrons via complex II in the electron transport chain (ETC) (Li *et al.*, 2016). Succinate dehydrogenase may also trigger the reverse flow of electrons through complex I, allowing for NADH production (Tretter *et al.*, 2016). The data suggests that SDH inhibition by cyclen tetrahydrochloride was mediated by iron (Fe) chelation; iron-sulphur (FeS) clusters are essential for electron transfer through complex II of the ETC and are therefore important for mitochondrial function and energy production (Lee and Roh, 2023; Hsu *et al.*, 2020). The sequestering of Fe by cyclen tetrahydrochloride would thus inhibit the formation of FeS clusters and minimise electron flow in the ETC, decreasing ATP production and triggering the

observed decrease in cell viability. According to Flora *et al*. (2008), metal chelators such as calcium disodium ethylenediamine tetraacetic acid ($CaNa_2EDTA$) compromise the function of SDH activity due to high affinity for thiol groups within iron-containing proteins and enzymes (Kontoghiorghes and Kontoghiorghe, 2020; Flora *et al.*, 2008). Interestingly, 1,4,7,10-tetraazacyclododecane (DMC), a derivative of cyclen, inhibited cell growth in HeLa and A459 cells after a 72-hour treatment and attributed to DMC being a stable metal chelator (Yang *et al.*, 2007).

A decrease in cell viability is often associated with reduced ATP levels since cells rely on ATP for various biochemical reactions involved in cell maintenance (Yong *et al.*, 2019). In this study, cyclen tetrahydrochloride decreased ATP (Figure 4.3 A and C) for both cell lines, which is consistent with decreased cell viability (Figure 4.1). Interestingly, research has shown that certain metal ions can inhibit the function of Na^+/K^+-ATPase and Mg^{2+}-ATPase. Thus, chelation of these metals would restore function and enhance ATP catabolism, contributing to the depleted ATP in this study (Krstić *et al.*, 2005). Moreover, the reduction in ATP levels is tied to a decrease in $\Delta\Psi m$ (Figure 4.3 B and D). This is because the $\Delta\Psi m$ is established by the proton pump in complexes I, III, and IV in the ETC, and the energy in this electrochemical gradient is used to make ATP (Neupane *et al.*, 2019; Zorova *et al.*, 2018). The result implies dysfunction of the mitochondrial ETC, possibly through cyclen tetrahydrochloride chelation of Fe. This will interfere with the ETC by disrupting the flow of electrons, dissipating the proton gradient generated by complexes I, III and IV and consequently preventing ATP production (Petronek *et al.*, 2019). Ultimately, the decreased $\Delta\Psi m$ indicates that the ETC was hampered, disrupting the proton gradient, and causing leakage of electrons. Similarly, Tian *et al.* (2017) investigated a half-sandwich ruthenium(II) complex with an N-N-chelated imino-pyridyl ligand as an anti-cancer agent, concluding ROS-mediated disruption of the $\Delta\Psi m$ causing cell death in A549 cancer cells (Li *et al.*, 2021; Tian *et al.*, 2017).

Decreased $\Delta\Psi m$ has the potential to uncouple reactions of oxidative phosphorylation and produce ROS. Indeed, the susceptibility of metals like Fe, Zn(II), magnesium and Cu(II) for chelation by cyclen tetrahydrochloride may account for uncoupling oxidative phosphorylation and depolarisation of the electrochemical gradient, with subsequent influx of calcium that may generate ROS (Gulcin and Alwasel, 2022; Timoshnikov *et al.*, 2022). Unpaired electrons leaked from complexes I and III reduce oxygen molecules in the mitochondria into superoxide anions ($O_2^{\bullet-}$), thus generating the first reactive oxygen species (ROS) (Berry *et al.*, 2018). The $O_2^{\bullet-}$ is the precursor for other ROS and RNS associated with

oxidative stress (Arfin *et al.*, 2021; Berry *et al.*, 2018); $O_2^{\bullet-}$ can be dismutated to the non-radical ROS, hydrogen peroxide (H_2O_2), or react with nitric oxide (NO) to form peroxynitrite ($OONO^-$) (Berry *et al.*, 2018). Nitric oxide is produced by three isoforms of nitric oxide synthase (NOS); this study focused on the effects of inducible NOS (iNOS) (Kashfi *et al.*, 2021). The ROS/RNS interacts with lipids, protein and DNA; lipid peroxidation occurs when hydrogen is abstracted from polyunsaturated fatty acids (PUFAs) in cell membranes by ROS/RNS and is a biomarker of oxidative stress (Recknagel *et al.*, 2020).

In this study, cyclen tetrahydrochloride induced increased ROS and RNS that interacted with lipids to induce lipid peroxidation as indicated by the increased MDA concentration in MCF-7 and MDA-MB-231 cells (Figure 4.4 A and C); MDA is an end-product of lipid peroxidation (De Leon and Borges, 2020; Recknagel *et al.*, 2020). Nitrosative stress was evident for the MDA-MB-231 cells (Figure 4.5 F) but not for MCF-7 cells (Figure 4.5 C), and it agrees with the relative changes for iNOS (Figure 4.5 B and E). The *OGG1* gene expression was also significantly increased (Figure 4.4 B and D), possibly in response to increased DNA oxidation by ROS or damage induced by the products of lipid peroxidation (Recknagel *et al.*, 2020; Wang *et al.*, 2018b). The upregulated gene expression *OGG1* results in the increased transcription of OGG1 repair protein via the BER pathway by excision of 8-oxoG from the mitochondrial genome (Wang *et al.*, 2018b). A study conducted by Mcoyi *et al*. (2020) elucidated that 1,4,7-triazacyclononane (TACN), a metal chelator, caused minimal oxidative damage in HepG2 cells since TACN may have sequestered essential metals from the Fenton reaction to decrease the production of hydroxyl radicals and MDA was reduced (Mcoyi *et al.*, 2020).

Increased ROS/RNS are counteracted by antioxidants, which neutralise ROS to prevent oxidative stress. The dismutation of $O_2^{\bullet-}$ to H_2O_2 is accomplished by superoxide dismutase (SOD2) (Hayes *et al.*, 2020). The unaffected SOD2 in MCF-7 (Figure 4.6 A) cells and downregulation in MDA-MB-231 cells (Figure 4.7 A) by cyclen tetrahydrochloride suggests that less H_2O_2 was formed, and $O_2^{\bullet-}$ would be shunted to RNS production. Thus, the observed lipid and DNA oxidation (Figure 4.4) would be attributed to $O_2^{\bullet-}$ and $ONOO^-$. The low intracellular GSH and increased *Gpx-1* (Figure 4.6 B and C) in MCF-7 cells suggest that the antioxidant system was recruited to repair lipid damage, and replenishment of GSH was associated with upregulation of *Gpx-1*. However, the decrease in Nrf2 (Figure 4.6 D) conflicts with this observation in MCF-7. Interestingly, cyclen tetrahydrochloride downregulated *Gpx1* in MDA-MB-231 cells, correlating with depleted GSH and downregulation of Nrf2 (Figure 4.7 B, C and D). The targeting of the cell membrane by ROS and RNS decreased capacity for repair, which culminates in the loss of

membrane integrity and causes irreversible cellular damage (Recknagel *et al.*, 2020). This may account for the loss of cell viability (Figure 4.2) and the extracellular lactate dehydrogenase (LDH) induced by cyclen tetrahydrochloride in this study (Figure 4.11 A and C). In contrast, previous research indicates that chelating agent ferrozine can form α-bonds with metal ions, predominantly Fe, thereby forming complexes that act as secondary antioxidants which can reduce redox potential by stabilising oxidised metal ions (Gulcin and Alwasel, 2022; Karawita *et al.*, 2005; Gordon, 1990). Ultimately, the oxidative injury induced by cyclen tetrahydrochloride suggests inadequate response by antioxidants and resultant oxidative stress that may trigger cellular responses that commit the MCF-7 and MDA-MB-231 cells to die by apoptosis or necrosis (Ibrahim and O'Sullivan, 2020).

The NF-κB pathway plays a crucial role in the cellular response to oxidative stress, demonstrating both anti- and pro-oxidant potential (Kim *et al.*, 2019). This study increased *NF-κB* expression significantly for MDA-MB-231 cell line and non-significantly for MCF-7 cells (Figure 4.5 A and D). Upregulated NF-κB is known to stimulate the transcription and activation of cytokines such as interlukin-1 (IL-1) or tumour necrosis factor (TNF), thereby inducing a chronic inflammatory state, membrane blebbing and apoptotic body formation that may be associated with apoptosis or necrosis (Kim *et al.*, 2019; Speranza *et al.*, 2007). The results revealed contrasting effects for *TNF-α*; its expression was significantly downregulated in MCF-7 (Figure 4.8 B) and upregulated considerably in MDA-MB-231 cell line (Figure 4.8 D). Tolouian *et al.* (2023) indicated that the metal chelator, cisplatin, induced ROS generated apoptosis by increasing genes associated with extrinsic apoptosis, such as TNF-α, and facilitated Bak/Bax activation in kidney cells (Tolouian *et al.*, 2023). These findings contradict the results in this study since caspase 8 (Figure 4.8 A and C) was downregulated in both cell lines and *TNF-α* was downregulated in MCF-7 (Figure 4.8 B), suggesting that extrinsic apoptosis did not occur. Interestingly, apoptosis was not induced via the intrinsic pathway as caspase 9 decreased (Figure 4.9 A). However, increased caspase 3/7 (Figure 4.10 A) and externalised phosphatidylserine (Figure 4.10 B) suggest that apoptosis was executed in MCF-7 cells. According to preliminary study conducted by Yang *et al*. (2007), DMC was the first macrocyclic polyamine to induce apoptosis in HeLa cells effectively; however, the mechanism of action still needs to be investigated further (Yang *et al.*, 2007).

Past literature has often denoted necrosis as an undesirable therapeutic pathway since its uncontrolled and unregulated processes (Kim *et al.*, 2019). However, accumulating evidence infers that necrotic cell death is carried out by complex signal transduction pathways and execution mechanisms (Gong *et al.*,

2019; Berghe *et al.*, 2010). According to Kim *et al*. (2019), pathways of programmed necrosis such as necroptosis, pyroptosis, and ferroptosis are inherently more immunogenic than their apoptotic counterpart (Kim *et al.*, 2019). This is due to the ability to support homeostasis and immunity by releasing inflammatory cytokines and danger-associated molecular patterns (DAMPs), changing the micro-environment towards a pro-inflammatory state (Kim *et al.*, 2019). This study revealed that the MCF-7 cell line had increased necrotic (Figure 4.11 B) and apoptotic cells (Figure 4.10 B) that can be associated with necroptosis (Figure 4.12 A, B and C). In contrast, only necrotic activity was evident in MDA-MB-231 cells, inferring necrosis (Figure 4.11 D) (Khorsandi *et al.*, 2017).

According to Vercammen *et al*. (1998), necroptosis was first reported in a seminal study wherein inhibition of caspase 8 sensitised fibroblasts to TNF-α-induced necrotic death (Kim *et al.*, 2019; Vercammen *et al.*, 1998). This correlates with decreased caspase 8 activity and *TNF-α* (Figure 4.8) induced by cyclen tetrahydrochloride for MCF-7 and MDA-MB-231 cells. Necroptosis is dependent on receptor-interacting protein kinase 1 (RIPK1), RIPK3 and mixed lineage kinase domain-like (MLKL) proteins to carry out its actions of cell death (Yang *et al.*, 2023). When caspase 8 is absent, it requires the formation of a necrosome produced by the RIPK1/RIPK3 complex assembly. The auto- and trans-phosphorylation of RIPK1 and RIPK3 enable recruitment and activation of MLKL, followed by oligomerisation, thus leading to plasma membrane insertion that is associated with phosphatidylinositol phosphates and disrupts the plasma membrane integrity (Kim *et al.*, 2019). The RIPK1/RIPK3 complex also facilitates mitochondrially derived ROS production, reinforcing the necrosome's stability (Kim *et al.*, 2019). Once the plasma membrane is disrupted, the cell is flagged with necroptotic cell death, displaying typical lytic morphology similar to primary necrosis (Kim *et al.*, 2019; Gong *et al.*, 2019; Berghe *et al.*, 2010). Besides the RIPK1/RIPK3 complex, TNF-α and TNF-receptor can bind to RIPK1 and stimulate the recruitment of TNFR1-associated death domain (TRADD), a cellular inhibitor of apoptosis proteins 1/2 (cIAP1/2) and TNF receptor-associated factor 2/5 (TRAF2/5) that forms complex I (Kim *et al.*, 2019; Gong *et al.*, 2019). Activated complex I will recruit FADD to form complex II and carry out apoptosis in the presence of caspase activity (Gong *et al.*, 2019).

In this study, cyclen tetrahydrochloride decreases in *TNF-α* expression and caspase 8 activity is associated with increased *RIPK1, RIPK3* and *MLKL* (Figure 4.12) for both cell lines. However, the increase in *RIPK3* (Figure 4.12 B) in the IC_{50}-treated MCF-7 cells is associated with downregulated *RIPK1* (Figure 4.12 A). However, *MLKL* was still upregulated (Figure 4.12 C) and is associated with

cell membrane rupture implied by LDH externalisation in this study (Figure 4.11 A). Thus, cyclen tetrahydrochloride induced ROS-mediated necroptosis within the MCF-7 cell line. The MDA-MB-231 cells were unable to overcome the nitrosative stress as indicated by increased oxidants (Figure 4.5 E and F), decreased antioxidants (Figure 4.7) and upregulated *NF-κB* (Figure 4.5 D) and *TNF-α* (Figure 4.8 D), thus RNS-mediated necroptosis (Figure 4.12 D, E and F) was induced by cyclen tetrahydrochloride treatment in MDA-MB-231 cells.

CHAPTER 6: CONCLUSION

Breast cancer is a fear that all women face globally, and its persistent top ranking for incidence and mortality, as well as projected statistics, do little to alleviate this fear. Moreover, the debilitating side effects associated with current treatment options translate to decreased quality of life. It is, therefore, imperative that novel therapeutics are investigated. This study investigated the effects of a synthetic metal chelating compound, 1,4,7,10-tetraazacyclododecane (cyclen) tetrahydrochloride in MCF-7 and MDA-MB-231 cells.

The findings of this study are summarised in Figure 6.1. Cyclen tetrahydrochloride decreased cell viability in both MCF-7 and MDA-MB-231 cells, coupled with decreased ATP production and $\Delta\Psi m$, possibly demonstrating mitochondrial dysfunction. The MCF-7 cells experienced oxidative stress, which was implied by oxidative DNA damage and lipid peroxidation that correlated with LDH leakage and diminished antioxidant defence; GSH, SOD2, and Nrf2 were decreased. Also, RNS was reduced. The increased necrosis and execution of apoptosis despite a seeming lack of initiation (caspase 8 and caspase 9 decreased) suggested cell death via necroptosis. Indeed, *MLKL, RIPK1* and *RIPK3* were upregulated despite downregulated *TNF-α*, concluding that cyclen tetrahydrochloride induced ROS-mediated necroptotic cell death in MCF-7 cells. The MDA-MB-231 cells yielded similar results but were unable to overcome the nitrosative stress induced by cyclen tetrahydrochloride treatment. This was implied by the upregulated expression of *NF-κB* associated with increased iNOS and NO production, thereby resulting in *TNF-α* upregulation and increased necrosis. Thus, MDA-MB-231 incurred necroptotic cell death induced by nitrosative stress in cyclen tetrahydrochloride treated cells.

The contrasting effects may be attributed to the estrogen receptor (ER) effects on cellular metabolism; MCF-7 cells are estrogen-positive, while MDA-MB-231 cells are estrogen-negative. Both the null hypothesis and alternative hypothesis were rejected since the study showed that the subtype specific cell lines had varying responses to stress-induced cell death mechanisms. Some limitations exist due to the constraints of this study's time, funding, research design, materials, quality of the cultured cells, methodology, generalisation of results and lack of relevant prior literature, which may have impacted the concluding findings. Therefore, the mechanisms require more specific research, and effects on normal cell lines need to be investigated. Future studies should also consider a time-dependent approach to

evaluate cyclen tetrahydrochloride's unclear cytotoxic effects, oxidant, and antioxidant nature. These studies can include the use of *in vivo* animal models to determine the precise mechanism of action.

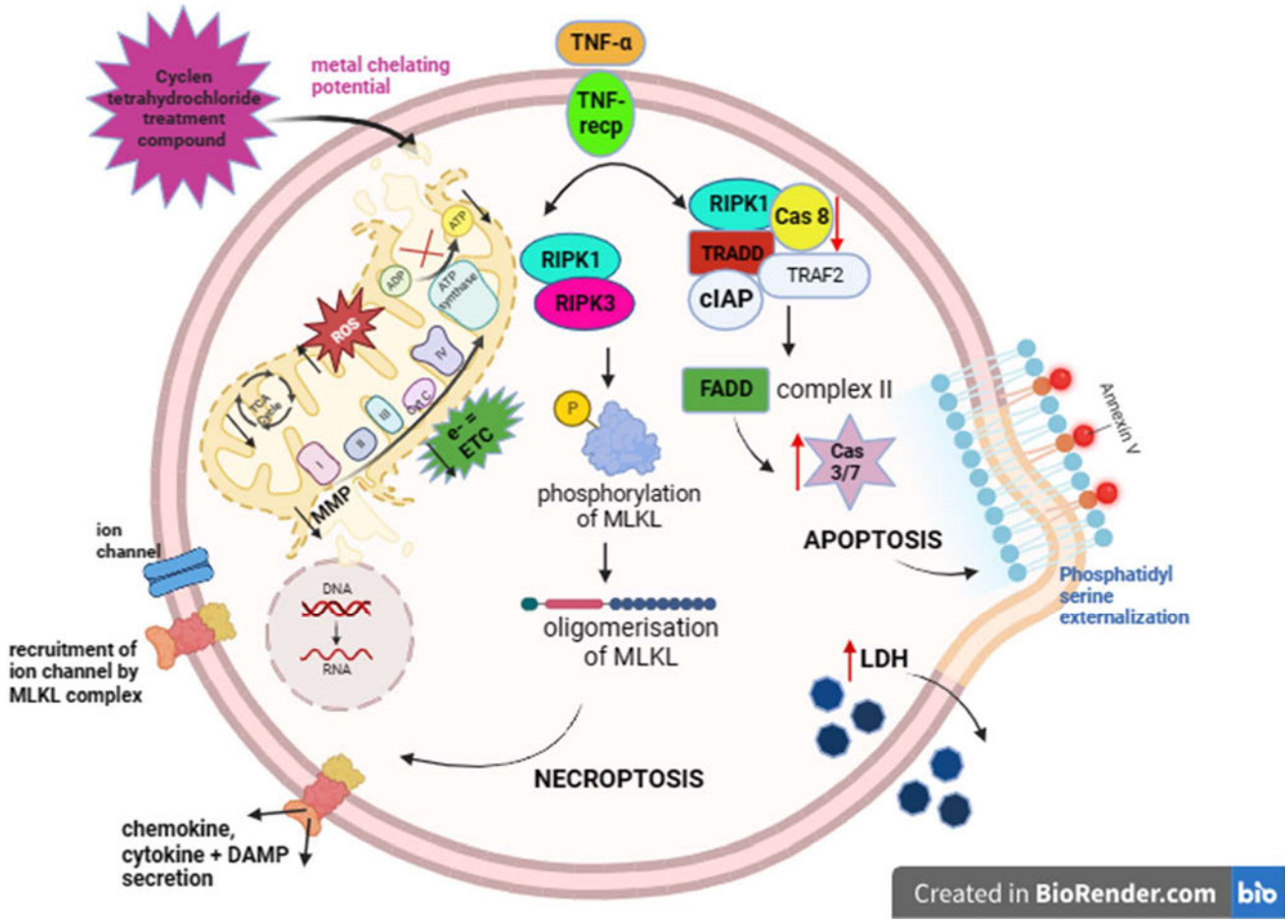

Figure 6.1: The schematic overview of the biochemical effects of cyclen tetrahydrochloride on oxidative stress, nitrosative stress, apoptosis, and necroptosis in MCF-7 and MDA-MB-231 cells (Prepared by author, 2024).

REFERENCES

ALDRICH, S. 2020. Cyclen tetrahydrochloride. *webpage*.

ANDELE, K. J. D. 2020. *BIOINSPIRED NANODRUGS FOR CANCER THERAPY.* Università Ca'Foscari Venezia.

ARFIN, S., JHA, N. K., JHA, S. K., KESARI, K. K., RUOKOLAINEN, J., ROYCHOUDHURY, S., RATHI, B. & KUMAR, D. 2021. Oxidative stress in cancer cell metabolism. *Antioxidants,* 10**,** 642.

ARNOLD, M., MORGAN, E., RUMGAY, H., MAFRA, A., SINGH, D., LAVERSANNE, M., VIGNAT, J., GRALOW, J. R., CARDOSO, F. & SIESLING, S. 2022. Current and future burden of breast cancer: Global statistics for 2020 and 2040. *The Breast,* 66**,** 15-23.

ASLANTÜRK, Ö. S. 2018. In vitro cytotoxicity and cell viability assays: principles, advantages, and disadvantages. *Genotoxicity-A predictable risk to our actual world,* 2**,** 64-80.

BARREIRO, E. 2016. Role of protein carbonylation in skeletal muscle mass loss associated with chronic conditions. *Proteomes,* 4**,** 18.

BASHEER, L. & KEREM, Z. 2015. Interactions between CYP3A4 and dietary polyphenols. *Oxidative medicine cellular longevity,* 2015.

BERGHE, T. V., VANLANGENAKKER, N., PARTHOENS, E., DECKERS, W., DEVOS, M., FESTJENS, N., GUERIN, C., BRUNK, U., DECLERCQ, W. & VANDENABEELE, P. 2010. Necroptosis, necrosis and secondary necrosis converge on similar cellular disintegration features. *Cell Death*

Differentiation, 17**,** 922-930.

BERRY, B. J., TREWIN, A. J., AMITRANO, A. M., KIM, M. & WOJTOVICH, A. P. 2018. Use the protonmotive force: mitochondrial uncoupling and reactive oxygen species. *Journal of molecular biology,* 430**,** 3873-3891.

BERTHOIS, Y., KATZENELLENBOGEN, J. A. & KATZENELLENBOGEN, B. S. 1986. Phenol red in tissue culture media is a weak estrogen: implications concerning the study of estrogen-responsive cells in culture. *Proceedings of the National Academy of Sciences,* 83**,** 2496-2500.

BHOO-PATHY, N., HARTMAN, M., YIP, C.-H., SAXENA, N., TAIB, N. A., LIM, S.-E., IAU, P., ADAMI, H.-O., BULGIBA, A. M. & LEE, S.-C. 2012. Ethnic differences in survival after breast cancer in South East Asia. *PLoS One,* 7**,** e30995.

BISTONI, G. & FARHADI, J. 2015. Anatomy and physiology of the breast. *Plastic Reconstructive Surgery: Approaches Techniques,* 31**,** 477-485.

BOLIGON, A. A., MACHADO, M. M. & ATHAYDE, M. L. J. M. C. 2014. Technical evaluation of antioxidant activity. 4**,** 517-522.

BUTTERICK, T. A., DUFFY, C. M., LEE, R. E., BILLINGTON, C. J., KOTZ, C. M. & NIXON, J. P. 2014. Use of a caspase multiplexing assay to determine apoptosis in a hypothalamic cell model. *Journal of visualized experiments: JoVE*.

CALI, J. J., MA, D., SOBOL, M., SIMPSON, D. J., FRACKMAN, S., GOOD, T. D., DAILY, W. J., LIU, D. J. E. O. O. D. M. & TOXICOLOGY 2006. Luminogenic cytochrome P450 assays. 2**,** 629-645.

CALI, J. J., SOBOL, M., MA, D., UYEDA, H. T. & MEISENHEIMER, P. 2009. CYP3A4 P450-Glo® Assays with Luciferin-IPA: The Most Sensitive and Selective Bioluminescent CYP3A4 Assay. *Promega Corporation*.

CERVELLO, M., EMMA, M. R., AUGELLO, G., CUSIMANO, A., GIANNITRAPANI, L., SORESI, M., AKULA, S. M., ABRAMS, S. L., STEELMAN, L. S. & GULINO, A. 2020. New landscapes and horizons in hepatocellular carcinoma therapy. *Aging,* 12**,** 3053.

CHHIKARA, B. S. & PARANG, K. 2023. Global Cancer Statistics 2022: the trends projection analysis. *Chemical Biology Letters,* 10**,** 451-451.

CHOW, W.-H., DONG, L. M. & DEVESA, S. S. 2010. Epidemiology and risk factors for kidney cancer. *Nature Reviews Urology,* 7**,** 245-257.

CIRERA, S. & BUSK, P. K. 2014. Quantification of miRNAs by a simple and specific qPCR method. *RNA Mapping: Methods Protocols***,** 73-81.

COLLELUORI, G., PERUGINI, J., BARBATELLI, G. & CINTI, S. 2021. Mammary gland adipocytes in lactation cycle, obesity and breast cancer. *Reviews in Endocrine Metabolic Disorders,* 22**,** 241-255.

CREE, I. A. 2011. Principles of cancer cell culture. *Cancer Cell Culture: Methods Protocols***,** 13-26.

DAMIANI, E. & WALLACE, H. M. 2018. Polyamines and cancer. *Polyamines***,** 469-488.

DE LEON, J. A. D. & BORGES, C. R. 2020. Evaluation of Oxidative Stress in Biological Samples Using the Thiobarbituric Acid Reactive Substances Assay. *JoVE***,** e61122.

DHANALAKSHMI, M. & ANANDATHANGADURAI, S. 2020. Evaluation Of Anticancer Effect Of Ethanolic Extract Of Lepidagathis Pungens Nees., Whole Plant By Mtt Assay-An In Vitro Study. *European Journal of Molecular Clinical Medicine,* 7**,** 1027-1038.

DWIECKI, P. M., MICHALAK, T. K. & MUSZALSKA-KOLOS, I. 2021. Assessment of the properties of terbinafine hydrochloride and the search route for antifungal agents. *Journal of Molecular Structure***,** 132225.

EL SAFADI, M., BHADBHADE, M., SHIMMON, R., BAKER, A. T. & MCDONAGH, A. M. 2017. Cyclen-based chelators for the inhibition of Aβ aggregation: Synthesis, anti-oxidant and aggregation evaluation. *Inorganic Chemicals,* 467**,** 343-350.

FENG, Y., SPEZIA, M., HUANG, S., YUAN, C., ZENG, Z., ZHANG, L., JI, X., LIU, W., HUANG, B. & LUO, W. 2018. Breast cancer development and progression: Risk factors, cancer stem cells, signaling pathways, genomics, and molecular pathogenesis. *Genes diseases,* 5**,** 77-106.

FINKEL, T. & HOLBROOK, N. J. 2000. Oxidants, oxidative stress and the biology of ageing. *Nature Reviews Urology,* 408**,** 239-247.

FLORA, S., MITTAL, M. & MEHTA, A. 2008. Heavy metal induced oxidative stress & its possible reversal by chelation therapy. *Indian Journal of Medical Research,* 128**,** 501-523.

GOLBEDAGHI, R., TABANEZ, A. M., ESMAEILI, S. & FAUSTO, R. 2020. Biological applications of macrocyclic Schiff base ligands and their metal complexes: a survey of the literature (2005–2019). *Applied Organometallic Chemistry,* 34**,** e5884.

GONG, Y., FAN, Z., LUO, G., YANG, C., HUANG, Q., FAN, K., CHENG, H., JIN, K., NI, Q. & YU, X. 2019. The role of necroptosis in cancer biology and therapy. *Molecular cancer,* 18**,** 1-17.

GONZALVEZ, F. 2008. *The role of cardiolipin in the regulation of mitochondria-dependent apoptosis.* University of Glasgow.

GORDON, M. 1990. The mechanism of antioxidant action into vitro *Food antioxidants***,** 1-18.

GRELA, E., KOZŁOWSKA, J. & GRABOWIECKA, A. 2018. Current methodology of MTT assay in bacteria–A review. *Histochemicals,* 120**,** 303-311.

GULCIN, İ. & ALWASEL, S. H. 2022. Metal ions, metal chelators and metal chelating assay as antioxidant method. *Processes,* 10**,** 132.

HANAHAN, D. & WEINBERG, R. A. 2011. Hallmarks of cancer: the next generation. *Cell Death,* 144**,** 646-674.

HAYES, J. D., DINKOVA-KOSTOVA, A. T. & TEW, K. D. 2020. Oxidative stress in cancer. *Cancer Cell Culture: Methods Protocols*.

HILLER, C., HÜBNER, U., FAJNOROVA, S., SCHWARTZ, T. & DREWES, J. 2019. Antibiotic microbial resistance (AMR) removal efficiencies by conventional and advanced wastewater treatment processes: A review. *Science of the Total Environment,* 685**,** 596-608.

HSU, M. Y., MINA, E., ROETTO, A. & PORPORATO, P. E. 2020. Iron: an essential element of cancer metabolism. *Cells,* 9**,** 2591.

IBRAHIM, O. & O'SULLIVAN, J. 2020. Iron chelators in cancer therapy. *Biometals,* 33**,** 201-215.

JACOBS, I., TALJAARD-KRUGELL, C., WICKS, M., CUBASCH, H., JOFFE, M., LAUBSCHER, R., ROMIEU, I., LEVY, R. B., RAUBER, F. & BIESSY, C. 2022. Degree of food processing and breast cancer risk in black urban women from Soweto, South African: the South African Breast Cancer study. *British Journal of Nutrition***,** 1-12.

JAN, R. 2019. Understanding apoptosis and apoptotic pathways targeted cancer therapeutics. *Advanced pharmaceutical bulletin,* 9**,** 205.

KAMILOGLU, S., SARI, G., OZDAL, T. & CAPANOGLU, E. 2020. Guidelines for cell viability assays. *Food Frontiers,* 1**,** 332-349.

KARAWITA, R., SIRIWARDHANA, N., LEE, K.-W., HEO, M.-S., YEO, I.-K., LEE, Y.-D. & JEON, Y.-J. 2005. Reactive oxygen species scavenging, metal chelation, reducing power and lipid peroxidation inhibition properties of different solvent fractions from Hizikia fusiformis. *European Food Research Technology,* 220**,** 363-371.

KASHFI, K., KANNIKAL, J. & NATH, N. 2021. Macrophage reprogramming and cancer therapeutics: role of iNOS-derived NO. *Cells,* 10**,** 3194.

KAUR, P., MEHTA, R. G., SINGH, B. & ARORA, S. 2019. Development of aqueous-based multi-herbal combination using principal component analysis and its functional significance in HepG2 cells. *BMC complementary alternative medicine,* 19**,** 1-17.

KEHINDE, I., KHAN, R., NLOOTO, M. & GORDON, M. 2021. Modulatory influences of antiviral bioactive compounds on cell viability, mRNA and protein expression of cytochrome P450 3A4 and P-glycoprotein in HepG2 and HEK293 cells. *Bioorganic Chemistry,* 107**,** 104573.

KHORSANDI, L., ORAZIZADEH, M., NIAZVAND, F., ABBASPOUR, M., MANSOURI, E. & KHODADADI, A. 2017. Quercetin induces apoptosis and necroptosis in MCF-7 breast cancer cells. *Bratislavske lekarske listy,* 118**,** 123-128.

KIM, E. H., WONG, S.-W. & MARTINEZ, J. 2019. Programmed necrosis and disease: we interrupt your regular programming to bring you necroinflammation. *Cell Death Differentiation,* 26**,** 25-40.

KOFF, J. L., RAMACHANDIRAN, S. & BERNAL-MIZRACHI, L. 2015. A time to kill: targeting apoptosis in cancer. *International journal of molecular sciences,* 16**,** 2942-2955.

KONTOGHIORGHES, G. J. & KONTOGHIORGHE, C. N. 2020. Iron and chelation in biochemistry and medicine: new approaches to controlling iron metabolism and treating related diseases. *Cells,* 9**,** 1456.

KRASOVEC, G., HORKAN, H. R., QUÉINNEC, É. & CHAMBON, J.-P. 2022. The constructive function of apoptosis: More than a dead-end job. *Frontiers in Cell Developmental Biology,* 10**,** 1033645.

KRSTIĆ, D., KRINULOVIĆ, K. & VASIĆ, V. 2005. Inhibition of Na+/K+-ATPase and Mg2+-ATPase by metal ions and prevention and recovery of inhibited activities by chelators. *Journal of Enzyme Inhibition Medicinal Chemistry,* 20**,** 469-476.

KUPCHO, K., PETERS, C. & NILES, A. 2017. Real-time assessment of apoptosis and necrosis.

KUPCHO, K., SHULTZ, J., HURST, R., HARTNETT, J., ZHOU, W., MACHLEIDT, T., GRAILER, J., WORZELLA, T., RISS, T. & LAZAR, D. 2019. A real-time, bioluminescent annexin V assay for the assessment of apoptosis. *Apoptosis,* 24**,** 184-197.

LAKSHMANAN, I. & BATRA, S. K. 2013. Protocol for apoptosis assay by flow cytometry using annexin V staining method. *Bio-protocol,* 3**,** e374-e374.

LEAL-ESTEBAN, L. C. & FAJAS, L. J. 2020. Cell cycle regulators in cancer cell metabolism. *Biochimical Biophysical -Molecular Basis of Diseases,* 1866**,** 165715.

LEE, J. & ROH, J.-L. 2023. Targeting Iron-Sulfur Clusters in Cancer: Opportunities and Challenges for Ferroptosis-Based Therapy. *Cancers,* 15**,** 2694.

LEJAULT, P., DUSKOVA, K., BERNHARD, C., VALVERDE, I. E., ROMIEU, A. & MONCHAUD, D. 2019. The scope of application of macrocyclic polyamines beyond metal chelation. *European Journal of Organic Chemistry,* 2019**,** 6146-6157.

LI, S., WU, L., FENG, J., LI, J., LIU, T., ZHANG, R., XU, S., CHENG, K., ZHOU, Y. & ZHOU, S. 2016. In vitro and in vivo study of epigallocatechin-3-gallate-induced apoptosis in aerobic glycolytic hepatocellular carcinoma cells involving inhibition of phosphofructokinase activity. *Scientific reports,* 6**,** 1-18.

LI, X., WANG, Y., LI, M., WANG, H. & DONG, X. 2021. Metal complexes or chelators with ROS regulation capacity: Promising candidates for cancer treatment. *Molecules,* 27**,** 148.

LIGUORI, I., RUSSO, G., CURCIO, F., BULLI, G., ARAN, L., DELLA-MORTE, D., GARGIULO, G., TESTA, G., CACCIATORE, F. & BONADUCE, D. 2018. Oxidative stress, aging, and diseases. *Clinical interventions in aging,* 13**,** 757.

LIU, Z.-Q., MAHMOOD, T. & YANG, P.-C. 2014. Western blot: technique, theory and trouble shooting. *North American journal of medical sciences,* 6**,** 160.

LIVAK, K. J. & SCHMITTGEN, T. D. J. M. 2001. Analysis of relative gene expression data using real-time quantitative PCR and the 2− ΔΔCT method. 25**,** 402-408.

MAHMOOD, T. & YANG, P.-C. 2012. Western blot: technique, theory, and trouble shooting. *North American journal of medical sciences,* 4**,** 429.

MALIK, J. A., AHMED, S., JAN, B., BENDER, O., AL HAGBANI, T., ALQARNI, A. & ANWAR, S. 2022. Drugs repurposed: An advanced step towards the treatment of breast cancer and associated challenges. *Biomedicine Pharmacotherapy,* 145**,** 112375.

MCOYI, S., AMOAKO, D. G., SOMBORO, A. M., KHUMALO, H. M. & KHAN, R. B. 2020. The molecular effect of 1, 4, 7-triazacyclononane on oxidative stress parameters in human hepatocellular carcinoma (HepG2) cells. *Journal of Biochemical Molecular Toxicology,* 34**,** e22607.

MEZZATESTA, C. & BORNHAUSER, B. C. 2019. Exploiting necroptosis for therapy of acute lymphoblastic leukemia. *Frontiers in Cell Developmental Biology,* 7**,** 40.

MHLANGA, P., PERUMAL, P. O., SOMBORO, A. M., AMOAKO, D. G., KHUMALO, H. M. & KHAN, R. B. 2019. Mechanistic insights into oxidative stress and apoptosis mediated by tannic acid in human liver hepatocellular carcinoma cells. *International journal of molecular sciences,* 20**,** 6145.

MILNE, R. L., KUCHENBAECKER, K. B., MICHAILIDOU, K., BEESLEY, J., KAR, S., LINDSTRÖM, S., HUI, S., LEMAÇON, A., SOUCY, P. & DENNIS, J. 2017. Identification of ten variants associated with risk of estrogen-receptor-negative breast cancer. *Nature genetics,* 49**,** 1767-1778.

MIYAI, T., TOYONO, T., KITAMOTO, K., FUKUSHIMA, M., YOSHIDA, J., SHIRAKAWA, R., NAKAGAWA, S., JURKUNAS, U. V., USUI, T. J. I. O. & SCIENCE, V. 2018. Endoplasmic reticulum stress decreases mitochondrial membrane potential and upregulates PARK2 expression in corneal endothelium. 59**,** 4436-4436.

MIZIAK, P., BARAN, M., BŁASZCZAK, E., PRZYBYSZEWSKA-PODSTAWKA, A., KAŁAFUT, J., SMOK-KALWAT, J., DMOSZYŃSKA-GRANICZKA, M., KIEŁBUS, M. & STEPULAK, A. 2023. Estrogen Receptor Signaling in Breast Cancer. *Cancers,* 15**,** 4689.

MOMENIMOVAHED, Z. & SALEHINIYA, H. 2019. Epidemiological characteristics of and risk factors for breast cancer in the world. *Breast Cancer: Targets Therapy,* 11**,** 151.

MOORE, C. 2009. Introduction to western blotting. *AbD serotec*, 4-20.

MURPHY, N., SHULTZ, J., ZHOU, W. & WOOD, K. V. J. C. N. 2008. Detecting Toxicological Responses in Cells with the Bioluminescent GSH-GLO™ Glutathione Assay.

NEUPANE, P., BHUJU, S., THAPA, N. & BHATTARAI, H. K. 2019. ATP synthase: structure, function and inhibition. *Biomolecular concepts,* 10, 1-10.

PARHAMIFAR, L., ANDERSEN, H. & MOGHIMI, S. M. 2013. Lactate dehydrogenase assay for assessment of polycation cytotoxicity. *Nanotechnology for Nucleic Acid Delivery: Methods Protocols*, 13-22.

PETRONEK, M. S., SPITZ, D. R., BUETTNER, G. R. & ALLEN, B. G. 2019. Linking cancer metabolic dysfunction and genetic instability through the lens of iron metabolism. *Cancers,* 11, 1077.

PFEFFER, C. M. & SINGH, A. T. 2018. Apoptosis: a target for anticancer therapy. *International journal of molecular sciences,* 19, 448.

PRASAD, S. & SRIVASTAVA, S. K. J. 2020. Oxidative stress and cancer: chemopreventive and therapeutic role of triphala. *Antioxidants,* 9, 72.

PROMEGA, C. 2016. P450-Glo™ Assays.

PROMEGA, C. 2017. RealTime-Glo™ Annexin V Apoptosis and Necrosis Assay.

PUBCHEM 2024. Cyclododecane - National Center for Biotechnology Information *PubChem Compound Summary for CID 9268*.

RECKNAGEL, R. O., GLENDE, E. A. & BRITTON, R. S. 2020. Free radical damage and lipid peroxidation. *Hepatotoxicology.* CRC press.

REDDY, P., PRADEEP, S., GOPINATH, S., RAMU, R., KOLLUR, S. P. & SHIVAMALLU, C. 2022. Anti-breast cancer potential of MnO2 nanoparticles using Terminalia chebula fruit extract against MCF-7 cell line through in vitro cell cycle and apoptotic studies. *Materials Today: Proceedings*.

REIBENSPIES, J. & ANDERSON, O. 1990. Structure of 1, 4, 7, 10-tetraazacyclododecane tetrahydrochloride. *Crystallographical Section C: Crystal Structure Communications,* 46, 163-165.

ROCHA, C. R. R., KAJITANI, G. S., QUINET, A., FORTUNATO, R. S. & MENCK, C. F. M. 2016. NRF2 and glutathione are key resistance mediators to temozolomide in glioma and melanoma cells. *Oncotarget,* 7, 48081.

SANDNES, R. W., GACEK, M. & UNDHEIM, K. 1999. A Simple Synthesis of the Macrocycle 1, 4, 7, 10-Tetraazacyclododecane. *Chemical form,* 30, no-no.

SHEN, X.-T., ZHANG, Y.-Z., XIAO, F., ZHU, J. & ZHENG, X.-D. 2017. Effects on cytotoxicity and antibacterial properties of the incorporations of silver nanoparticles into the surface coating of dental alloys. *Journal of Zhejiang University-SCIENCE B,* 18**,** 615-625.

SIEGEL, R. L., MILLER, K. D., WAGLE, N. S. & JEMAL, A. J. C. C. J. C. 2023. Cancer statistics, 2023. 73**,** 17-48.

SPERANZA, L., DE LUTIIS, M., SHAIK, Y., FELACO, M., PATRUNO, A., TETÈ, A., MASTRANGELO, F., MADHAPPAN, B., CASTELLANI, M. & CONTI, F. 2007. Localization and activity of iNOS in normal human lung tissue and lung cancer tissue. *The International journal of biological markers,* 22**,** 226-231.

SULTAN, M. T., ANWAR, M. J., IMRAN, M., KHALIL, I., SAEED, F., NEELUM, S., ALSAGABY, S. A., AL ABDULMONEM, W., ABDELGAWAD, M. A. & HUSSAIN, M. 2023. Phytochemical profile and pro-healthy properties of Terminalia chebula: A comprehensive review. *International Journal of Food Properties,* 26**,** 526-551.

SUN, X., TANG, S., HOU, B., DUAN, Z., LIU, Z., LI, Y., HE, S., WANG, Q. & CHANG, Q. 2021. Overexpression of P-glycoprotein, MRP2, and CYP3A4 impairs intestinal absorption of octreotide in rats with portal hypertension. *BMC gastroenterology,* 21**,** 1-15.

SUN, Y.-S., ZHAO, Z., YANG, Z.-N., XU, F., LU, H.-J., ZHU, Z.-Y., SHI, W., JIANG, J., YAO, P.-P. & ZHU, H.-P. 2017. Risk factors and preventions of breast cancer. *International journal of biological sciences,* 13**,** 1387.

SWAIN, S. M., SHASTRY, M. & HAMILTON, E. 2023. Targeting HER2-positive breast cancer: Advances and future directions. *Nature Reviews Drug Discovery,* 22**,** 101-126.

TIAN, M., LI, J., ZHANG, S., GUO, L., HE, X., KONG, D., ZHANG, H. & LIU, Z. 2017. Half-sandwich ruthenium (ii) complexes containing N^ N-chelated imino-pyridyl ligands that are selectively toxic to cancer cells. *Chemical Communications,* 53**,** 12810-12813.

TIMOSHNIKOV, V. A., SELYUTINA, O. Y., POLYAKOV, N. E., DIDICHENKO, V. & KONTOGHIORGHES, G. J. 2022. Mechanistic Insights of Chelator Complexes with Essential Transition Metals: Antioxidant/Pro-Oxidant Activity and Applications in Medicine. *International journal of molecular sciences,* 23**,** 1247.

TOLOUIAN, R., TOLOUIAN, A., DASTAN, F., FARHANGI, V., PEYMANI, P., SAEIFAR, S., MONTES, O. F. B., MOHMOODNIA, L., KHOSRAVIFARSANI, M. & SADIGHPOUR, T. 2023. Antioxidants and cisplatin nephrotoxicity; an updated review on current knowledge. *Journal of Nephropharmacology,* 12.

TOSATO, M., LAZZARI, L. & MARCO, V. D. 2022. Revisiting Lead (II)-1, 4, 7, 10-tetraazacyclododecane-1, 4, 7, 10-tetraacetic Acid Coordination Chemistry in Aqueous Solutions: Evidence of an Underestimated Thermodynamic Stability. *ACS omega*.

TOWNSEND, D. M., TEW, K. D. & TAPIERO, H. 2003. The importance of glutathione in human disease. *Biomedicine Pharmacotherapy,* 57**,** 145-155.

TRETTER, L., PATOCS, A. & CHINOPOULOS, C. 2016. Succinate, an intermediate in metabolism, signal transduction, ROS, hypoxia, and tumorigenesis. *Biochimical Biophysical-Bioenergetics,* 1857**,** 1086-1101.

VERCAMMEN, D., BEYAERT, R., DENECKER, G., GOOSSENS, V., VAN LOO, G., DECLERCQ, W., GROOTEN, J., FIERS, W. & VANDENABEELE, P. 1998. Inhibition of caspases increases the sensitivity of L929 cells to necrosis mediated by tumor necrosis factor. *The Journal of experimental medicine,* 187**,** 1477-1485.

VISHWAKARMA, A., WANY, A., PANDEY, S., BULLE, M., KUMARI, A., KISHOREKUMAR, R., IGAMBERDIEV, A. U., MUR, L. A. & GUPTA, K. J. 2019. Current approaches to measure nitric oxide in plants. *Journal of experimental botany,* 70**,** 4333-4343.

WANG, Q., JIANG, J., YING, G., XIE, X.-Q., ZHANG, X., XU, W., ZHANG, X., SONG, E., BU, H. & PING, Y.-F. 2018a. Tamoxifen enhances stemness and promotes metastasis of ERα36+ breast cancer by upregulating ALDH1A1 in cancer cells. *Cell research,* 28**,** 336-358.

WANG, R., HAO, W., PAN, L., BOLDOGH, I. & BA, X. 2018b. The roles of base excision repair enzyme OGG1 in gene expression. *Cellular Molecular Life Sciences,* 75**,** 3741-3750.

WANG, Z., LI, Z., YE, Y., XIE, L. & LI, W. J. O. M. 2016. Oxidative stress and liver cancer: etiology and therapeutic targets. *Oxidative medicine cellular longevity,* 2016.

WORLD HEALTH ORGANISATION 2021. Breast cancer newsroom.

YADAV, P., YADAV, R., JAIN, S., VAIDYA, A. J. C. B. & DESIGN, D. 2021. Caspase-3: a primary target for natural and synthetic compounds for cancer therapy. 98**,** 144-165.

YANG, L., LIANG, F., LIU, M., ZHENG, C., WAN, S., XIONG, X., ZHANG, X., SHEN, C. & ZHOU, X. 2007. HeLa cells apoptosis induced by 1, 7-dimethyl-1, 4, 7, 10-tetraazacyclododecane. *Bioorganic medicinal chemistry letters,* 17**,** 1818-1822.

YANG, Y., CHEN, Y., WU, J. H., REN, Y., LIU, B., ZHANG, Y. & YU, H. 2023. Targeting regulated cell death with plant natural compounds for cancer therapy: A revisited review of apoptosis, autophagy-dependent cell death, and necroptosis. *Phytotherapy Research,* 37**,** 1488-1525.

YIN, L., DUAN, J.-J., BIAN, X.-W. & YU, S.-C. J. B. C. R. 2020. Triple-negative breast cancer molecular subtyping and treatment progress. *Breast Cancer Research,* 22**,** 1-13.

YONG, J., BISCHOF, H., BURGSTALLER, S., SIIRIN, M., MURPHY, A., MALLI, R. & KAUFMAN, R. J. 2019. Mitochondria supply ATP to the ER through a mechanism antagonized by cytosolic Ca2+. *Elife,* 8**,** e49682.

ZOROVA, L. D., POPKOV, V. A., PLOTNIKOV, E. Y., SILACHEV, D. N., PEVZNER, I. B., JANKAUSKAS, S. S., BABENKO, V. A., ZOROV, S. D., BALAKIREVA, A. V. & JUHASZOVA, M. 2018. Mitochondrial membrane potential. *Analytical biochemistry,* 552**,** 50-59.

APPENDICES

APPENDIX A: MTT CELL VIABILITY VS. TREATMENT CONCENTRATIONS

The MTT assay revealed a dose-dependent decrease in MCF-7 (IC_{50} = 168.4µM, IC_{20} = 41.69µM) and MDA-MB-231 (IC_{50} = 561µM, IC_{20} = 302.9µM) cell viability when cells were treated with 0-1000µM cyclen tetrahydrochloride dilutions for 48 hours (Table A.1 and A.2).

Table A.1: Cell viability changes depending on treatment concentration for MCF-7 cells determined by the MTT assay.

Average absorbances	Treatment concentration (µM)	log con	% cell viability
1.385	0	0	100
1.374	12.5	1.09691001	99
0.981	25	1.39794001	71
0.990	50	1.69897	72
0.911	100	2	66
0.711	250	2.39794001	51
0.366	500	2.69897	26
0.087	1000	3	6

Table A.2: Cell viability changes depending on treatment concentration for MDA-MB-231 cells determined by the MTT assay.

Average absorbances	Treatment concentration (μM)	log con	% cell viability
0.914	0	0	100
1.124	12.5	1.09691001	123
1.179	25	1.39794001	129
1.049	50	1.69897	115
0.948	100	2	104
0.742	250	2.39794001	81
0.512	500	2.69897	56
0.218	1000	3	24

APPENDIX B: QUANTIFICATION OF NITRITES

The quantification of nitrites using a standard curve determined by the NOS assay for MCF-7 and MDA-MB-231 cells, treated with cyclen tetrahydrochloride treatments for 48 hours (Table B.1 and Figure B.1).

Table B.1: The determination of the nitrates and nitrites by standard reference curve.

Standard nitrite concentration (µM)	OD1	OD2	OD3	average	Av-blank
0	0.214	0.206	0.213	0.210	0.000
12.5	0.269	0.318	0.267	0.294	0.084
25	0.301	0.300	0.326	0.301	0.091
50	0.438	0.431	0.455	0.435	0.225
75	0.472	0.544	0.541	0.508	0.298
100	0.628	0.627	0.629	0.628	0.418
150	0.656	0.833	0.282	0.745	0.535
200	1.027	0.996	1.044	1.012	0.802

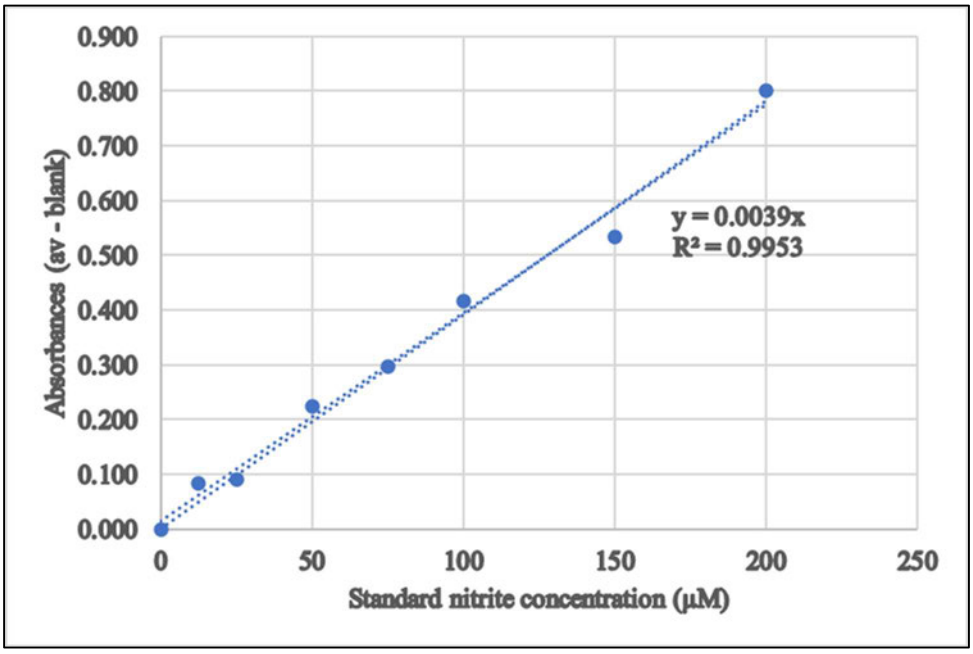

Figure B.1: Standard curve for nitrite and nitrate concentrations.

APPENDIX C: PROTEIN STANDARDISATION

The quantification of proteins using the bicinchoninic acid (BCA) assay determined by western blotting for MCF-7 and MDA-MB-231 cells, treated with cyclen tetrahydrochloride treatments for 48 hours (Table C.1, Figure C.1 and Table C.2).

Table C.1: Protein Quantification and Standardisation using Bovine Serum Albumin (BSA).

Protein standard concentrations (mg/ml)	Abs 1	Abs 2	Average	Av - blank
0	0.105	0.103	0.104	0
0.2	0.373	0.324	0.3485	0.2445
0.4	0.48	0.498	0.489	0.385
0.6	0.606	0.617	0.6115	0.5075
0.8	0.805	0.874	0.8395	0.7355
1	0.941	1.034	0.9875	0.8835

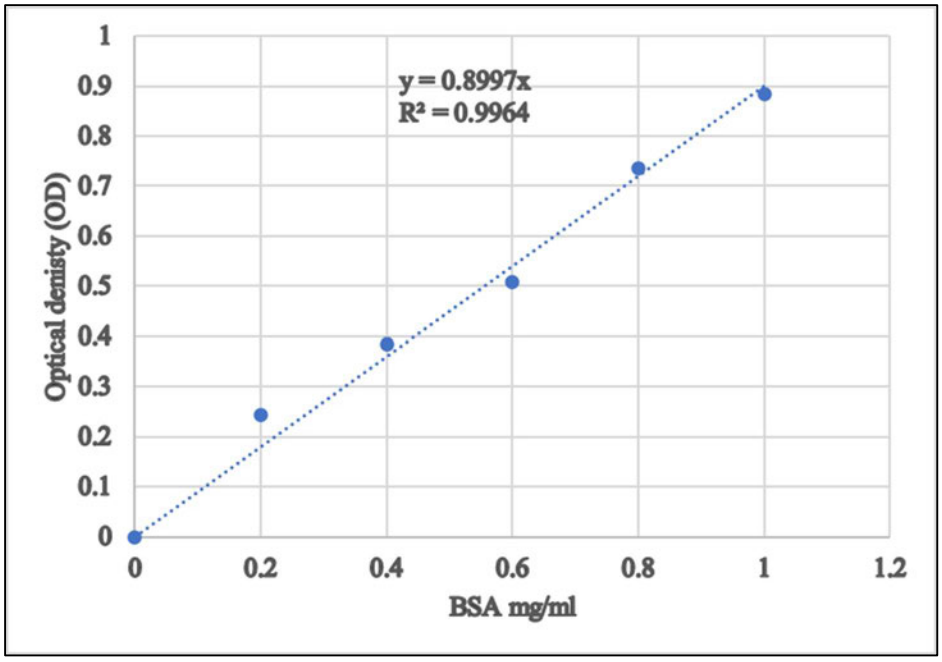

Figure C.1: Standard curve using a range of known BSA concentration. The straight-line equation was used to determine sample protein concentrations by means of the BCA assay.

APPENDIX D: qPCR MELT CURVES

The melt curves obtained from amplification of specified genes determined by qPCR, when treated with cyclen tetrahydrochloride for 48 hours (Figure D.1, D.2, D.3, D.4, D5, D.6 and Figure D.7).

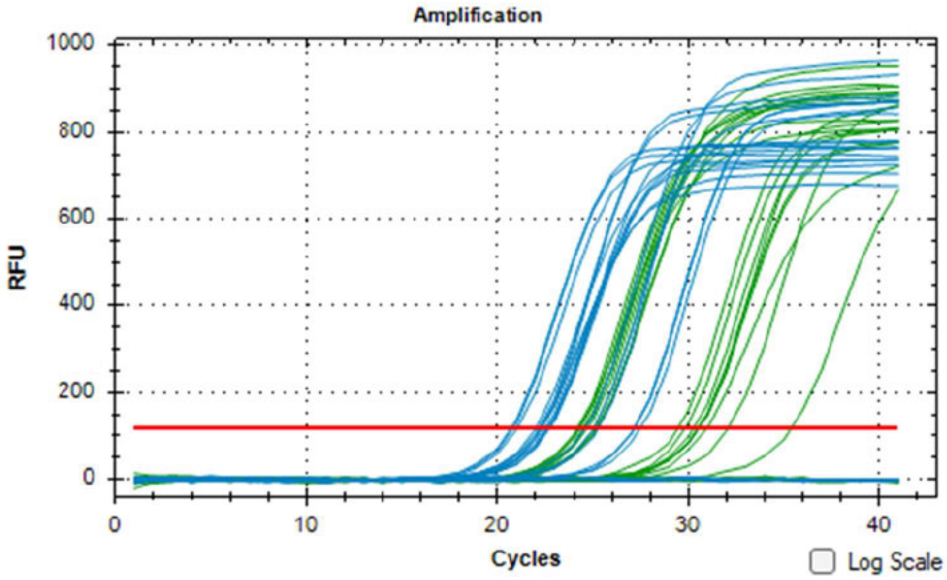

Figure D.1: The gene amplification of *MLKL*.

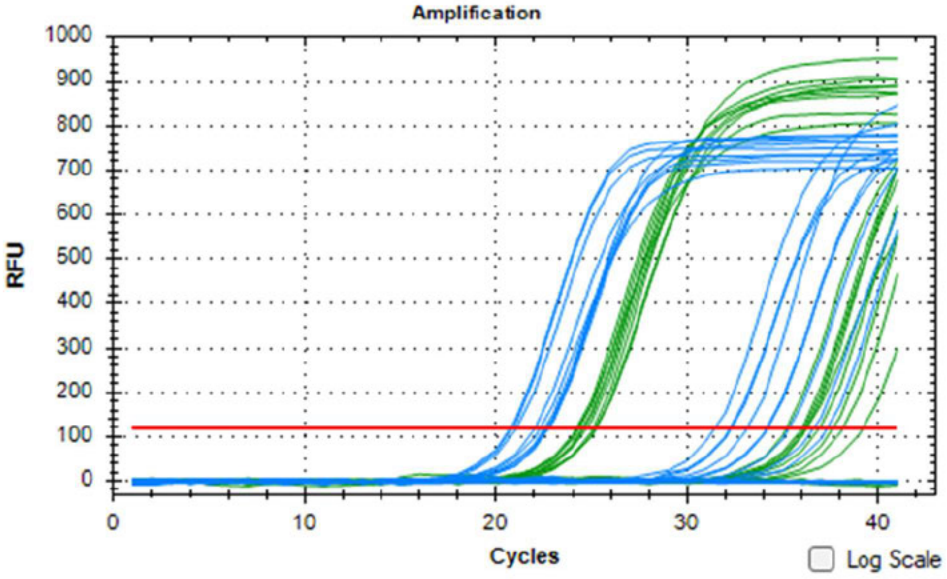

Figure D.2: The gene amplification of *RIPK1*.

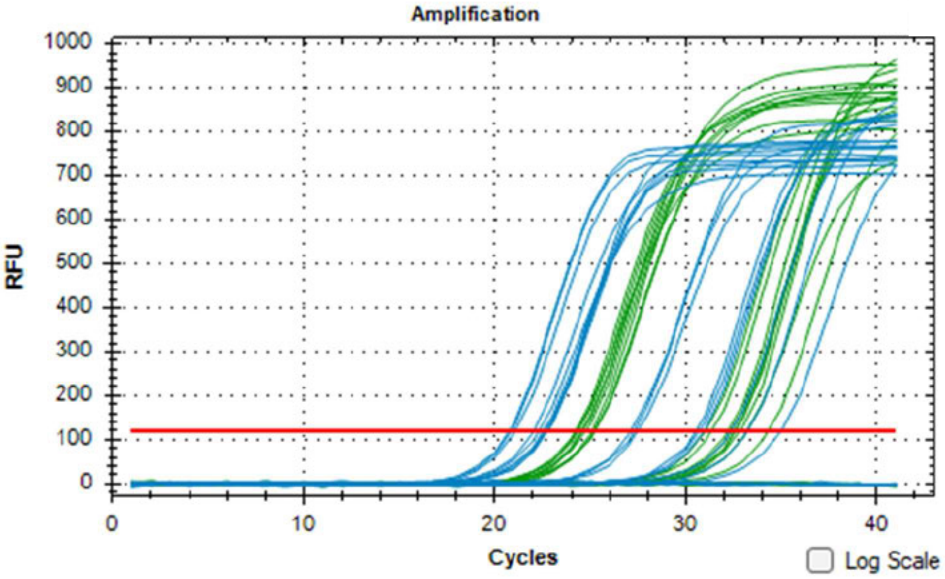

Figure D.3: The gene amplification of *RIPK3*.

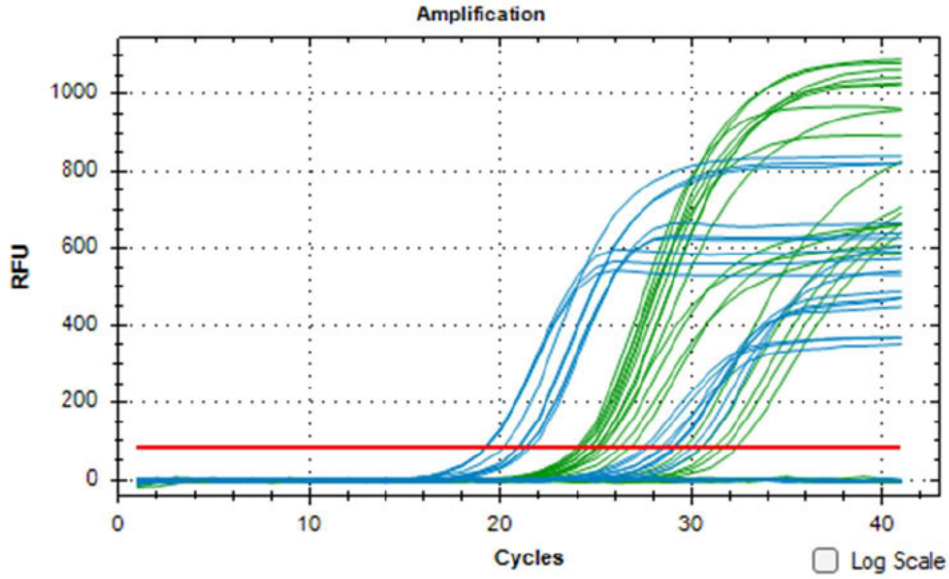

Figure D.4: The gene amplification of *NF-KB*.

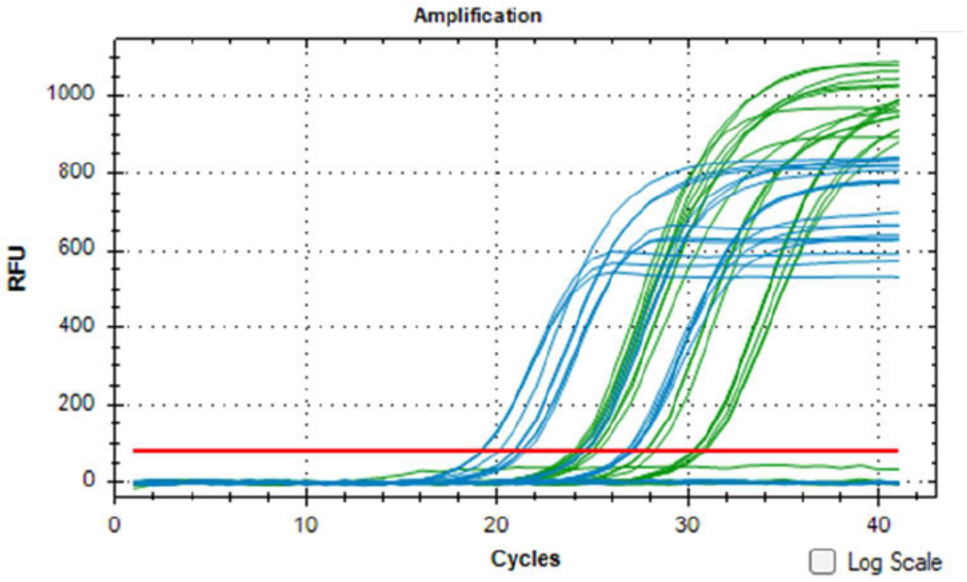

Figure D.5: The gene amplification of *Gpx1*.

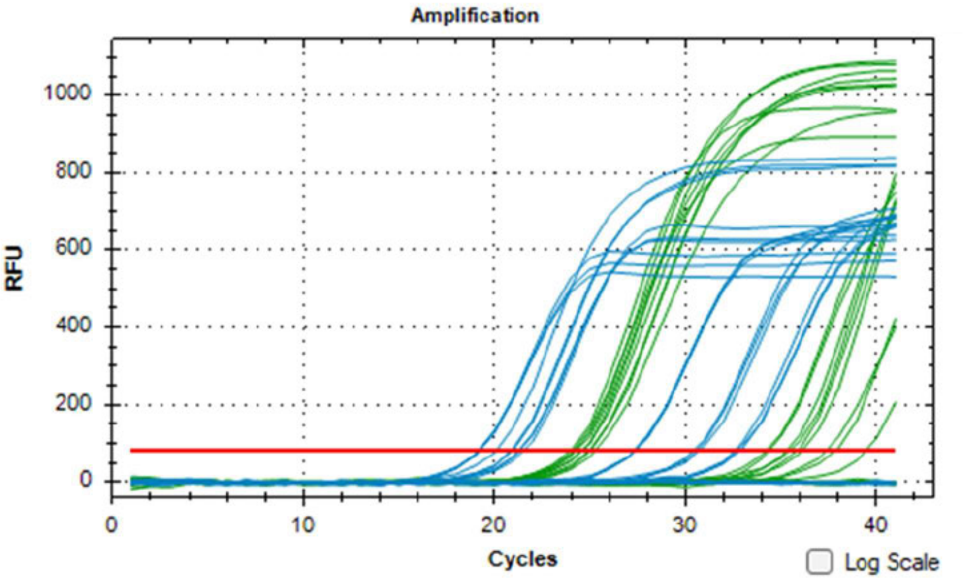

Figure D.6: The gene amplification of *OGG1*.

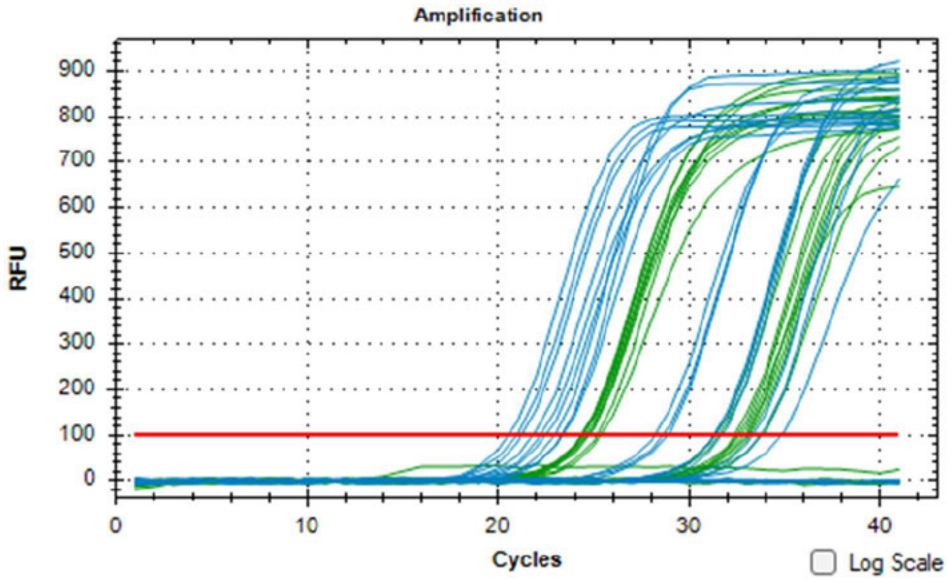

Figure D.7: The gene amplification of *TNF-a.*

APPENDIX E: ETHICS SUPPORT

Ethics approval and renewal letter.

UNIVERSITY OF KWAZULU-NATAL
INYUVESI YAKWAZULU-NATALI

21 December 2022

Ms Mikayla Libby Munsamy (218016363)
School of Laboratory Medicine & Medical Science
Howard College

Dear Ms Munsamy,

Protocol reference number: BREC/00005021/2022
Project title: The mechanistic pathways of oxidative stress and apoptosis in response to synthetic compound Cyclen tetrahydrochloride in oestrogen-positive (MCF-7) and oestrogen-negative (MDA-MB-231) human breast cancer cells.
Degree: MMedSc

EXPEDITED APPLICATION: APPROVAL LETTER

A sub-committee of the Biomedical Research Ethics Committee has considered and noted your application.

The conditions have been met and the study is given full ethics approval and may begin as from 21 December 2022. Please ensure that any outstanding site permissions are obtained and forwarded to BREC for approval before commencing research at a site.

This approval is valid for one year from 21 December 2022. To ensure uninterrupted approval of this study beyond the approval expiry date, an application for recertification must be submitted to BREC on RIG on the appropriate BREC form 2-3 months before the expiry date.

Any amendments to this study, unless urgently required to ensure safety of participants, must be approved by BREC prior to implementation.

Your acceptance of this approval denotes your compliance with South African National Research Ethics Guidelines (2015), South African National Good Clinical Practice Guidelines (2020) (if applicable) and with UKZN BREC ethics requirements as contained in the UKZN BREC Terms of Reference and Standard Operating Procedures, all available at http://research.ukzn.ac.za/Research-Ethics/Biomedical-Research-Ethics.aspx.

BREC is registered with the South African National Health Research Ethics Council (REC-290408-009). BREC has US Office for Human Research Protections (OHRP) Federal-wide Assurance (FWA 678).

The sub-committee's decision will be noted by a full Committee at its next meeting taking place on 14 February 2023.

Yours sincerely,

[redacted]

Prof D Wassenaar
Chair: Biomedical Research Ethics Committee

UNIVERSITY OF KWAZULU-NATAL
INYUVESI YAKWAZULU-NATALI

23 November 2023

Ms Mikayla Libby Munsamy (218016363)
School of Laboratory Medicine & Medical Science
Howard College

Dear Ms Munsamy,

Protocol reference number: BREC/00005021/2022
Project title: The mechanistic pathways of oxidative stress and apoptosis in response to synthetic compound Cyclen tetrahydrochloride in estrogen-positive (MCF-7) and estrogen-negative (MDA-MB-231) human breast cancer cells.
Degree: MMedSci

RECERTIFICATION APPLICATION APPROVAL NOTICE

Approved:	21 December 2023
Expiration of Ethical Approval:	21 December 2024

I wish to advise you that your application for recertification for the above study has been noted and approved by a subcommittee of the Biomedical Research Ethics Committee (BREC). The start and end dates of this period are indicated above.

Note to PI: In Future please provide more info to assist BREC in determining current stage of study.

If any modifications or adverse events occur in the project before your next scheduled review, you must submit them to BREC for review. Except in emergency situations, no change to the protocol may be implemented until you have received written BREC approval for the change.

The committee will be notified of the above approval at its next meeting to be held on 12 December 2023.

Yours sincerely

[redacted]

Ms A Marimuthu
(for) Prof D Wassenaar
Chair: Biomedical Research Ethics Committee

APPENDIX F: TURNITIN REPORT

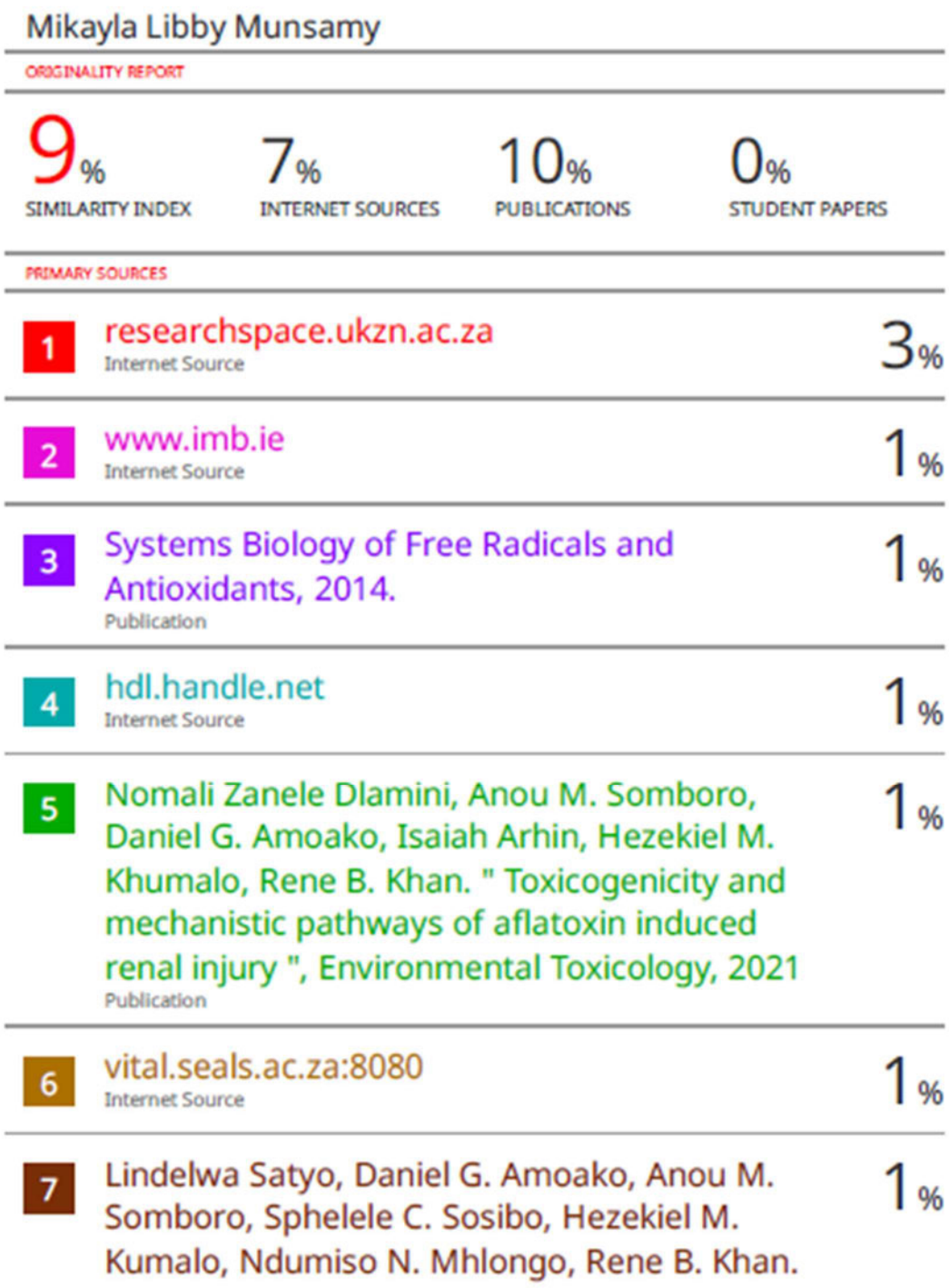

Mikayla Libby Munsamy

ORIGINALITY REPORT

9%	7%	10%	0%
SIMILARITY INDEX	INTERNET SOURCES	PUBLICATIONS	STUDENT PAPERS

PRIMARY SOURCES

1	researchspace.ukzn.ac.za Internet Source	3%
2	www.imb.ie Internet Source	1%
3	Systems Biology of Free Radicals and Antioxidants, 2014. Publication	1%
4	hdl.handle.net Internet Source	1%
5	Nomali Zanele Dlamini, Anou M. Somboro, Daniel G. Amoako, Isaiah Arhin, Hezekiel M. Khumalo, Rene B. Khan. " Toxicogenicity and mechanistic pathways of aflatoxin induced renal injury ", Environmental Toxicology, 2021 Publication	1%
6	vital.seals.ac.za:8080 Internet Source	1%
7	Lindelwa Satyo, Daniel G. Amoako, Anou M. Somboro, Sphelele C. Sosibo, Hezekiel M. Kumalo, Ndumiso N. Mhlongo, Rene B. Khan.	1%

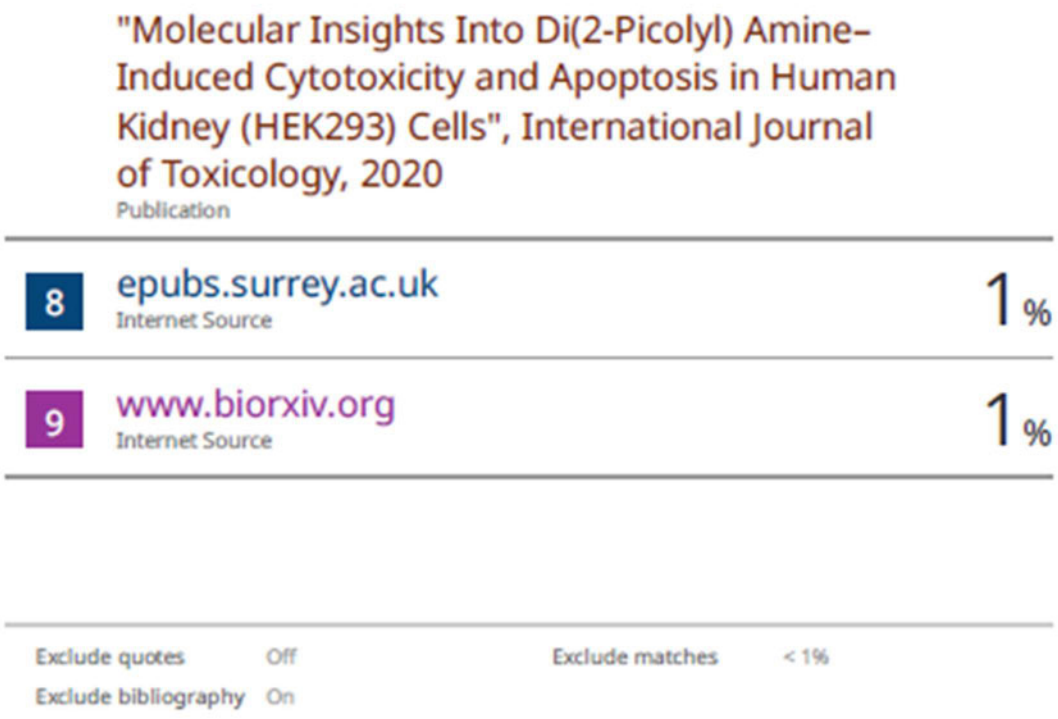
"Molecular Insights Into Di(2-Picolyl) Amine–Induced Cytotoxicity and Apoptosis in Human Kidney (HEK293) Cells", International Journal of Toxicology, 2020
Publication
8
epubs.surrey.ac.uk
Internet Source
1 %
9
www.biorxiv.org
Internet Source
1 %
Exclude quotes Off
Exclude bibliography On
Exclude matches < 1%